First tephrostratigraphic results of the DEEP site record from Lake Ohrid (Macedonia, Albania)

N. Leicher[1], G. Zanchetta[2], R. Sulpizio[3,4], B. Giaccio[5], B. Wagner[1], S. Nomade[6], A. Francke[1], and P. Del Carlo[7]

[1] Institute of Geology and Mineralogy, University of Cologne, Zuelpicher Str. 49a, 50674 Cologne, Germany

[2] Dipartimento di Scienze della Terra, University of Pisa, via S. Maria 53, 56126 Pisa, Italy

[3] Dipartimento di Scienze della Terra e Geoambientali, University of Bari, via Orabona 4, 70125 Bari, Italy

[4] Istituto per la Dinamica dei Processi Ambientali (IDPA) CNR, via M. Bianco 9, Milan, Italy

[5] Istituto di Geologia Ambientale e Geoingegneria, CNR, Via Salaria Km 29,300, Monterotondo, Roma, Italy

[6] Laboratoire des sciences du climat et de l'environnement, UMR 8212, CEA/CNRS/UVSQ et Université Paris-Saclay F-91198 Gif-Sur-Yvette, France

[7] Istituto Nazionale di Geofisica e Vulcanologia, Sezione di Pisa, via della Faggiola 32, 56126, Pisa, Italy

Correspondence to: N. Leicher (n.leicher@uni-koeln.de)

Abstract

A tephrostratigraphic record covering the Marine Isotope Stages (MIS) 1–15 was established for the DEEP site record of Lake Ohrid (Macedonia/Albania). Major element analyses (SEM-EDS/WDS) were carried out on juvenile fragments extracted from 12 tephra layers (OH-DP-0115 to OH-DP-2060). The geochemical analyses of the glass shards of all of these layers suggest an origin from the Italian volcanic provinces. They include: the Y-3 (OH-DP-0115, 26.68–29.42 ka cal BP), the Campanian Ignimbrite/Y-5 (OH-DP-0169, 39.6±0.1 ka), and the X-6 (OH-DP-0404, 109±2 ka) from the Campanian volcanoes, the P-11 of the Pantelleria Island (OH-DP-0499, 133.5±2 ka), the Vico B (OH-DP-0617, 162±6 ka) from the Vico volcano, the Pozzolane Rosse (OH-DP- 1817, 457±2 ka), and the Tufo di Bagni Albule (OH-DP-2060, 527±2 ka) from the Colli Albani volcanic district, and the Fall A (OH-DP-2010, 496±3 ka) from the Sabatini volcanic field. Furthermore, a comparison of the Ohrid record with tephrostratigraphic records of mid-distal archives related to the Mediterranean area allowed the recognition of the equivalents of other less known tephra layers, such as the TM24a/POP2 (OH-DP-0404, 102±2 ka) recognised in the Lago Grande di Monticchio and the Sulmona basin, the CF-V5/PRAD3225 (OH-DP-0624, ca. 163±22 ka) identified in the Campo Felice basin/Adriatic Sea, the SC5 (OH-DP-1955, 493.1±10.9 ka) recognised in the Mercure basin, and the A11/12 (OH-DP-2017, 511±6 ka) sampled at the Acerno basin, whose specific volcanic sources are still poorly constrained. Additionally, one cryptotephra (OH-DP-0027) was identified by correlation of the potassium XRF intensities from the DEEP site with those from a short core of a previous study from Lake Ohrid. In these cores, a maximum in potassium is caused by glass shards, which were correlated with the Mercato tephra (8.43– 8.63 ka cal BP) from Somma-Vesuvius. The presented tephrostratigraphic work allows, for the first time, the extension of a consistent part of the Middle Pleistocene tephrostratigraphy of Italian volcanoes as far as to the Balkans. The establishment of the tephrostratigraphic framework for the Lake Ohrid record provides important, independent tie-points for the age-depth model of the DEEP site sequence, which is a prerequisite for paleoclimatic and -environmental reconstructions. Furthermore, this age-depth model will help to improve and re-evaluate the chronology of other, both undated and dated tephra layers from other records. Thus, the Lake Ohrid record is candidate to become the template for the central Mediterranean tephrostratigraphy, especially for the hitherto poorly known and explored lower Middle Pleistocene period.

1 Introduction

Volcanic explosive eruptions produce pyroclastic material, called tephra (gr. τεφρα = ash), which is ejected into the atmosphere and distributed by the prevailing wind systems. Tephra settles down from the atmosphere in a relatively short time (days-weeks) as isochronous event marker horizons into all kind of geological archives downwind of the volcano. By determining the unique geochemical and physical fingerprint of such a tephra horizon, tephra layers (from different archives) can be identified, characterised, and correlated with each other in order to obtain a tephrostratigraphic framework. If tephra horizons can be dated directly (e.g., $^{40}Ar/^{39}Ar$) or indirectly (e.g., ^{14}C dating on overlying or underlying sediments, varve counting, age modelling) and correlated with tephra horizons in other archives, also the ages can be transferred to these other archives.

The Italian volcanism was characterized by an intense explosive activity during the entire Quaternary (Peccerillo, 2005). Consequently, the surrounding Mediterranean region became an ideal setting for tephrochronological studies (tephrostratigraphy and tephrochronometry, cf. Sarna-Wojcicki, 2013), which provide a key tool for a wide spectrum of Quaternary science subjects (e.g. Lowe, 2011). After Keller et al. (1978) set up the first tephrostratigraphic scheme for the central Mediterranean region, numerous studies on marine and terrestrial archives have spatially and temporally extended and improved this initial stratigraphy for the Holocene and Late Pleistocene (Paterne et al., 1986, 1988, 2008; Vezzoli, 1991; Calanchi et al., 1998; Narcisi and Vezzoli, 1999; Siani et al., 2004; Calanchi and Dinelli, 2008; Zanchetta et al., 2011; Tamburrino et al., 2012; Insinga et al., 2014; Satow et al., 2015; Tomlinson et al., 2015). Despite this noticeable progress over the last decades, tephrochronological work in the period > 200 ka is still challenging due to incomplete knowledge on the eruption history and limited geochemical analysis. Some records from the Italian Peninsula cover specific intervals of the Early to Middle Pleistocene and can be used as proximal (Karner et al., 2001; Rouchon et al., 2008; Marra et al., 2009, 2014; Palladino et al., 2010; Giaccio et al., 2013a) or relatively distal (Karner et al., 1999; Munno and Petrosino, 2007; Roulleau et al., 2009; Russo Ermolli et al., 2010; Giaccio et al., 2013b, 2014, 2015; Petrosino et al., 2014a, b, 2015; Sagnotti et al., 2014) archives of deposits from volcanic complexes. Sediment records spanning continuously > 200 ka are extremely rare in the Mediterranean region. To date, there are only two continuous records covering the entire Middle and parts of the Early Pleistocene of the Mediterranean region, which are the Calabrian Ridge core KC01B (Lourens, 2004; Insinga et al., 2014) and

the peat record from Tenaghi Philippon, Greece (Tzedakis, 1993; St. Seymour et al., 2004; Pross et al., 2007). However, both records are limited in the tephrostratigraphy to the Holocene and upper Middle Pleistocene.

Lake Ohrid is located on the Balkan Peninsula and is one of the oldest lakes of Europe (Wagner et al., 2014). Over 1.2 Ma of continuous sediments were recovered from Lake Ohrid during the ICDP (International Continental Scientific Drilling Program) deep drilling campaign SCOPSCO (Scientific Collaboration on Past Speciation Conditions in Lake Ohrid). Previous tephrochronological studies on sediment cores from Lake Ohrid covered the last 135 ka and revealed the lake's unique potential as distal tephra archive of Italian volcanoes (e.g. Sulpizio et al., 2010).

Here, we present first tephrostratigraphic and tephrochronological results of the uppermost 247.8 m composite depth (mcd) of the main drill site (DEEP site) in the central part of the lake, which covers continuously the last 637 ka (Francke et al., 2016). The correlation of the discovered tephra layers to known and dated equivalent tephra horizons from proximal and distal archives enables dating of the Lake Ohrid succession. The transfer of these ages to the Lake Ohrid record provides important, independent tie-points for an age-depth model complemented by orbital tuning (Francke et al., 2016), which is a precondition for environmental and climate reconstructions. The correlation of tephra layers between different geographical archives, both terrestrial and marine, is crucial for a synchronisation of paleoclimatic and paleoenvironmental changes on a regional and global scale.

2 Regional setting

Lake Ohrid (40°54'–41°10' N, 20°38'–20°48' E) is located in the Balkan Peninsula (cf. Fig. 1a) and shared between Albania and the Former Yugoslav Republic of Macedonia (FYROM). The lake is 30 km long, 15 km wide, covers an area of 358 km^2, and is situated at an altitude of 693 m above sea level (a.s.l.). The lake basin has a simple tub-like shape with a volume of 55.4 km^3 and a maximum water depth of 293 m (Lindhorst et al., 2015). The lake is oligotrophic today due to the large water volume and the low nutrient availability (Wagner et al., 2010), and has a specific conductivity of ca. 200 μScm^{-1} and a pH of around 8.4 (Matter et al., 2010) in the surface waters. The hydrological characteristics are mainly controlled by a relatively low water input of 37.9 m^3s^{-1}, of which ~50% derives from karst aquifers (Matzinger et al., 2006a, b). The natural catchment area is relatively small with 1042 km^2 (Matzinger et al., 2006b; Wagner et al., 2008). Lake Ohrid is situated within the Lake Ohrid Basin, which is a 40 km

long N–S trending graben structure in the Dinarides-Albanides-Hellenides mountain belt. The basin formation was initiated during a late phase of Alpine orogeny in the Miocene as a pull-apart basin in a short transtensional phase and consequently widened by an E-W extensional phase since the Pliocene (Lindhorst et al., 2015). The exact age of the formation of the lake is still unknown and subject of several studies within the SCOPSCO project.

In the N and NE of the basin Palaeozoic metamorphic rocks crop out, which are superimposed by Triassic to Early Jurassic karstified platform carbonates (cf. Fig. 1b) in the E, NW and at the up to 2300 m a.s.l. high Galičica Mountains in the SE (Robertson and Shallo, 2000). Jurassic ophiolites and Tertian conglomerates form the Mocra Mountains of the SW part of the graben shoulder (Robertson and Shallo, 2000). Mesozoic intrusions of rhyolites and diabases are locally preserved in between the limestones and dolomites in the NE (Hoffmann et al., 2010). The plains in the N and S of Lake Ohrid are covered with lacustrine and alluvial plain sediments of Quaternary age (Watzin et al., 2002). The occurrence of a hydrothermal field near Kosel in the north of the Lake Ohrid Basin is most likely fault related since no hints for volcanic activity in younger times have been found during detailed field mapping (Reicherter et al., 2011).

3 Materials and methods

During the ICDP deep drilling campaign at Lake Ohrid in spring 2013 six parallel holes were drilled at the main drill site, the DEEP site (cf. Fig. 1b), down to a maximum sediment depth of 569 m below lake floor (b.l.f.). The coring location (40 m distance between the individual holes) can be averaged to 41°02’57” N and 20°42’54” E with a water depth of 243 m.

The cores of the DEEP site sequence were opened lengthwise, visually described, and subsequently scanned by X-ray fluorescence with an ITRAX core scanner (Cr- tube, 30mA 30 kV, COX Ltd, Sweden) at the University of Cologne. Based on the core description and the XRF data the uppermost 247.8 mcd of the DEEP site sequence were correlated to a composite profile (Francke et al., 2016). The core halves were visually screened for conspicuous horizons showing changes in macroscopic grain size or colour to identify potential tephra layers. Smear slides of these horizons were then checked for the occurrence of glass shards and micro-pumices using a Leitz DM EP polarization microscope. Once a tephra layer was identified, bulk samples were taken from the respective horizon and embedded in epoxy resin. The epoxy pucks were polished to avoid compositional variations due to topographic effects and carbon-coated to enable conductivity during the following SEM and EDS/WDS-analysis. A first screening of major element compositions of single glass shards and micro-pumice was done using a SEM

Philips XL30 equipped with an energy dispersive spectroscope (EDS) EDAX DX4. Operating conditions were adjusted at 20 kV accelerating energy, 200–500 nm beam diameter, 9–10 A beam current, 100 s live time with 2100–2400 shots per second, and ZAF correction (Z: atomic number; A: absorption; and F: fluorescence). The initial calibration, using four reference standards (albite, olivine and the glasses CFA47 and KE12), and the performance of the machine are described in detail by Marianelli and Sbrana (1998). In order to obtain more accurate quantitative analysis and to enlarge the comparability/reproducibility with existing datasets, a second screening of the samples was performed using the more common wavelength dispersive spectrometer (WDS) technique at the Istituto di Geologia Ambientale e Geoingegneria of the Italian National Research Council (IGAG-CNR, Rome). A Cameca SX50 electron microprobe equipped with a five wavelength dispersive spectrometer was set to the following operating conditions: 15 kV; beam current, 15 nA; beam diameter, 10–15 mm; and counting time 20 s per element. Wollastonite (Si and Ca), corundum (Al), diopside (Mg), andradite (Fe), rutile (Ti), orthoclase (K), jadeite (Na), phlogopite (F), potassium chloride (Cl), baritina (S), and metals (Mn) were used as standards. Titanium contents were corrected for the overlap of the Ti and K peaks. Two international secondary standards (Kanui augite and rhyolite RLS132 glasses, from the United States Geological Survey) were analysed prior sample measurements to evaluate the accuracy of the analyses. The mean analytical precision was < 1% for SiO_2 and up to 1, 5, 15, 30, and > 50% for all the elements in concentration range of 15-30, 5-15, 1-5, 1-0.3, and < 0.3 wt %, respectively. All geochemical compositions were recalculated as being 100% water-free. The geochemically classification of the composition of shards and micro-pumice was done with the total alkali vs. silica (TAS) diagram (Le Bas et al., 1986). Identified tephra layers are labelled unambiguously with the site name (OH-DP for Ohrid-DEEP) and the correlated bottom depth of each layer (e.g. “OH-DP-corr. depth in dm”).

4 Results and Discussion

The uppermost 247.8 mcd of sediments from the DEEP site sequence mainly consist of fine-grained hemipelagic sediments with some intercalated coarse-grained beds, which were classified as event layer such as tephra and mass movement deposits. A detailed lithological description and the discussion of sedimentological processes and paleoenvironmental information is given by Francke et al. (2016). Interglacial sediments indicate high amounts of calcite and organic matter, whereas glacial sediments are dominated by clastic, terrigenous components.

In total, 34 macroscopic tephra layers were recognized in the upper 247.8 mcd of the DEEP site sequence (Fig. 2). 12 out of the 34 macroscopic tephra and one cryptotephra horizon have been unambiguously correlated with known eruptions of Italian volcanoes and represent the focus of the present paper. A detailed geochemical description and interpretation of the remaining tephra layers, which are not all analysed yet, and a discussion of potential ages and origins will be given elsewhere, as it is beyond the scope of this paper.

A local origin of the tephra layers from the direct surrounding of Lake Ohrid is highly unlikely, as there is no volcanic activity recorded for the Quaternary (cf. Fig.1). Potential volcanic sources within the Mediterranean area are the Italian provinces, the Hellenic Arc, or the Anatolian provinces. Pyroclastic deposits from the Hellenic Arc and the Anatolian provinces, mainly high-silica calc-alkaline tephra, were primarily dispersed in eastern directions (Druitt et al., 1995, 1999; Aksu et al., 2008; Hamann et al., 2010; Sulpizio et al., 2013; Sumita and Schmincke, 2013; Keller et al., 2014; Tomlinson et al., 2015), and so far have not been found in the sediment records of Lake Ohrid (Sulpizio et al., 2010) and nearby Lake Prespa (Damaschke et al., 2013). Furthermore, they were not found in the numerous studied tephrochronological successions from the Tyrrhenian, Adriatic, or Western Ionian Sea.

Mainly eastern distribution is also assumed for Italian tephra layers, and some of them were even found in the Eastern Mediterranean and Aegean Sea (Margari et al., 2007; Sulpizio et al., 2010; Karkanas et al., 2015; Satow et al., 2015). All tephra layers discussed here show an alkaline affinity, which is only known from the Italian volcanic provinces in the Mediterranean region (Peccerillo, 2005). The existing records from lakes Ohrid and Prespa only contain tephra from Italian volcanoes, which was transported by the prevailing westerlies with E–SE directions in the upper atmospheric wind system. The Quaternary Italian volcanism is classified in several magmatic provinces (Washington, 1906; Peccerillo, 2005), which are mainly located along the Tyrrhenian coast of the Italian Peninsula, in the Tyrrhenian Sea, and in the Sicily channel, between 500 and 1000 km apart of Lake Ohrid (Fig. 1). In the studied succession (< 637 ka) explosive volcanic activity of Italian volcanoes is known so far from the Roman province (Vulsini, Vico, Sabatini, Colli Albani), the Ernici-Roccamonfina area (Mt. Ernici, Roccamonfina), the Campania province (Somma-Vesuvio, Campi Flegrei, Procida, Ischia), the Pontine Islands (Ventotene, Santo Stefano), the Mount Vulture, the Aeolian Arc (Alicudi, Filicudi, Salina, Lipari, Vulcano, Panarea, Stromboli)), and the Sicily province (Mt. Etna, Ustica, Pantelleria,Fig. 1, Peccerillo, 2005). The products of these Italian volcanoes span a wide

compositional field ranging from subalkaline to alkaline and from mafic to silicic, depending on their geodynamic setting or mantle source (Lustrino et al., 2011). Most of them have a potassium or a high potassium affinity (Roman, Roccamonfina, Campanian, and Pontine Islands) and their large chemical similarity or overlap in composition makes tephrostratigraphic work very challenging (Sulpizio et al., 2010). An origin from one of these provinces is supposed by the (high) alkaline phonolitic and trachytic compositions of most of the tephra layers found in the DEEP site sequence. However, some of the tephra layers in the DEEP site succession show more specific and unique compositions, which allow more straightforward correlations to the Pantelleria Islands and Somma-Vesuvius (Peccerillo, 2005), or the silica undersaturated, low evolved pyroclastic products of Colli Albani (Giaccio et al., 2013a).

4.1 OH-DP-0027/Mercato

Cryptotephra OH-DP-0027 was recognized by correlating the patterns of the XRF potassium curve of the DEEP site record with those of the nearby core Co1262 (cf. Fig. 1, Wagner et al., 2012). In both cores, a potassium peak is observed in the same stratigraphic position, which in core Co1262 is caused by the presence of glass shards of cryptotephra Co1262-709. In the DEEP site sequence, the corresponding peak culminates at about 2.775 mcd. A microscopic inspection of the interval 2.770-2.780 mcd revealed the occurrence of glass shards. Since cryptotephra is dispersed in the sediment and do not form a continuous distinct horizons, the exact depth of the tephra isochron was set to the maximum of the K-peak (2.775 mcd), most likely representing the maximum shard concentration.

The discovered volcanic particles of OH-DP-0027 are highly vesicular micro-pumices having spherical or elongated vesicles and glass shards with thick septa or a platy shape. The composition of OH-DP-0027 is Na-phonolitic (Table 1, Figure 2a) and thus similar to cryptotephra Co1262-709 (Wagner et al., 2012) and the associated cryptotephra horizons OT0702-3 from Lake Ohrid (Vogel et al., 2010) and PT0915-2 from Lake Prespa (Damaschke et al., 2013). The geochemical composition (cf. Table 1, Suppl. I Fig. a), and the stratigraphic position of OH-DP-0027 suggest a correlation with the aforementioned cryptotephra horizons and their supposed origin, the Pomici di Mercato (PdM) eruption from the Somma-Vesuvius volcano. The PdM eruption is the only known eruption in the Late Pleistocene and early Holocene having such a composition in the central Mediterranean region (Mele et al., 2010; Santacroce et al., 2008).

The products of the PdM eruption are found as two distinct layers TM6a and TM6b in the Lago Grande di Monticchio record (Wulf et al., 2004). The double layer were interpreted as due to shortly interrupted eruptive phases of the eruption (Mele et al., 2011). OH-DP-0027 and the associated Ohrid cryptotephra horizons match better with TM6b (Table 1), which represents the main Plinian and initial phase of the eruption (Wulf et al., 2004). A correlation with the PdM eruption is also established for a tephra found in the Veliko Jezero on the Island of Mljet (Croatia), where even more than two eruptive phases are indicated (Jahns and van den Bogaard, 1998). Also in sediment cores from the Adriatic Sea, such as KET8218 (V1, Paterne et al., 1988), IN68-9, IN68-5 and RF95-11 (125, 259, 320 cm respectively, Calanchi and Dinelli, 2008), AD91-17 (190-191, 195-196 cm, Marchini et al., 2014), or from MD90-918 (210/223 cm, Caron et al., 2012) tephra layers were correlated with the PdM eruption (cf. Suppl. I Figure a).

Santacroce et al. (2008) reviewed several existing ^{14}C ages on proximal deposits of the Mercato eruption and suggested a maximum age of 9010–8750 year cal BP. This age is somewhat younger than the varve age obtained from the Lago Grande di Monticchio record for TM6b (9680±480 year BP; Wulf et al., 2004). The most reliable age of 8630-8430 year cal BP comes probably from ^{14}C dating of charcoals collected at the basal part of the proximal fallout deposit (Zanchetta et al., 2011).

4.2 OH-DP-0115 / Y-3

Tephra layer OH-DP-0115 (11.492–11.507 mcd) is 1.5 cm thick, brownish-greyish in colour and has sharp upper and lower boundaries. OH-DP-0115 comprises both highly vesicular micro-pumices with elongated vesicles and bubble-wall and -junction glass shards. The glass composition is mainly trachytic tending towards the phonolitic field in the TAS-diagram (Fig. 3b, Table 1), which suggests a correlation with the prominent marine tephra layer Y-3 from the Campanian area (cf. Table 1, Suppl. I Fig. b; Keller et al., 1978; Albert et al., 2015). The slightly heterogeneous major element composition, with a low and a high silica end-member (</> 62 wt.% SiO_2) is defined by Albert et al. (2015) as the diagnostic characteristic of the Y-3 tephra and perfectly matches the OH-DP-0115 tephra (cf. Fig.3b, Tab. 1, Suppl. I Fig. b). The most probable source of the Y-3 tephra is the Campi Flegrei (CF) caldera (Di Vito et al., 2008; Zanchetta et al., 2008; Albert et al., 2015), but to date none of the suggested proximal counterparts of different eruptions could be unambiguously assigned as its origin (Albert et al., 2015). Furthermore, the former most accepted correlation of the Y-3 tephra with the

intracaldera VRa and the mid-distal SMP1e/CE1 deposits (Sulpizio et al., 2003; Di Vito et al., 2008) is rejected, because new geochemical data gained on the Y-3 type locality (marine cores M25/4-12, RC9 191) separate the Y-3 from other CF eruptions of the Tufi Biancastri/NYT series (Tomlinson et al., 2012; Albert et al., 2015).

The Y-3 tephra is known as a widespread stratigraphic marker found in different archives in the Central and Eastern Mediterranean region, such as the Lago Grande di Monticchio (TM15, Wulf et al., 2004; Tomlinson et al., 2012), the Southern Adriatic Sea core MD90-917 (920/17, Zanchetta et al., 2008), Lake Ohrid (OT0520-2; OT0700-1; OT0702-4; JO 187, summarized in Sulpizio et al., 2010), Lake Prespa (PT0915-5, Damaschke et al., 2013), and the Tenaghi Philippon peat record in Greece (TP 9.70, Albert et al., 2015). These correlations are validated by the low and high silica end-member (Albert et al., 2015). The correlations of the marine tephra layers C-7 (Tyrrhenian and Adriatic Sea, Paterne et al., 1988), A2/B2 (C106/C45, Munno and Petrosino, 2004), and the terrestrial S19 layer (Munno and Petrosino, 2007) with the Y-3 tephra were not revaluated by Albert et al. (2015) due to restricted data sets, but seem to be likely.

Since no proximal equivalents could be unambiguously identified so far, the ages from these proximal correlations (e.g., 31–30 ka cal BP, Zanchetta et al., 2008) have to be rejected (Albert et al., 2015). However, a Bayesian age-depth model based on multiple radiocarbon ages above and below the TP 9.70 tephra of the Tenaghi Phillipon record provides an age of 28.68-29.42 ka cal BP (Albert et al., 2015). This is probably the best age estimate, which is supported by radiocarbon ages from other distal archives, for example the ^{14}C-age of 28.78-29.98 ka cal BP obtained at the top of the Ohrid tephra OT07042-4/Y-3 (Vogel et al., 2010). The Y-3 tephra represents an important marker in the Mediterranean area, linking marine and terrestrial archives close to the Marine Isotope Stage 3/2 transition and the North Atlantic Heinrich Stadial 3 (HS3).

4.3 OH-DP-0169 / Y-5 CI

Tephra OH-DP-0169 (16.783–16.933 mcd) has a thickness of 15 cm, which is the thickest tephra layer found within this part of the DEEP site sequence and can be visually separated into two units. The lower unit (OH-DP-0169a) has a sharp boundary at the bottom, is 2 cm thick and pale yellow in colour, whereas the upper unit (OH-DP-0169b) is 13 cm of pale brown, coarser material. The uppermost centimetres of the upper unit are mixed with lacustrine

sediments and have an uneven top boundary, which is probably due to a difficult penetration during coring. Both units comprise elongated vesicle bearing micro-pumices, bubble-wall and -junction shards with thick septa, and have the same trachytic to phono-trachytic glass composition (Fig. 3c, Table 1). The characteristic trachytic to phonotrachytic alkaline composition of OH-DP-0169 (cf. Fig.3c, Suppl. I Fig. c) and its remarkable thickness allow an unambiguous correlation with the Campanian Ignimbrite (CI) eruption (Orsi et al., 1996; Civetta et al., 1997; Pappalardo et al., 2002) and the marine tephra layer Y-5 (Keller et al., 1978; Thunell et al., 1979). The comparison of major element oxides such as Al_2O_3, FeO_{TOT}, and CaO strongly support the correlation with the Y-5/CI deposits and exclude other possible correlation with pre-CI deposits described in Tomlinson et al., 2012 (cf. Suppl. I Fig. c). Additionally, the CI/Y-5 was also recognized in previous studies at lakes Ohrid and Prespa (OT0520-3; OT0700-2; OT0701-1; OT0702-6; JO-244; PT0704-3 summarized in Sulpizio et al., 2010).

The proximal deposits of the CI are described to have a trimodal composition, which resulted from the different timing and dynamic of extraction and mingling of two layered compositionally different magmas (Civetta et al., 1997; Pappalardo et al., 2002; Marianelli et al., 2006). According to Civetta et al. (1997), OH-DP-0169 belongs to the most evolved composition (K_2O/N_2O 1.1-1.35) and only some shards can be assigned to the intermediate group (K_2O/N_2O 1.37-1.42, cf. Suppl. II). The third, least evolved group (K_2O/Na_2O >2) was not found in OH-DP-0169 most likely due to its relatively low abundance in distal settings and the limited number of analysis of OH-DP-0169. Indeed, the least-evolved group is associated with the less energetic phase of the eruption of the late caldera collapse that generated more dense pyroclastic flows that did not reach great distance from the vent (Civetta et al., 1997). Thus, they are likely less representative in very distal settings also because the intermediate and most evolved group form more than 85 % of the eruptive volume (Civetta et al., 1997).

As the two optical units of OH-DP-0169 (a+b) cannot be geochemically discriminated based on major elements, the initial Plinian phase (cf. Marianelli et al., 2006) may correspond with the lower, pale yellow and more fine-grained part (OH-DP-0169a), while the main ignimbrite phase probably corresponds with the upper, pale brown and coarser part (OH-DP-0169b).

The CI/Y-5 tephra layer, originating from the Campi Flegrei (e.g. Pappalardo et al., 2002), is the most widely dispersed tephra marker in the Mediterranean region. It was found, for example, in sediment cores from the Lago Grande di Monticchio (TM-18, Wulf et al., 2004),

the San Gregorio Magno basin, (S-17, Munno and Petrosino, 2007) the Greek island of Lesvos (ML 2, Margari et al., 2007), and the Tenaghi Philippon peat record (TP-CI, Lowe et al., 2012). Furthermore, it was identified in the Tyrrhenian Ses cores KET- 8022, -8004, -8003, -8011 (C-13, Paterne et al., 1988; Ton-That et al., 2001), in the Adriatic Sea cores PRAD1-2 (PRAD1653, Bourne et al., 2010) and KET8218 (C-13, Paterne et al., 1988), in the Ionian Sea cores KC01B (I-3, Insinga et al. 2014) and RC9 191/V110 69 (Y-5, Keller et al. 1978), and in the Levantine and Aegean Sea cores (RC 9 183, -181, V10 58 (Y-5) Keller et al., 1978; LC21 (4.925) Lowe et al., 2012, Satow et al., 2015). To date, the most distal finding is in the Russian Plain, 2500 km away from its source (Pyle et al., 2006; Giaccio et al., 2008).

The ages for the CI cluster around 40 ka BP. The varve chronology of Lago Grande di Monticchio yielded an age of 36.77 ka BP (Wulf et al., 2006). $^{40}Ar/^{39}Ar$ dating on single sanidine crystals revealed ages of 37.1±0.4 ka(Deino et al., 1994), 41.1±2.1 ka (Ton-That et al. (2001) and 39.28±0.11 ka (De Vivo et al., 2001), with the latter regarded as the best age, as it derives from proximal deposits.

4.4 OH-DP-0404 / TM24a POP2

Tephra layer OH-DP-0404 (40.456–40.486 mcd) is a 3 cm thick dark reddish brown horizon with sharp stratigraphic contacts at the top and bottom. The layer comprises elongated vesicular micro-pumices and thick walled bubble-wall shards. Glass composition analyses reveal a mainly phonolitic composition with some shards scattering around the intersection of tephriphonolitic, trachyandesitic, and trachytic fields in the TAS-diagram (Fig. 3d, Table 1) The geochemical signature is similar, even if somewhat more variable, to tephra OT-0702-8 (cf. Fig.3d, Suppl. I Fig. d), found in Ohrid core Co1202 (Vogel et al., 2010), which is correlated with the Monticchio tephra TM24a (Wulf et al., 2004; Wulf et al., 2012). The TM24a tephra was first correlated with the prominent marine X-5 layer (Keller et al., 1978), but this correlation was later revised and the older Monticchio tephra TM25 was correlated with the X-5 layer (Wulf et al., 2012). The proximal or the marine tephra counterparts of TM24a remain unknown so far. Based on major element compositions, OH-DP-0404 can be further correlated with the recently found POP2 tephra in the Popoli section from the Sulmona basin (Regattieri et al., 2015), which is also correlated with the TM24a tephra (cf. Table1, Suppl. I Fig. d). A correlation of OH-DP-0404 with marine tephra layers from core CM92-42 (710 cm) and core RF93-77 (797 cm), which were also correlated with the TM24 (Calanchi and Dinelli, 2008), is likely, however, there is no differentiation between the bifurcation of tephra TM24 (a+b) in

these marine tephra layers. According to the Monticchio varve record, TM24a has an age of 101.8±5 ka BP (Wulf et al., 2012), which matches well the age of 102.0±2.4 ka obtained from the age-model of the Sulmona basin (Regattieri et al., 2015).

4.5 OH-DP-0435 / X-6

Tephra OH-DP-0435 (43.498–43.513 mcd) is a 1.5 cm thick, greyish brown layer with sharp top and bottom contacts. The horizon comprises highly vesicular micro-pumices and bubble wall shards with thick septa having a low alkali ratio (LAR) trachytic glass composition with only few shards plotting in the phonolitic field. This geochemical composition and the position below OH-DP-0404/TM24a/POP2 suggest a correlation of OH-DP-0435 with the marine tephra layer X-6 (core 22M-60, Keller et al., 1978). The correlation is supported by the geochemically similarity of OH-DP-0435 with the Ohrid tephra layers OT0702-9 (Vogel et al., 2010) and JO-575 (Caron et al., 2010), which were also correlated with the X-6 layer (cf. Fig.3e; Suppl. I Fig. e). Equivalents of the X-6 tephra are also found in marine cores KET8004 and -8022 of the Tyrrhenian Sea (C-31, Paterne et al., 2008), the Adriatic Sea cores PRAD1-2 (PRAD-2812, Bourne et al., 2015), and the Ionian Sea cores KC01B (I-9, Insinga et al., 2014), and KET82-22 (C-31, Paterne et al., 2008). Furthermore, the X-6 is known from the terrestrial records of the Lago Grande di Monticchio (TM27, Wulf et al., 2012), the San Gregorio Magno basin (S10, Munno and Petrosino, 2007), the Cilento coastline (SM1-2/SA, Marciano et al., 2008; CIL2, Giaccio et al., 2012), and the Popoli section of the Sulmona basin (POP4, Regattieri et al., 2015). The origin of the X-6 is assigned to an unknown eruption of the Campanian area (Keller et al., 1978; Paterne et al., 2008; Wulf et al., 2012).

Based on $^{40}Ar/^{39}Ar$ dating, the age of tephra layer X-6 is 107±2 ka (Kraml, 1997), which fits to the varve-based age of ca. 108.3±5.4 ka BP of the TM-27 layer in Lago Grande di Monticchio (Wulf et al., 2012) and the interpolated age of 107 ka of the C-31 tephra layer (Paterne et al., 2008). More recently, a $^{40}Ar/^{39}Ar$ age of 108.9±1.8 ka was obtained on X-6 equivalent deposits of the Cilento offshore area (t1 tephra, Iorio et al., 2014), which matches well the interpolated age of the Popoli section (109.0±1.5 ka, Regattieri et al., 2015).

4.6 OH-DP-0499 / P-11

The OH-DP-0499 (49.937–49.947 mcd) tephra layer is 1 cm thick, olive brown, and characterised by a sharp bottom and a diffuse top boundary. It comprises elongated vesicular

micro-pumices and larger platy bubble wall shards. OH-DP-0499 has a distinct bimodal glass chemical composition, with a clearly separated trachytic and a rhyolitic group (Fig. 3f, Table 1). The shards can be classified as comendites and pantellerites (cf. Al_2O_3-FeO_{TOT} diagram, Fig.4), which unambiguously assign them to an origin from the Pantelleria Island, the only source of these type of magmas in the central Mediterranean region (Peccerillo, 2005). The twofold composition is explained by a chemically zoned magma chamber, in which peralkaline rocks originating from mantle-derived parental magma and trachytic magma differentiated in a low-pressure magma chamber by crystal-liquid fractionation (Civetta et al., 1984).

The stratigraphic position of OH-DP-0499, below the X-6 tephra (OH-DP-0435), infers a definite correlation with the P-11 tephra (cf. Fig. 3f) found in the Ionian Sea core KET82-22 (Paterne et al., 2008), since other widespread eruptions of the Pantelleria Island are much younger (ca. 77 ka, P-10, Paterne et al., 2008; 45.7 ka, Green Tuff, Scaillet et al., 2013). Furthermore, the geochemical fingerprint of OH-DP-0499 is identical to those of the two cryptotephra layers OT0702-10 (Vogel et al., 2010) and JO-941 (Caron et al., 2010), which were found previously in Lake Ohrid sediments and correlated with the P-11 (cf. Suppl. I Fig. f). A more proximal core from the Sicily Channel (ODP 963A) comprises three pantelleritic layers (ODP2-4) in a similar stratigraphic position (Tamburrino et al., 2012). ODP2 shows a somewhat different geochemical composition (benmoritic part) compared to OH-DP-0499/P-11 (cf. Table1, Suppl. I Fig. f). ODP3 and ODP4 indicate a very similar composition, but ODP3 is formed as a distinct horizon, whereas ODP4 is a cryptotephra (Tamburrino et al., 2012). Due to chronological concerns, Tamburrino et al. (2012) correlated ODP3 with the P-11, which is supported by their climastratographic position at the transition from MIS 6 to 5 (cf. Zanchetta et al., this issue). As only one pantelleritic layer is found in distal archives, ODP2 was precluded due to chemical considerations, ODP4 is a cryptotephra, a correlation of ODP3 with the P-11 layer is the most likely and supposes that this tephra is the most widespread.

OH-DP-0499 can be further correlated with the ML5 tephra found on Lesovs Island (Margari et al., 2007), as already suggested by Vogel et al. (2010) for the OT0702-10 tephra. The ML5 tephra was previously correlated with the younger Green Tuff/Y-6, but the geochemical data support a correlation with the older P-11 tephra. In more recent studies, Karkanas et al. (2015) correlated a pantelleritic cryptotephra (THP-TII5) found in the Theopetra cave in central Greece with the P-11 and its equivalents. Satow et al. (2015) found a cryptotephra (LC21 10.345) in the Aegean Sea core LC21, which he ascribed to one of the ODP2-4 tephra layers. The position

of LC21 10.345 in the *G. ruber* $\delta^{18}O$ record of LC21 implies a correlation with ODP3 and P-11 based on the position in the respective isotope records. Nevertheless, it has to be stated that only the rhyolitic endmember of P-11 was found in the records from LC21 and Theopetra. The typical comenditic trachytic part is not found in these archives, which is probably due to a different dispersal of the twofold zonation of the magma chamber (rhyolitic/trachytic part) tapped at different phases of the eruption. This is also indicated by an internal zonation of the OPD3 layer. Whereas the bottom of ODP3 has a pantelleritic composition, its top shows comenditic trachytic compositions (Tamburrino et al., 2012). This suggests that the rhyolitic pantelleritic part was erupted first and dispersed over a larger area, while the comenditic trachytic part is distributed only in a smaller, northern sector. Changes of the plume direction and dispersal during an eruption are likely due to changes in the aerodynamic characteristics of the erupted material or in the high and low atmosphere dynamics (Sulpizio et al., 2008, 2013).

Proximal counterparts of the P-11 are the ignimbrite deposits of the P-unit on Pantelleria Island (Mahood and Hildreth, 1986; Paterne et al., 2008; Tamburrino et al., 2012). These proximal P-unit deposits provide inhomogeneous $^{40}Ar/^{39}Ar$ ages between 123±1.6 ka and 135±1.2 ka, with large internal age variations suggesting xenocrystic contamination (Rotolo et al., 2013). The mean age of the P-unit (129±5.9 ka) is in broad accordance with the non-radiometric ages from the distal deposits. The age-depth model of core KET82-22, based on orbital tuning of the oxygen isotope and sapropel stratigraphy, provided an age of 130.6±5 ka for the P-11 tephra (Paterne et al., 2008). This age matches well the age of 128.1 ka of ODP3, which is inferred from correlation of benthic and planktonic foraminifera $\delta^{18}O$ curves of core ODP-963A with the SPECMAP stack curve (Incarbona et al., 2008; Tamburrino et al., 2012). The correlation of LC21 10.345 with P-11 provides an age of 133.5±2 ka, based on the correlation of the surface-water foraminiferal $\delta^{18}O$ record of LC21 to the high resolution U/Th dated Soreq Cave $\delta^{18}O$ record (Grant et al., 2012, Satow et al., 2015).

4.7 OH-DP-0617 / Vico "Ignimbrite B"

The tephra layer OH-DP-0617 (61.701–61.726 mcd) is a yellowish brown, 2.5 cm thick deposit with sharp bottom and top contacts. The very fine-grained glass shards have various forms, being highly vesicular with circular and oval bubbles. Micropumices with elongated vesicles are rare. The characteristic homogenous phonolitic composition of OH-DP-0617 (Fig. 3f, Table 1) is very similar to the composition of tephra OT0701-6 (cf. Fig. 5a), which was found in the Ohrid core Co1201 (Sulpizio et al., 2010). OT0701-6 was previously correlated with the marine

tephra C-20 and the proximal deposits of the SA3-b eruption from the Campanian area (Sulpizio et al., 2010). However, the stratigraphic position of OH-DP-0617 below the X-6/C-31/OH-DP-0435 and P-11/OH-DP-0499 tephra suggests that and OH-DP-0617 and OT0706-1 rather correlate with the CF-V4 tephra from the Campo Felice Basin (Giraudi et al., 2011). The CF-V4 tephra is correlated with the "Ignimbrite B" of the Vico volcano (Vico B, Ronciglione Formation, Bear et al., 2009), which also has a large geochemical similarity to the Ohrid tephra layers OH-DP-0617/OT0701-6 (cf. Table 1, Fig. 5a). So far, equivalents of this Vico eruption were not found in other archives. Laurenzi and Villa (1987) $^{40}Ar/^{39}Ar$ dated the Ignimbrite B in a proximal setting to 157±3 ka.

4.8 OH-DP-0624 / CF-V5/ PRAD3225

Tephra OH-DP-0624 (62.367–62.413 mcd) is 4.6 cm thick, of olive brown colour, and has a sharp bottom and more diffuse top transition. It comprises micro-pumices with elongated vesicles, cuspate glass shards, and non-vesicular, blocky, porphyric particles, bearing prismatic microlites and phenocrysts. In the uppermost diffuse part, volcanic fragments are mixed with authigenic siderite crystals. The glass composition spans from the phonotephritic to the phonolitic field of the TAS-diagram (Fig. 3g, Table 1). This characteristic is also observed for tephra OT0701-7 in core Co1201 from Lake Ohrid (Sulpizio et al., 2010). OT0701-7 was first subdivided into three different chemical groups (a-b-c), of which OT0701-7b tentatively was correlated with the tephra layer OT0702-8/TM24a/X-5 (Sulpizio et al., 2010). However, this correlation is not supported by the stratigraphic position of OT0701-7 below OT0701-6, as the latter correlates well with OH-DP-0617. Furthermore, OT0702-8/TM24a is correlated with OH-DP-0404, which is embedded by sediments of interglacial MIS5, whereas glacial sediments encompass OT0701-7 (Sulpizio et al., 2010). Also the glass composition of OT0701-7, showing a linear geochemical trend rather than two different geochemical populations, makes a correlation with OH-DP-0624 more likely (Fig. 5b).

The peculiar geochemical trend of OH-DP-0624 (cf. Fig. 3g, Fig. 5b) matches the marine tephra PRAD3225 from the Adriatic Sea (Bourne et al., 2015), which is tentatively correlated with the tephra 322 from core RF95-7 and with the TM38 tephra from the Lago Grande di Monticchio record (Wulf et al., 2012). Tephra 322 was assigned to the Vico D eruption (Calanchi and Dinelli, 2008), which is dated to ca. 138 ka (Laurenzi and Villa, 1987). TM38 has an age of 125.6±6.3 ka according to the varve chronology of the Lago Grande di Monticchio record (Wulf et al., 2012). However, the ages of TM38 and 322/Vico D are significantly too young for the

stratigraphic position of OH-DP-0624 below the OH-DP-0617/Vico B and dated to ca. 157±3 ka. Another marine counterpart of OH-DP-0624 could be tephra C-42 with its phonotephritic composition (core DED8708, Paterne et al., 2008), but the published average values do not allow a robust correlation.

The most reliable equivalent of OH-DP-6024/OT0701-7/PRAD3225 is probably found in the Campo Felice basin in the Apennine chain. The geochemical composition and the stratigraphic position of the CF-V5 tephra, which was found in this basin directly below the CF-V4 tephra (Giraudi and Giaccio, 2015) correlates well with the composition and stratigraphic position of the OH-DP-6024 directly below the OH-DP-0617 tephra. Giraudi and Giaccio (2015) tentatively suggest that the CF-V5 tephra is an equivalent of the Pitigliano Tuff from the Latera caldera in the Vulsini volcanic complex (Turbeville, 1992a). Although the geochemical dataset is limited, a similar characteristic trend is observed in CF-V5 and OH-DP-0624/OT071-7/PRAD3225 (cf. Fig. 5b). $^{40}Ar/^{39}Ar$ dating on proximal deposits of the Pitigliano Tuff provided ages of 158±11 ka and 155±11 ka (Turbeville, 1992b, a) and the overlying Vico Ignimbrite B tephra limits the minimum age to 157±3 ka.

4.9 OH-DP-1817 / Pozzolane Rosse

Tephra layer OH-DP-1817 (181.744–181.769 mcd) is a dark brownish layer with a thickness of 2.5 cm and sharp bottom and top contacts. The layer contains mostly non-vesicular, blocky porphyric shards with a high content of microlites and phenocrysts, mostly leucite. Vesicular cuspate shards are rare and are also porphyritic. OH-DP-1817 has a low evolved K-foiditic composition (Fig. 3h, Table 1), which is only known from the Italian volcanoes of the Colli Albani volcanic district, and more sporadically in Vulture volcano (Peccerillo, 2005). However, as the activity of the Vulture volcano clustered between ~740 to 610 ka and around 140 ka (Villa and Buettner, 2009), the most relevant source of foiditic tephra is the Colli Albani caldera, of which the Middle Pleistocene explosive activity was characterized by very high-energetic events (e.g., Marra et al., 2009). The most widespread Colli Albani tephra is from the Pozzolane Rosse eruption (Giaccio et al., 2013a) of the Tuscalano-Aretemsio phase (~560-360 ka; Marra et al., 2011).

A direct chemical correlation of OH-DP-1817 with proximal Pozzolane Rosse pyroclasts is difficult, because of the lack of a comprehensive geochemical dataset. Marra et al. (2009) describe the proximal type localities (within the Colli Albani volcanic district) of the Pozzolane

Rosse pyroclastic products, but only the mean value of one geochemical analysis is published (AH-20-PRa). Another, more comprehensive data set for the composition of the proximal Pozzolane Rosse pyroclastics was provided by Freda et al. (2010), who however reported only the composition of the basal sub-Plinian fallout. Therefore, the correlation OH-DP-1817/Pozzolane Rosse (cf. Fig. 3h, 5c, Suppl. I Fig. g) is mainly based on the major element data of the $^{40}Ar/^{39}Ar$ dated distal equivalents of the Pozzolane Rosse units, which occur diffusely in the fluvial-lacustrine successions of the Apennine intermountain basins of Paganica-San Demetrio-Castelnuovo and Sulmona, east of Colli Albani (Galli et al., 2010; Giaccio et al., 2013a). Giaccio et al. (2013a) separates the Pozzolane Rosse distal equivalents into two sublayers, which differ chemically and morphologically. OH-DP-1817 matches both compositions of the less evolved composition (group a) of the lower layer and the more evolved composition (group b) of the upper sublayer (cf. Fig. 3h). Besides the geochemical correlation, microtextural features, such as the scoria character (dense, few vesicles) of the shards and the huge number of juvenile crystals, suggest the components of the lower sub-layer prevail in OH-DP-1817. Giaccio et al. (2013a) correlate the lower sublayer (group a) to the proximal Pozzolane Rosse basal fallout and the upper sublayer to the phoenix cloud of the main pyroclastic flow-forming phase. According to Freda et al. (2011), the Pozzolane Rosse eruption sequence encompasses from bottom to top the Vallerano lava flow, the main Pozzolane Rosse pyroclastic units (basal fallout and main pyroclastic flow unit) and the scoria lapilli fallout deposits. Recently, the products of the Pozzolane Rosse eruption were also found in the Campo Felice basin (layer CF-V11) where it marks the local glacier advancement of the MIS 12 glacial (Giraudi and Giaccio, 2015). Pronounced glacial conditions are also recorded in the lacustrine sediments across the Pozzolene Rosse of the Sulmona basin (Regattieri et al., 2016).

The age of the Pozzolane Rosse eruption is well constrained by several $^{40}Ar/^{39}Ar$-ages. The pyroclastic products are dated to 457±4 ka at a proximal site (Karner et al., 2001), which is confirmed by the distal equivalent found in the Sulmona Basin (457±2 ka, Giaccio et al., 2013a). These ages are further supported by $^{40}Ar/^{39}Ar$-ages of 457±5 ka from a lava flow below and of 442±2 ka from a relatively thin succession of fallout deposits on top (Marra et al., 2009).

4.10 OH-DP-1955 / SC5

The tephra layer OH-DP-1955 (195.536–195.566 mcd) is 3 cm thick and has a sharp bottom and a diffuse top boundary. The greyish layer comprises blocky, non-vesicular glass shards and porphyric micro-pumices containing leucite crystals. The composition is mainly phonolitic to

trachy-andesitic with some shards plotting in the tephri-phonolitic field (Fig. 3h, Table 1). According to the stratigraphic position, OH-DP-1955 was deposited prior to ca. 460 ka, since it is found below OH-DP-1817/Pozzolane Rosse (457±2 ka). Proximal deposits of the active volcanoes in Italy older than 450 ka are only barely explored. From the more distal archives, the tephra layer SC5 from the Mercure Basin (Giaccio et al., 2014) shows a trachytic-andesitic to phonolitic trend similar to that of OH-DP-1955 (cf. Fig. 3h). Oxide plots (cf. Fig 6a, Suppl. I Fig. h) of major element clarify that this composition shows a linear magmatic trend and the occurrence of two different populations of tephra can be ruled out. Investigated sources for OH-DP-1955 and its potential equivalent SC5 are very limited. Sr-isotope ratios of tephra layer SC5 reveal an origin from the Roccamonfina volcano (Giaccio et al., 2014). $^{40}Ar/^{39}Ar$ dating provided an age of 493.1±10.9 ka for the SC5 tephra (Giaccio et al., 2014), which thus represents a poorly known eruption from the Roccamonfina volcano attributable to the Rio Rava stage dated between ~600 and 439 ka (Rouchon et al., 2008). Despite a similar age, a potential correlation of OH-DP-1955 with Fall B (490±4 ka) from the Tufi Terrosi con Pomici Bianche eruptive cycle (TTPB, 499±3-490±4 ka) of the Sabatini volcanic field (Sottili et al., 2004; Marra et al., 2014) is unlikely. The composition of the Fall B deposits is somehow different, having e.g. lower FeO_{TOT} (~1.1 wt.%), and CaO (1.5 wt%.) but higher K_2O (3.4 wt.%) contents (cf. Fig. 6a, Table 1).

4.11 OH-DP-2010 / Fall A

OH-DP-2010 (201.034–201.049 mcd) is a reddish-brown, 1.5 cm thick layer with a sharp lower and an undulated upper boundary. It comprises morphological different volcanic fragments, which range from non-vesicular, microlite-bearing blocky, glass shards, to medium vesicular cuspate glass shards, and elongated vesicular micropumices. The tephri-phonolitic to phonolitic composition of tephra OH-DP-2010 (Fig. 3i, Table 1) and its characteristic high potassium content suggest an origin from the Roman province. The low Cl content of OH-DP-2010 (cf. Table 1) is typical for Middle Pleistocene Sabatini products (Giaccio et al., 2014; Palladino et al., 2014) and supports an origin from the TTPB eruptive cycle of the Sabatini volcanic district (Sottili et al., 2004; Marra et al., 2014). The major element composition and the stratigraphic position suggest that OH-DP-2010 correlates with the proximal and distal products of the oldest eruptive unit Fall A (cf. Fig. 3i; Fig. 6b). The reddish colour of OH-DP-2010 can be attributed to the reddish, terracotta-like, thermally metamorphosed clay lithics, which are a diagnostic characteristic of the proximal Fall A deposits (Sottili et al., 2004). However, the proximal

deposits of Fall A apparently show a smaller compositional range (cf. Marra et al., 2014) than OH-DP-2010 and other distal archives, such as the Mercure Basin (SC3) and the Sulmona Basin (SUL 5-1c), whose correlation is corroborated by Sr-isotope analyses (Giaccio et al., 2014). Similar major element composition (cf. Table 1, Fig. 6b) suppose also a correlation of OH-DP-2010/Fall A with the Acerno tephra A9 (Petrosino et al., 2014b) and FIC-12.9 from Ficoncella site (Aureli et al., 2015).

Sottili et al. (2004) describe a bifurcation of the Fall A at the type section Isola Farnese at the Sabatini volcanic district with a lower sublayer A1 and an upper sublayer A2 both comprising alternating layers of white pumice and grey scoria clasts. Whereas the white pumices of these eruptive units are more evolved and trachy-phonolitic, the grey scoria clasts have a phono-tephritic to tephri-phonolitic composition (Marra et al., 2014). The reason for the wider compositional spectrum of distal Fall A deposits (e.g. OH-DP-2010, SC3) could be the lack of data for the less evolved, upper grey pumices of the proximal zoned Fall A. A correlation of the older Grottarossa Pyroclastic Sequence (GPRS, Karner et al., 2001) of the Sabatini volcano (Marra et al., 2014) with the chemically similar and less evolved part of OH-DP-2010 can be excluded, since the GPRS and Fall A are temporally well distinct events, as testified by field (Sottili et al., 2004) and $^{40}Ar/^{39}Ar$ chronological evidence (Marra et al., 2014).

According to $^{40}Ar/^{39}Ar$ dating, the lower Fall A1 has an age of 499±3 ka and the upper Fall A2 has an age of 496±3 ka (Marra et al., 2014). However, unpublished age–depth interpolations from distal equivalents reveal slightly older ages, with 510±3 ka for SC3 at the Mercure Basin, and with 502±4 ka for the A9 at the Acerno Basin.

4.12 OH-DP-2017 / A11/A12

Tephra layer OH-DP-2017 (201.747–201.782 mcd) is whitish to yellowish, 3.5 cm thick, and has sharp bottom and top boundaries. The horizon contains highly vesicular cuspate glass shards with a varying morphology and septa thickness. The homogenous trachytic composition of OH-DP-2017 (Fig. 3j, Table 1) excludes an origin from Roman and Roccamonfina provinces, which mainly produced phonolites and tephro-phonolites during the Middle Pleistocene (cf. Giaccio et al., 2014). However, two very similar trachytic layers (A11/A12) are found in the Acerno Basin sequence (Petrosino et al., 2014b). They have a similar stratigraphic position and a similar glass chemical composition (cf. Fig. 3j+6c, Table 1) compared with OH-DP-2017 (Petrosino et al., 2014b). An unambiguous correlation of OH-DP-2017 with one of the both layers is not

possible due to their indistinguishable major element composition (Table 1). Tephra SC2 from the Sulmona Basin was tentatively also correlated based on chemical affinities and its stratigraphic position with the A11/A12 (Giaccio et al., 2014). However, differences in the composition (higher FeO_{TOT}, SiO_2) do not support an unambiguous correlation of SC2 with OH-DP-2017 or A11/12 (cf. Fig 6c) and suggest that they may derive from the same source, but from different eruptions.

According to the geochemical characteristics, an origin of A11/12 from the Campanian area was proposed (Petrosino et al., 2014b). Proximal products of the Campanian area date back to ca. 290 ka only (Seiano Ignimbrite, Rolandi et al., 2003). Distal deposits, such as found in the Montalbano Jonico succession (around 720 ka, V5, V7, Petrosino et al., 2014c) and the Sulmona Basin (ca. 723 ka, SC1-35.30/SUL2-1, Giaccio et al., 2013b), suggest also older activity of the Campanian area, which may have produced OH-DP-2017/A11/A12. Although Sr-isotope ratios indicate that tephra layer SC2 originate from the Ponza Island, the lack of Middle Pleistocene pyroclastic rocks on Ponza Island contradicts this correlation and an origin of SC2 from the Campanian area appears more likely (Giaccio et al., 2014).

Sanidine crystals of the Acerno tephra A11 yielded a $^{40}Ar/^{39}Ar$ age of 514±5.6 ka (Petrosino et al., 2014b). As A12 is located only 12 cm below A11, which amounts to an age difference of a few hundred years according to the sedimentation rate between the two tephra (Petrosino et al., 2014b), the difference in age is negligible and the age of 514±5.6 ka can be transferred from the A11 to OH-DP-2017 tephra.

4.13 OH-DP-2060 / Tufo di Bagni Albule

Tephra OH-DP-2060 (206.060–206.080 mcd) is a 2 cm thick, brownish-greyish tephra layer with a sharp bottom and a more diffuse upper boundary. The layer comprises mainly non-vesicular, porphyritic (leucite and sanidine), blocky glass shards. Furthermore, numerous diatoms and weathered calcite were found during microscope analysis. The characteristic K-foiditic composition (Fig. 3j, Table 1) suggests an origin from the Colli Albani volcanic district. According to the stratigraphic position of OH-DP-2060 with a presumed age older than 510 ka, it can be assigned to the Tufo del Palatino-Tufo di Bagni Albule eruptive cycle of the Colli Albani volcanic district (Karner et al., 2001; Giaccio et al., 2013a). Glass composition data are only published for the upper pyroclastic flow Tufo di Bagni Albule (TBA or Tufo di Acque Albule), which is separated by a paleosol from the lower Tufo del Palatino (TP) ignimbrite

(Marra et al., 2009). A geochemical comparison of the TBA with the proximal data of the Via Tiburtina section AH-23 (within the Colli Albani volcanic district, Marra et al., 2009) and the distal equivalent found in the Sulmona Basin (SUL1-6 site 2, Giaccio et al., 2013a) reveals a good correlation with OH-DP-2060 (cf. Table 1, Fig. 6d). A relatively thick, foiditic tephra with Tufo del Palatino-Tufo di Bagni Albule products was also found in a core from the Fucino basin in the Apennine chain (Giaccio et al., 2013a). In the Intra-Apennine Carsoli Basin, a chemically very similar deposit, the so-called the Oricola tuff was found (Stoppa et al., 2005) and later correlated with TBA from the Colli Albani volcanic district based on chronological, isotopic, and major element composition affinities (Giaccio et al., 2013a). The carbonate content of the Oricola tuff (Peccerillo, 2005; Stoppa et al., 2005), which is also noticed in OH-DP-2060, is typical for Colli Albani products, because the magma chambers are situated in Mesozoic limestones (Giordano et al., 2006). TP and TBA in proximal deposits indicate geochronologically indistinguishable ages of 530±2 and 527±2 ka (Marra et al., 2009), which are in a good agreement with the age obtained for the Oricola tuff (ca. 531 ka, Bosi et al., 1991). As long as no compositional glass data is available for the TP, the TBA is the most likely equivalent of OH-DP-2060 and an age of 527±2 ka can be assumed for this tephra.

4.14 Reassessing and homogenizing the age of the DEEP site tephra layers

The obtained tephrochronological information from the dated equivalents of the DEEP site tephra layers were used to develop a robust chronology for the DEEP site proxy series, for both the sediment core and the borehole successions (cf. Baumgarten et al., 2015; Francke et al., 2016). For this purpose, 11 out of the presented 13 tephra layers were selected based on the strength of correlation and their geochronological reliability. Except for the Y-3, TM24a/POP2, and P-11 tephra, all ages are radiometric ages, whereas the ages of these three tephra layers were taken from the respective age-depth models. The high number of ^{14}C ages above and below the Y-3 equivalent of the Tenaghi Philippon record (Albert et al. 2015) allow a reliable age interpolation, similar to the POP2 tephra from the Sulmona basin, where tephra layers above and below are precisely $^{40}Ar/^{39}Ar$ dated (Regattieri et al., 2015). The only available $^{40}Ar/^{39}Ar$ ages of the P-11 tephra scatter between 123±1.6 ka and 135±1.2 ka. Currently, the most reliable age of P-11 is likely that obtained from the age-depth model of core LC21, which is tuned to the extensively U/Th-dated Soreq Cave speleothem record (Satow et al., 2015; Zanchetta et al., 2015).

In order to achieve a homogenous set of ages, all $^{40}Ar/^{39}Ar$ ages have been recalculated relative to the same flux standard and the total ^{40}K decay constant of Steiger and Jäger (1977). Since the flux standards Fish Canyon sanidine (FCs) and Alder Creek sanidine (ACs-2) are intercalibrated, all ages were recalculated to an age of 1.194 Ma for ACs, which corresponds to FCs at 28.02 Ma (Nomade et al., 2005). This choice was made because most of the published ages were calculated using these two flux standards. However, several calibrations of the $^{40}Ar/^{39}Ar$ chronometer are currently in use, which yield ages that can vary by ~1% in the time range of the Pleistocene (e.g. Kuiper et al., 2008; Renne et al., 2010; Phillips and Matchan, 2013). As long as it is not the purpose of this work to decipher, which calibration is the more accurate and that the implied difference in calibrated age is within the current reported fully propagated uncertainties at 2σ level, we decided to keep ages as they were published without necessarily endorsing the flux standards values used. The results are indicated in Table 2.

The age obtained from the suggested correlation OH-DP-0624/CF-V5 with the Pitigliano Tuff was recalculated, but not included in the age model, as the tephrostratigraphical correlation is not very robust (cf. discussion OH-DP-0624) and the 2σ error bar is relatively large (Table 2). Furthermore, the age of the directly overlying tephra OH-DP-0617/Vico B represents a more reliable tie-point in this part of the sequence. The original/recalculated age of Fall A 499/496±3 ka was not selected as a first order tie point for the age-depth model shown in Francke et al. (2016), because of the age-depth interpolations of the Acerno Basin and the Mercure Basin: They suggest an older age for distal Fall A, making the published age for the proximal Fall A questionable.

In order to obtain a first overview of the chronology of the DEEP site sequence, an age-depth plot (Fig. 7) with all tephrochronological information was created. The homogenous distribution of ages vs. depth suggests a relatively constant sedimentation rate of the DEEP site succession for the upper 247.8 m. As shown in Fig. 7, the unreliability of the $^{40}Ar/^{39}Ar$ age of Fall A at 496±3 ka becomes more obvious. The tephra OH-DP-1955/SC5 dated to 493±11 ka is located 5.48 m above OH-DP-2010/Fall A, whilst the OH-DP-2017/A11 dated to 514±6 ka is located only 0.73 m below this layer. Accepting an age of 496±3 ka for Fall A would imply a distinct change in the sedimentation rates, with interpolated sedimentation rates of 1.8 m ka^{-1} above and 0.04 m ka^{-1} below, which differ substantially from a mean sedimentation rate of 0.39 m ka^{-1} for the entire sequence. However, there is no lithological evidence justifying such a conspicuous change in sedimentation rate. The radiometric dating of Fall A was done on

deposits from Cava Rinaldi, which were correlated with Fall A only using trace element ratios (Zr/Y vs. Nb/Y plot) and chronological constraints, because the deposits have been too altered to use major element compositions (Marra et al., 2014). Although this method is helpful to distinguish between the different Italian provinces and between the different volcanic districts (Marra et al., 2011; Marra et al., 2014), it may be not suitable to distinguish between single eruptions, with similar composition. Moreover, the intense alteration of the deposits makes an unequivocal correlation difficult and the obtained age for Fall A is probably too young. Following the correlation of OH-DP-2010 with distal deposits of the SC3 in the Mercure and the A9 in the Acerno basin, an age of between 502 and 510 ka seems to be more likely and would be consistent with more constant sedimentation rates in the DEEP site record.

4.15 Resulting tephrostratigraphy of the Lake Ohrid record

The Middle Pleistocene Italian tephrostratigraphic framework was extended for the first time beyond Italy to the Balkan region. The 13 identified tephra layers (OH-DP-0027-2060) of the DEEP sequence link the Lake Ohrid record with numerous terrestrial and marine records of the Mediterranean region (Fig. 8) at least back to MIS13. Since the last 160 kyrs are recorded in many archives, tephra layers found in Lake Ohrid of this period were also found in numerous other records and give a dense framework of tie points for this period. However, for the period between MIS 7 and MIS 11, no correlations could be established for the Lake Ohrid sequence so far, but at least 13 tephra layers between OH-DP-0624 (>160 ka) and OH-DP-1817 (<450 ka) indicate activity and widespread eruptions of Italian volcanoes. On the other hand, Lake Ohrid provides a very long and continuous record of stratigraphically ordered Middle Pleistocene tephra, which represents a reference section for other discontinuous and short successions in which the stratigraphic order of tephra is unknown or not well constrained. In spite of this potential, tephrostratigraphic and volcanologic implications based on the lower part of the record below P-11 are premature, because the succession is not fully analysed and more detailed investigations are needed to complete and improve the tephrostratigraphic framework. Even still at this preliminary stage of the study, the recognition of tephra layers from volcanic provinces, which were thought to be poorly active or even inactive at the time of tephra deposition, such as the ca. 490 ka old OH-DP-1955/SC5 tephra from the Roccamonfina volcano, or the ca. 510 ka old OH-DP-2017/A11/12 tephra from the Campanian Volcanic Zone, provide insights for exploring and improve our knowledge about volcanic activity of the

different provinces. Furthermore, their widespread distribution to the Balkan suggests that some of them were rather large magnitude eruptions and represent widespread marker horizons.

The connection to different records within the Mediterranean region also reveals the possibility to review different distribution patterns of specific eruptions, which probably will change substantially in the light of the Lake Ohorid data (e.g. OH-DP-0499/P-11/THP-TII-5). Moreover, this established tephrostratigraphic framework can be used as a powerful tool for the synchronization of different archives in order to address at very fine temporal and stratigraphic resolution relevant paleoclimate and paleoenvironmental issues (cf. Zanchetta et al., 2015).

5 Conclusions

The results of the first tephrostratigraphic study of the DEEP site succession from Lake Ohrid allowed us to recognize 34 macroscopic tephra, 12 out of which and one cryptotephra, all originating from the Italian volcanism, were correlated with their proximal or distal counterparts. Tephra layers found in the previous studies have been re-identified and were utilized as helpful markers for setting up the uppermost part of the new tephrostratigraphy of the DEEP site record. In the light of the longer tephra succession presented in this paper, the previously established correlations have been either confirmed or, in some cases, revised (e.g. OH-DP-0617/OT0701-6 and OH-DP-0624/OT0701-7). Furthermore, tephrostratigraphy was successfully applied for the succession older than the already inspected 135 ka of Lake Ohrid's history. On the whole, the following correlations are here proposed: OH-DP-0027/Mercato tephra (8.43-8.63 ka cal BP), OH-DP-0115/Y-3 (28.68-29.42 ka cal BP), OH-DP-0169/Y-5 (39.6±0.1 ka), OH-DP-0404/TM24a/POP2 (102±2.4 ka), OH-DP- 0435/X-6 (109±2 ka), OH-DP-0499/P-11 (133.5±2 ka), OH-DP-0617/Vico "Ignimbrite B" (162±6 ka), OH-DP-0624/CF-V5/Pitigliano Tuff (163±22 ka), OH-DP-1817/Pozzolane Rosse (457±2 ka), OH-DP-1955/SC5 (493.1±10.9 ka), OH-DP-2010/Fall A (496±3 ka), OH-DP-2017/A11/12 (511±6 ka), and OH-DP-2060/Tufo di Bagni Albule (527±2 ka).

The ages of 11 of the correlated tephra layers were used to contribute first order tie points to develop a robust age-depth model of the uppermost 247.8 mcd of the DEEP succession, which is a fundamental pillar for the development of the different multi-proxy paleoclimatic-environmental and evolutionary studies, which are in progress. Furthermore, this age-depth model has the potential to refine our chronological knowledge of some relevant marker tephra found in the Lake Ohrid succession (e.g. Fall A), and to provide a first chronological framework for a number of currently poorly known tephra, which, however, can be potentially found

elsewhere and thus indirectly dated by simple geochemical fingerprinting. In this perspective, the data presented in this paper provide a further important step forward for extending back in time, and well beyond the current chronological limit, a robust and reliable Middle Pleistocene tephrostratigraphy in central Mediterranean area.

Appendix A: Supplementary Material

Supplemenent I: Harker diagrams of established correlations of the Ohrid tephra layers OH-DP-0027-1955.

Supplement II: Full data set of WDS-analysis of Ohrid tephra layers OH-DP-0027-2060

Acknowledgements

The SCOPSCO Lake Ohrid drilling campaign was funded by ICDP, the German Ministry of Higher Education and Research, the German Research Foundation, the University of Cologne, the British Geological Survey, the INGV and CNR (both Italy), and the governments of the republics of Macedonia (FYROM) and Albania. Logistic support was provided by the Hydrobiological Institute in Ohrid. Drilling was carried out by Drilling, Observation and Sampling of the Earth's Continental Crust's (DOSECC) and using the Deep Lake Drilling System (DLDS). Special thanks are due to Beau Marshall and the drilling team. Ali Skinner and Martin Melles provided immense help and advice during logistic preparation and the drilling operation.

Table 1. Average major element glass composition (normalised to 100 %) of investigated tephra layers OH-DP-0027–OH-DP-2060 of the DEEP site sequence, the discussed correlations, and the standards used for evaluation of the accuracy of the analyses. All data of the Ohrid tephra layers were obtained using an electron microprobe outfitted with WDS. The "Total" is given as analytical total, and the tephra layers printed in italic are not correlated with the respective Ohrid tephra and are discussed only. The full dataset of OH-DP-0027–OH-DP-2060 is given in the Supplement II.

		SiO_2	TiO_2	Al_2O_3	FeO_{TOT}	MnO	MgO	CaO	Na_2O	K_2O	P_2O_5	F	Cl	SO_3	Total	Tot. Alkali	Alk. Ratio
OH-DP-0027	$\bar{x}$	59.29	0.17	20.70	2.19	0.18	0.19	2.33	8.10	6.81	0.03	0.67	0.59	0.06	97.49	14.91	0.84
n=15	*s*	1.12	0.06	0.88	0.94	0.07	0.37	1.31	0.38	0.63	0.02	0.13	0.06	0.03	1.75	0.91	0.06
OT0702-3	$\bar{x}$	59.10	0.17	21.58	1.95	0.17	0.16	1.76	7.56	7.02	-	-	0.52	-	100.00	14.58	0.93
n=9	*s*	0.51	0.08	0.12	0.11	0.06	0.09	0.13	0.53	0.26	-	-	0.03	-	-	0.66	0.07
Co1262-709	$\bar{x}$	58.59	0.17	21.81	1.84	0.16	0.12	1.67	8.20	6.94	0.00	-	0.51	-	100	15.14	0.85

n=12		*s*	0.39	0.08	0.49	0.12	0.06	0.08	0.22	0.50	0.29	0.00	-	0.03	-	-	0.36	0.08
PT0915-2		x̄	58.34	0.18	21.59	1.92	0.15	0.24	1.97	7.93	6.85	0.09	-	0.73	-	100.00	14.79	0.87
n=10		*s*	0.30	0.05	0.38	0.12	0.06	0.10	0.42	0.24	0.18	0.18	-	0.06	-	-	0.33	0.03
TM-6a		*x̄*	*59.98*	*0.30*	*20.61*	*2.24*	*0.13*	*0.16*	*2.42*	*5.58*	*8.02*	*0.08*	*0.08*	*0.51*	-	*97.67*	*13.60*	*1.51*
n=13		*s*	*0.93*	*0.09*	*0.51*	*0.46*	*0.04*	*0.07*	*0.39*	*1.03*	*0.82*	*0.12*	*0.00*	*0.15*	-	*0.91*	*0.57*	*0.38*
TM-6b		x̄	58.71	0.16	21.10	1.99	0.19	0.15	2.11	8.14	6.82	0.13	0.10	0.49	-	98.21	14.96	0.88
n=12		*s*	1.53	0.09	0.83	1.00	0.07	0.26	1.19	1.11	0.88	0.20	0.09	0.18	-	1.27	0.97	0.31
MJ1/VJ1		x̄	58.76	0.21	21.03	1.85	0.19	0.12	2.41	7.38	7.12	-	0.30	0.57	0.06	98.12	14.51	0.96
n=27		*s*	1.42	0.11	0.81	0.81	0.08	0.21	1.24	0.73	0.85	-	0.18	0.21	0.04	0.88	1.51	0.07
KET8218 V1		x̄	60.04	0.10	21.49	1.74	0.00	0.00	1.82	7.72	7.05	-	-			99.96	14.77	0.91
n=n.a.		*s*	-	-	-	-	-	-	-	-	-	-	-	-	-	-	-	-
IN68-9 125cm		x̄	59.50	0.09	21.26	1.71	0.11	0.14	1.81	7.72	7.14	-	-	0.52	-	93.40	93.40	0.92
n=20		*s*	0.78	0.02	0.34	0.17	0.06	0.12	0.43	0.57	0.62	-	-	0.08	-	3.53	3.53	0.11
IN68-5 259cm		x̄	58.81	0.09	21.21	1.79	0.12	0.10	1.75	8.18	7.40	-	-	0.55	-	95.54	15.58	0.91
n=15		*s*	0.36	0.03	0.15	0.10	0.06	0.07	0.09	0.37	0.13	-	-	0.04	-	1.82	0.33	0.05
RF95-11 320cm		x̄	59.10	0.11	20.60	1.89	0.13	0.08	1.88	7.58	8.13	-	-	0.50	-	95.94	15.71	1.08
n=21		*s*	0.76	0.05	0.26	0.30	0.06	0.05	0.36	0.67	0.45	-	-	0.12	-	1.64	0.84	0.11
RF95-11 320cm		x̄	61.43	0.27	18.46	2.95	0.12	0.32	1.97	5.29	8.52	-	-	0.67	-	94.95	13.81	1.65
n=3		*s*	0.56	0.06	0.09	0.24	0.07	0.28	0.19	0.83	0.94	-	-	0.21	-	1.18	0.40	0.24
MD90-918 210cm		x̄	58.71	0.14	21.82	1.78	0.17	0.17	1.74	8.06	6.80	-	-	0.60	-	-	14.86	0.85
n=9		*s*	0.47	0.08	0.23	0.11	0.10	0.06	0.16	0.35	0.15	-	-	0.11	-	-	0.38	0.04
MD90-918 223cm		x̄	58.82	0.12	21.88	1.72	0.13	0.11	1.81	8.27	6.60	-	-	0.53	-	100.00	14.88	0.80
n=12		*s*	0.61	0.10	0.28	0.15	0.12	0.06	0.53	0.37	0.81	-	-	0.09	-	-	1.00	0.10
AD94-17 190-191 cm		x̄	58.69	0.14	21.97	1.70	0.14	0.26	1.72	8.17	6.73	-	-	0.49	-	100.00	14.90	0.82
n=14		*s*	0.74	0.11	0.21	0.16	0.09	0.09	0.34	0.43	0.47	-	-	0.09	-	-	0.79	0.05
AD94-17 195-196cm		x̄	58.51	0.13	22.13	1.73	0.15	0.43	1.68	8.13	6.65	-	-	0.51	-	100.00	14.78	0.83
n=10		*s*	0.31	0.07	0.32	0.15	0.09	0.09	0.21	0.79	0.45	-	-	0.06	-	-	0.38	0.15
OH-DP-0115		x̄	61.60	0.38	18.24	3.43	0.12	0.70	2.67	3.43	9.32	0.10	0.14	0.46	0.11	95.49	12.76	2.77
n=16		*s*	0.89	0.03	0.17	0.32	0.05	0.16	0.32	0.44	0.44	0.04	0.09	0.10	0.06	1.98	0.15	0.45
OT0702-4		x̄	61.27	0.39	18.70	3.11	0.11	0.67	2.35	3.73	9.22	-	-	0.46	-	100.00	12.96	2.52
n=12		*s*	0.61	0.05	0.12	0.20	0.06	0.17	0.24	0.44	0.46	-	-	0.10	-	-	0.11	0.42
OT0520-2		x̄	61.88	0.29	18.63	2.92	0.03	0.50	2.20	4.18	8.82	-	-	0.54	-	100.00	12.99	2.15
n=12		*s*	0.50	0.08	0.18	0.22	0.06	0.15	0.18	0.45	0.49	-	-	0.13	-	-	0.09	0.35
JO187		x̄	60.99	0.40	18.74	3.26	0.11	0.68	2.38	3.59	9.43	-	-	0.42	-	100.00	13.02	2.68
n=10		*s*	0.71	0.10	0.10	0.26	0.07	0.15	0.25	0.48	0.41	-	-	0.09	-	-	0.28	0.46
OT0700-1		x̄	61.60	0.38	18.74	3.03	0.10	0.67	2.30	3.74	8.94	-	-	0.50	-	100.00	12.68	2.44
n=12		*s*	0.75	0.10	0.15	0.34	0.09	0.16	0.30	0.44	0.43	-	-	0.13	-	-	0.24	0.39
PT0915-5		x̄	60.85	0.40	18.92	3.40	0.11	0.79	2.37	3.60	8.94	0.01	-	0.62	-	100.00	12.54	2.57
n=12		*s*	0.87	0.08	0.27	0.37	0.07	0.19	0.30	0.58	0.56	0.03	-	0.19	-	-	0.27	0.56
M25/4-12	Y-3	x̄	61.32	0.37	18.27	3.23	0.12	0.62	2.42	3.64	9.41	0.11	-	0.50	-	96.22	13.04	2.69
n=33		*s*	0.89	0.03	0.26	0.34	0.05	0.19	0.26	0.62	0.69	0.04	-	0.18	-	1.35	0.17	0.61
RC9 191	Y-3	x̄	62.76	0.36	18.21	2.98	0.17	0.25	2.07	4.44	8.75	-	-	-	-	-	-	-
n=n.a.		*s*	0.36	0.03	0.16	0.21	0.12	0.12	0.15	0.19	0.26	-	-	-	-	-	-	-

TM-15	x̄	62.22	0.38	18.36	3.27	0.13	0.61	2.19	3.85	8.36	0.12	-	0.52	-	96.32	12.21	2.21
n=20	*s*	0.76	0.03	0.20	0.29	0.04	0.14	0.22	0.43	0.54	0.06	-	0.10	-	0.46	0.21	0.36
TP-9.70	x̄	61.79	0.37	18.28	3.17	0.10	0.59	2.40	3.78	9.19	0.12	-	0.54	-	96.46	12.97	2.48
n=42	*s*	0.78	0.04	0.17	0.31	0.04	0.14	0.22	0.47	0.47	0.04	-	0.12	-	1.42	0.19	0.41
S-19	x̄	62.17	0.31	18.77	2.96	0.08	0.49	2.13	4.20	8.90	-	-	-	-	100.01	13.10	2.12
n=n.a.	*s*	1.15	0.07	0.14	0.47	0.04	0.26	0.29	0.38	0.50	-	-	-	-	-	-	-
C106 A2	x̄	62.63	0.34	18.24	3.15	0.15	0.47	2.12	4.15	8.75	-	-	-	-	100.00	12.90	2.11
n=12	*s*	0.20	0.06	0.12	0.12	0.08	0.08	0.10	0.19	0.14	-	-	-	-	-	-	-
C45 B2	x̄	62.41	0.33	18.30	3.17	0.15	0.50	2.13	4.30	8.71	-	-	-	-	100.00	13.01	2.03
n=11	*s*	0.32	0.10	0.29	0.10	0.08	0.09	0.10	0.15	0.08	-	-	-	-	-	-	-
MD90-917 920–17	x̄	61.41	0.37	18.72	3.17	0.08	0.70	2.44	3.52	9.14	-	-	0.44	-	100.00	12.66	2.60
n=n.a.	*s*	0.86	0.10	0.17	0.38	0.08	0.21	0.33	0.40	0.40	-	-	0.09	-	-	-	-
KET8004 C-7	x̄	63.12	0.25	18.53	3.03	0.00	0.14	2.17	3.86	8.86	-	-	-	-	99.96	12.72	2.30
n=n.a.	*s*	0.90	0.08	0.21	0.39	0.00	0.13	0.33	0.52	0.42	-	-	-	-	-	-	-
KET8011 C-7	x̄	61.90	0.33	19.14	2.95	0.00	0.49	2.75	3.62	8.79	-	-	-	-	99.97	12.41	2.43
n=n.a.	*s*	-	-	-	-	-	-	-	-	-	-	-	-	-	-	-	-
OH-DP-0169b	x̄	61.76	0.43	18.86	3.01	0.25	0.36	1.86	5.96	7.47	0.04	0.33	0.83	0.05	97.04	13.43	1.26
n=18	*s*	0.29	0.03	0.15	0.09	0.03	0.02	0.09	0.28	0.19	0.02	0.07	0.07	0.02	1.25	0.29	0.08
OH-DP-0169a	x̄	61.69	0.41	18.89	3.04	0.26	0.34	1.78	6.28	7.28	0.04	0.36	0.85	0.05	98.78	13.56	1.17
n=25	*s*	0.44	0.03	0.14	0.09	0.04	0.02	0.04	0.56	0.15	0.02	0.07	0.04	0.02	1.56	0.57	0.17
OT0700-2	x̄	60.84	0.39	19.21	2.98	0.20	0.42	1.77	6.06	7.45	-	-	0.68	-	100.00	13.51	1.29
n=17	*s*	0.38	0.09	0.18	0.19	0.07	0.12	0.25	0.82	0.72	-	-	0.11	-	-	0.33	0.50
OT05020-3	x̄	61.88	0.29	18.63	2.92	0.03	0.50	2.20	4.18	8.82	-	-	0.54	-	100.00	12.99	2.15
n=12	*s*	0.50	0.08	0.18	0.22	0.06	0.15	0.18	0.45	0.49	-	-	0.13	-	-	0.09	0.37
OT0702-6	x̄	60.83	0.40	19.13	2.93	0.18	0.48	1.77	6.31	7.34	-	-	0.65	-	100.00	13.65	1.17
n=11	*s*	0.30	0.10	0.11	0.13	0.09	0.08	0.20	0.44	0.25	-	-	0.10	-	-	0.31	0.13
JO-244	x̄	60.64	0.42	19.18	2.96	0.21	0.40	1.81	6.22	7.48	-	-	0.69	-	100.00	13.69	1.21
n=18	*s*	0.57	0.08	0.24	0.16	0.05	0.12	0.21	0.36	0.31	-	-	0.10	-	-	0.20	0.13
OT0701-1/5	x̄	60.92	0.41	19.15	3.02	0.20	0.44	1.80	5.87	7.57	-	-	0.64	-	100.00	13.44	1.37
n=41	*s*	0.64	0.07	0.69	0.18	0.07	0.14	0.30	1.12	0.97	-	-	0.14	-	-	0.38	0.69
PT0704-3	x̄	60.83	0.42	19.14	3.03	0.23	0.47	1.77	5.86	7.59	-	-	0.65	-	100.00	13.46	1.53
n=105	*s*	0.58	0.09	0.23	0.26	0.09	0.16	0.32	1.01	0.82	-	-	0.13	-	-	0.42	0.69
RC9 191 Y-5	x̄	61.56	0.44	18.90	3.59	0.17	0.59	1.97	5.55	7.26	-	-	-	-	96.48	12.80	1.31
V10 58 Y-5	*s*	62.46	0.36	18.43	2.11	0.16	0.40	2.16	6.33	7.59	-	-	-	-	93.52	13.92	1.20
C-13	x̄	62.20	0.35	19.30	2.94	0.08	1.75	5.92	7.41	-	-	-	-	-	99.95	13.33	1.25
C-13	*s*	61.50	0.31	19.15	3.13	0.33	2.50	3.54	9.50	-	-	-	-	-	99.96	13.04	2.68
PRAD 1653	x̄	61.00	0.43	19.71	2.93	0.24	0.28	1.68	6.72	7.01	-	-	-	-	95.89	13.73	1.04
n=14	*s*	0.49	0.04	0.11	0.29	0.04	0.03	0.07	0.20	0.12	-	-	-	-	0.87	0.27	0.03
I-3	x̄	61.45	0.41	18.40	3.12	0.19	0.54	2.16	4.88	7.84	0.09	0.26	0.65	-	97.01	12.84	1.72
n=14	*s*	1.14	0.05	0.43	0.43	0.06	0.24	0.56	0.94	0.97	0.06	0.11	0.21	-	2.48	0.47	0.63
Lc 21 4.925	x̄	61.93	0.46	18.03	3.20	0.21	0.44	2.05	6.20	7.46	-	-	-	-	95.35	13.66	1.25
n=32	*s*	0.74	0.10	0.25	0.47	0.08	0.36	0.70	0.94	0.48	-	-	-	-	1.33	0.93	0.30
TM18	x̄	61.60	0.43	18.92	2.93	0.24	0.35	1.75	5.78	7.04	0.05	0.33	0.79	-	98.64	12.82	1.24

n=61	*s*	0.46	0.03	0.36	0.11	0.03	0.07	0.16	0.75	0.53	0.02	0.04	0.08	-	1.71	0.83	0.25
ML2	x̄	61.01	0.48	18.18	3.02	0.21	0.44	2.12	5.64	8.05	-	0.07	0.71	-	96.51	13.70	1.57
n=105	*s*	0.42	0.04	0.19	0.21	0.06	0.15	0.32	1.20	1.02	-	0.04	0.20	-	1.46	0.32	0.69
S-17	x̄	61.67	0.33	19.18	2.90	0.22	0.27	1.60	6.42	7.38	-	-	-	-	100.00	13.80	1.15
n=n.a.	*s*	0.22	0.14	0.10	0.10	0.10	0.08	0.11	0.30	0.20	-	-	-	-	-	0.50	-
Tenaghi Phlippon CI	x̄	63.29	0.40	19.42	3.32	0.20	0.45	2.09	5.20	8.48	0.10	-	-	-	96.42	13.69	1.99
n=3	*s*	0.39	0.03	0.28	0.26	0.06	0.20	0.47	1.69	1.27	0.06	-	-	-	0.88	0.46	1.13
pre CI deposits	x̄	*58.94*	*0.40*	*19.75*	*3.45*	*0.25*	*0.34*	*2.04*	*6.46*	*7.58*	-	-	*0.79*	-	*97.76*	*14.04*	*1.19*
n=68	*s*	*0.38*	*0.02*	*0.16*	*0.14*	*0.03*	*0.04*	*0.10*	*0.51*	*0.30*	-	-	*0.04*	-	*1.32*	*0.26*	*0.14*
OH-DP-0404	x̄	57.49	0.54	19.05	5.10	0.17	1.30	4.33	4.06	7.72	0.24	0.18	0.50	0.09	97.08	11.78	1.93
n=20	*s*	1.00	0.11	0.45	0.67	0.04	0.24	0.65	0.54	0.62	0.07	0.08	0.09	0.05	1.33	0.93	0.25
OT0702-8	x̄	57.60	0.55	19.49	4.48	0.16	1.22	3.77	4.18	8.09	0.01	-	0.46	-	100.00	12.26	1.94
n=12	*s*	0.46	0.08	0.15	0.33	0.07	0.15	0.32	0.18	0.43	0.02	-	0.05	-	-	0.43	0.15
TM-24a	x̄	57.64	0.49	18.99	4.26	0.14	1.12	3.99	4.24	8.37	0.24	-	0.52	-	100.00	12.61	1.97
n=35	*s*	1.14	0.06	0.19	0.46	0.02	0.22	0.56	0.14	0.31	0.06	-	0.04	-	0.01	0.31	0.11
POP2	x̄	59.71	0.42	18.43	3.79	0.17	0.73	2.94	4.26	8.61	0.09	0.14	0.54	0.15	96.28	12.87	2.02
n=26	*s*	1.10	0.07	0.11	0.62	0.05	0.25	0.57	0.17	0.34	0.05	0.07	0.06	0.06	1.34	0.48	0.07
RF93-77 797cm	x̄	59.41	0.41	19.17	3.69	0.10	0.77	2.84	4.36	8.75	-	-	0.50	-	97.24	13.11	2.01
n=n.a	*s*	0.41	0.08	0.10	0.18	0.07	0.15	0.20	0.36	0.30	-	-	0.07	-	0.81	0.66	-
CM92-42 710cm	x̄	59.19	0.41	19.20	3.74	0.08	0.81	2.99	4.25	8.84	-	-	0.49	-	97.65	13.09	2.08
n=n.a	*s*	0.39	0.07	0.17	0.22	0.05	0.11	0.22	0.30	0.23	-	-	0.07	-	1.46	0.53	-
OH-DP-0435	x̄	61.06	0.45	18.53	3.09	0.30	0.36	1.78	6.12	6.98	0.05	0.37	0.86	0.05	96.82	13.10	1.16
n=22	*s*	0.34	0.04	0.17	0.12	0.10	0.09	0.10	0.52	0.55	0.03	0.13	0.14	0.03	1.60	0.26	0.20
OT0702-9	x̄	61.15	0.46	18.82	3.09	0.29	0.39	1.68	6.39	7.03	-	-	0.71	-	100.00	13.42	1.12
n=15	*s*	0.30	0.06	0.12	0.14	0.09	0.10	0.08	0.62	0.50	-	-	0.14	-	-	0.20	0.20
JO575	x̄	61.20	0.47	18.74	2.97	0.29	0.38	1.65	6.54	7.04	-	-	0.72	-	100.00	13.58	1.09
n=20	*s*	0.43	0.08	0.17	0.15	0.08	0.08	0.11	0.61	0.45	-	-	0.12	-	-	0.32	0.17
22M-60 X-6	x̄	61.45	0.49	18.52	3.80	0.22	0.59	2.06	6.20	6.66	-	-	-	-	94.53	12.86	1.08
n=n.a.	*s*	-	-	-	-	-	-	-	-	-	-	-	-	-	-	-	-
TM27	x̄	61.43	0.46	18.57	2.85	0.23	0.40	1.84	6.32	7.25	0.06	-	0.71	-	97.86	13.57	1.17
n=22	*s*	0.40	0.02	0.09	0.13	0.06	0.08	0.11	0.66	0.50	0.04	-	0.14	-	1.40	0.24	0.19
POP4	x̄	61.49	0.45	18.26	3.08	0.25	0.38	1.77	5.84	7.36	0.04	0.28	0.75	0.05	97.05	13.20	1.28
n=31	*s*	0.42	0.03	0.11	0.11	0.07	0.06	0.08	0.52	0.43	0.02	0.10	0.14	0.03	1.31	0.28	0.17
S-10	x̄	62.38	0.40	18.86	2.81	0.24	0.29	1.61	6.02	7.39	-	-	-	-	-	13.41	1.23
n=n.a.	*s*	-	-	-	-	-	-	-	-	-	-	-	-	-	-	-	-
I-9	x̄	62.00	0.46	18.50	2.99	0.27	0.38	1.71	5.74	6.77	0.06	0.32	0.80	-	96.42	12.51	1.19
n=15	*s*	0.39	0.05	0.24	0.09	0.05	0.04	0.07	0.31	0.30	0.04	0.13	0.10	-	0.83	0.22	0.11
KET8004 DED8708 C-31	x̄	61.80	0.45	18.11	3.16	0.28	0.31	1.76	5.64	7.34	0.02	0.14	1.00	-	-	12.98	1.30
n=n.a.	*s*	0.50	0.09	0.19	0.17	0.11	0.16	0.21	0.54	0.60	0.03	0.08	0.25	-	-	1.14	-
KET8282 C-31	x̄	61.74	0.49	19.19	3.10	-	0.43	1.72	6.03	7.31	-	-	-	-	-	13.34	1.21
n=n.a.	*s*	0.34	0.08	0.11	0.18	-	0.08	0.14	0.71	0.68	-	-	-	-	-	1.39	-

KET8222 C-31	x̄	60.17	0.47	19.45	3.70	-	0.77	2.51	4.03	8.69	-	-	-	-	-	12.72	2.16
n=n.a.	*s*	0.12	0.04	0.04	0.20	-	0.06	0.25	0.55	0.62	-	-	-	-	-	1.17	-
PRAD2812	x̄	62.00	0.46	18.84	2.93	0.24	0.39	1.75	6.10	7.29	-	-	-	-	96.21	13.39	1.22
n=23	*s*	0.24	0.03	0.10	0.11	0.07	0.08	0.08	0.62	0.55	-	-	-	-	0.85	0.15	0.21
C1202 t1	x̄	60.16	0.45	18.36	3.30	0.32	0.31	1.77	7.34	6.60	0.17	0.30	0.91	-	96.82	13.94	1.05
n=20	*s*	0.28	0.12	0.25	0.22	0.11	0.08	0.11	0.21	0.21	0.12	0.18	0.06	-	1.81	0.26	0.03
CIL2	x̄	61.46	0.45	18.37	3.24	0.29	0.45	1.86	5.47	7.19	0.08	0.38	0.72	0.03	96.08	12.66	1.40
n=74	*s*	0.67	0.05	0.34	0.25	0.09	0.19	0.28	0.97	0.97	0.06	0.20	0.23	0.04	1.51	0.42	0.47
SM1	x̄	62.27	0.45	18.19	3.31	0.35	0.35	1.76	5.05	7.82	-	-	0.45	-	95.27	12.87	1.55
n=15	*s*	0.33	0.04	0.25	0.16	0.01	0.14	0.06	0.18	0.35	-	-	0.07	-	-	-	-
SM2	x̄	62.50	0.43	18.37	3.23	0.36	0.40	1.73	5.36	7.31	-	-	0.33	-	96.18	12.66	1.36
n=11	*s*	0.90	0.02	0.18	0.24	0.14	0.20	0.22	0.23	0.50	-	-	0.11	-	-	-	-
SA	x̄	62.21	0.41	18.50	3.34	0.22	0.42	1.80	4.77	7.94	-	-	0.39	-	96.36	12.71	1.66
n=16	*s*	0.24	0.07	0.17	0.09	0.10	0.07	0.09	0.21	0.16	-	-	0.10	-	-	-	-
OH-DP-0499	x̄	65.32	0.69	15.32	6.02	0.28	0.33	1.32	5.68	4.92	0.11	0.08	0.15	0.06	97.13	10.61	0.87
n=11 (trachyte)	*s*	1.06	0.08	0.88	0.31	0.04	0.09	0.25	0.36	0.09	0.04	0.05	0.05	0.02	1.70	0.41	0.05
OH-DP-0499	x̄	73.61	0.36	8.77	7.30	0.34	0.08	0.33	4.72	4.46	0.02	0.29	0.85	0.06	93.33	9.18	0.95
n=32 (pantellerite)	*s*	0.34	0.03	0.21	0.15	0.05	0.02	0.03	0.28	0.09	0.02	0.09	0.07	0.03	1.16	0.28	0.06
LC21 10.345	x̄	73.91	0.39	8.65	7.06	0.30	0.03	0.29	5.01	4.36	-	-	-	-	100.00	9.37	1.06
n=5	*s*	1.62	0.04	0.15	0.24	0.06	0.02	0.02	1.89	0.08	-	-	-	-	-	1.83	0.49
ODP3	x̄	65.05	0.75	15.61	5.66	0.29	0.41	1.43	5.85	4.78	0.15	0.07	0.10	-	96.81	10.64	0.95
n=14 (trachyte)	*s*	0.33	0.04	0.20	0.16	0.04	0.03	0.07	0.31	0.15	0.02	0.04	0.02	-	1.39	0.30	0.06
ODP3	x̄	73.58	0.39	9.40	6.63	0.32	0.10	0.31	4.83	4.43	0.02	0.24	0.68	-	94.78	9.25	1.40
n=4 (pantellerite)	*s*	0.98	0.02	1.21	0.83	0.02	0.05	0.01	0.61	0.11	0.01	0.08	0.17	-	2.21	0.64	0.10
TII5	x̄	75.46	0.38	8.99	7.28	0.22	0.06	0.30	6.24	4.59	-	-	-	-	95.94	10.82	0.74
n=15	*s*	0.57	0.04	0.14	0.28	0.09	0.02	0.03	0.30	0.26	-	-	-	-	0.69	0.31	0.85
ML5	x̄	66.22	0.75	14.33	6.05	0.30	0.27	1.16	5.59	4.99	-	-	-	-	95.86	10.58	0.90
n=6 (trachyte)	*s*	0.93	0.06	0.98	0.43	0.02	0.09	0.24	0.25	0.12	-	-	-	-	1.33	0.15	0.06
ML5	x̄	73.73	0.43	8.31	7.14	0.32	0.08	0.31	4.30	4.44					92.72	8.74	1.04
n=50 (pantellerite)	*s*	0.24	0.01	0.10	0.16	0.02	0.01	0.01	0.24	0.08					0.45	0.24	0.07
OT0702-10	x̄	66.18	0.43	16.23	5.96	0.23	0.20	0.84	5.85	5.79	-	0.13	-	-	100.00	11.64	0.99
n=3 (trachyte)	*s*	0.73	0.13	2.54	0.08	0.16	0.17	0.10	0.64	1.14	-	0.09	-	-	-	1.44	0.18
OT0702-10	x̄	72.52	0.41	9.34	6.70	0.31	0.12	0.34	5.06	4.50	-	0.71	-	-	100.00	9.55	0.91
n=6 (pantellerite)	*s*	0.72	0.08	1.12	0.36	0.05	0.06	0.06	0.64	0.28	-	0.07	-	-	-	0.56	0.17
JO941	x̄	72.28	0.37	8.54	6.79	0.29	0.10	0.29	6.33	4.39	-	0.69	-	-	100.00	10.71	0.69
n=13	*s*	0.26	0.11	0.09	0.10	0.09	0.21	0.05	0.18	0.09	-	0.05	-	-	-	0.14	0.48
KET8222 P-11	x̄	64.67	0.83	15.50	5.88	0.28	1.45	6.41	4.98	-	-	-	-	-	-	11.39	0.78
n=n.a. (trachyte)	*s*	0.68	0.10	0.71	0.19	0.14	0.20	0.27	0.19	-	-	-	-	-	-	0.46	-
KET8222 P-11	x̄	72.41	0.34	8.95	7.43	0.08	0.17	6.09	4.54	-	-	-	-	-	-	10.63	0.75
n=n.a. (pantellerite)	*s*	0.38	0.08	0.09	24.00	6.00	0.08	0.33	0.00	-	-	-	-	-	-	0.33	-
ODP2	x̄	*63.92*	*1.00*	*16.22*	*5.35*	*0.25*	*0.99*	*2.50*	*5.55*	*3.89*	*0.35*	*0.09*	*0.24*	-	*97.22*	*9.44*	*0.82*
n=18	*s*	*1.74*	*0.30*	*0.83*	*0.51*	*0.04*	*0.61*	*1.18*	*0.43*	*0.80*	*0.37*	*0.07*	*0.11*	-	*1.18*	*0.87*	*0.10*

ODP4	x̄	*65.10*	*0.72*	*15.89*	*5.72*	*0.30*	*0.38*	*1.41*	*5.62*	*4.72*	*0.14*	*0.05*	*0.15*	-	*96.33*	*10.35*	*0.90*
n=33 (trachyte)	*s*	*0.61*	*0.04*	*0.47*	*0.14*	*0.04*	*0.08*	*0.12*	*0.38*	*0.12*	*0.04*	*0.05*	*0.23*	-	*1.55*	*0.39*	*0.06*
ODP4	x̄	*74.58*	*0.40*	*8.70*	*6.98*	*0.36*	*0.07*	*0.29*	*4.25*	*4.33*	*0.03*	*0.30*	*0.73*	-	*93.45*	*8.55*	*1.35*
n=33 (pantellerite)	*s*	*0.18*	*0.02*	*0.00*	*0.04*	*0.06*	*0.01*	*0.01*	*0.26*	*0.09*	*0.02*	*0.01*	*0.04*	-	*0.39*	*0.22*	*0.05*
OH-DP-0617	x̄	60.15	0.43	19.77	2.75	0.15	0.42	2.38	5.04	8.85	0.05	0.49	0.24	0.12	94.36	13.89	1.76
n=13	*s*	0.33	0.02	0.28	0.09	0.04	0.02	0.06	0.16	0.26	0.02	0.10	0.02	0.04	1.62	0.16	0.10
CF5 V4	x̄	58.90	0.48	20.46	3.20	0.18	0.62	2.71	5.00	8.37	0.08	0.47	0.25	0.11	95.85	13.37	1.68
n=16	*s*	1.81	0.10	0.22	1.03	0.03	0.48	0.98	0.37	0.39	0.10	0.15	0.07	0.04	0.81	0.73	0.08
OT0701-6	x̄	59.58	0.44	20.04	2.76	0.13	0.51	2.31	5.24	8.80	-	-	0.18	-	100.00	14.04	1.68
n=15	*s*	0.22	0.07	0.12	0.14	0.09	0.08	0.09	0.15	0.16	-	-	0.04	-	-	0.10	0.08
Vico B	x̄	59.66	0.46	19.59	2.85	0.15	0.42	2.37	5.37	8.65	0.05	0.43	0.22	0.09	95.32	14.02	1.61
n=13	*s*	0.26	0.07	0.10	0.05	0.04	0.03	0.05	0.09	0.16	0.04	0.11	0.02	0.03	1.31	0.14	0.05
OH-DP-0624	x̄	51.40	1.02	18.17	8.00	0.19	3.09	8.36	3.20	5.88	0.68	0.19	0.34	0.37	97.77	9.08	1.84
n=19	*s*	3.60	0.22	0.62	2.13	0.03	1.17	2.48	0.68	1.45	0.28	0.06	0.08	0.17	1.29	2.08	0.18
OT0701-7	x̄	55.79	0.81	19.24	5.30	0.18	1.67	5.14	4.20	7.19	0.16	-	0.37	-	100.00	11.40	1.73
n=22	*s*	3.92	0.28	0.63	2.49	0.08	1.25	2.67	0.71	1.58	0.16	-	0.07	-	-	2.27	0.13
PRAD3225	x̄	57.82	0.68	19.12	4.15	0.19	1.05	4.05	4.88	8.08	-	-	-	-	97.21	12.95	1.65
n=11	*s*	2.77	0.16	0.39	1.73	0.01	0.90	2.00	0.60	1.10	-	-	-	-	1.19	1.68	0.06
CF5 V5	x̄	54.92	0.81	18.76	6.08	0.19	1.98	5.93	3.82	7.06	0.46	0.21	0.41	0.24	96.59	10.88	1.86
n=14	*s*	3.56	0.22	0.58	2.12	0.05	1.06	2.09	0.64	1.12	0.30	0.08	0.08	0.08	1.39	1.71	0.13
C-42	x̄	49.74	1.49	18.06	8.63	0.27	3.26	8.25	3.37	5.97	0.79	0.17	-	-	99.56	9.34	1.77
n=n.a.	*s*	1.08	0.30	0.26	0.61	0.17	0.21	0.56	0.13	0.24	0.19	0.05	-	-	-	0.37	-
Pittigliano tuff	x̄	58.89	0.60	19.65	3.42	-	0.15	0.78	3.69	4.16	8.59	0.08	0.21	-	98.41	12.75	2.09
n=3	*s*	1.71	0.11	0.37	1.36	-	0.01	0.66	1.58	0.50	1.56	0.00	0.13	-	0.61	1.65	0.48
OH-DP-1817	x̄	44.48	0.98	15.44	10.76	0.23	4.61	13.25	3.81	5.48	0.95	0.36	0.14	0.41	97.58	9.28	1.47
n=10	*s*	1.60	0.12	0.97	1.02	0.06	0.44	1.40	0.59	0.47	0.13	0.11	0.02	0.18	0.85	0.77	0.24
AH20-PRa	x̄	41.69	1.37	12.52	11.56	0.27	6.39	15.24	3.49	4.98	1.11	0.61	-	0.08	96.94	8.47	1.43
n=6	*s*	0.16	0.04	0.05	0.17	0.03	0.30	0.13	0.08	0.36	0.12	0.11	-	0.02	0.44	-	-
Sulmona Site 2	x̄	41.92	1.19	14.23	12.50	0.32	5.20	14.20	4.00	5.43	1.02	0.49	0.16	0.16	96.95	9.43	1.37
n=23	*s*	0.63	0.05	0.19	0.35	0.03	0.18	0.37	0.31	0.28	0.08	0.08	0.02	0.05	1.38	0.32	0.15
Sulmona Site 2a	x̄	43.01	1.17	14.77	11.53	0.28	4.75	13.59	3.83	6.07	1.00	0.45	0.14	0.14	97.61	9.90	1.64
n=30	*s*	1.40	0.15	0.94	1.16	0.06	1.01	1.57	0.41	1.46	0.13	0.12	0.02	0.07	1.12	1.21	0.60
Paganica site 5	x̄	43.47	1.10	15.34	10.87	0.29	4.78	13.15	3.75	6.42	0.82	0.45	0.14	0.27	96.70	10.17	1.80
n=18	*s*	1.86	0.16	1.76	1.20	0.07	1.19	2.17	0.98	1.32	0.17	0.16	0.05	0.12	1.22	1.70	0.54
Raiano site 3	x̄	43.68	1.06	14.49	10.62	0.27	5.24	13.69	3.53	6.53	0.88	0.44	0.13	0.21	97.79	10.06	1.85
n=22	*s*	1.04	0.21	1.42	0.76	0.05	1.06	1.55	0.31	1.20	0.13	0.11	0.02	0.14	0.66	1.30	0.34
PR basal fallout	x̄	42.83	1.41	12.65	11.60	0.22	6.51	16.30	2.96	4.42	1.10	0.48	-	0.03	97.96	7.38	1.49
n=10	*s*	0.17	0.11	0.11	0.09	0.04	0.10	0.29	0.06	0.11	0.06	0.14	-	0.03	0.86	0.14	0.04
CF7-V11	x̄	43.49	1.03	14.81	10.83	0.26	4.58	13.15	4.23	6.67	0.94	0.38	0.14	0.30	99.04	99.04	10.90
n=11	*s*	1.35	0.12	0.98	1.12	0.05	0.57	1.64	0.44	1.16	0.11	0.11	0.02	0.12	0.62	0.62	1.24

OH-DP-1955	x̄	57.53	0.57	20.51	4.03	0.18	0.56	4.55	4.78	6.97	0.09	0.31	0.23	0.21	96.70	11.75	1.47
n=18	*s*	1.49	0.10	0.47	0.34	0.04	0.07	0.52	0.72	1.55	0.02	0.11	0.05	0.05	1.83	1.90	0.33
SC5	x̄	58.42	0.48	21.16	3.01	0.20	0.36	4.41	4.84	6.63	0.14	0.33	0.24	0.18	94.64	11.47	1.38
n=17	*s*	1.37	0.09	0.98	0.74	0.08	0.16	0.52	0.52	0.69	0.10	0.18	0.10	0.14	1.55	0.91	0.20
Fall B	x̄	60.09	0.48	19.06	2.92	0.16	0.50	3.26	3.14	10.34	0.05	-	-	-	100.00	13.48	3.78
n=6	*s*	0.25	0.01	0.09	0.08	0.02	0.04	0.17	0.15	0.12	0.01	-	-	-	-	0.25	0.16
OH-DP-2010	x̄	54.03	0.76	18.14	6.33	0.15	1.77	6.23	3.08	8.66	0.35	0.32	0.08	0.49	97.59	11.73	2.87
n=22	*s*	3.62	0.17	0.72	1.75	0.03	0.81	1.81	0.49	0.89	0.19	0.11	0.03	0.16	1.77	1.10	0.43
Fall A	x̄	59.92	0.50	19.21	3.16	0.17	0.51	3.19	3.05	10.20	0.08	-	-	-	100.00	13.25	3.36
n=11	*s*	0.29	0.02	0.14	0.12	0.11	0.05	0.25	0.17	0.17	0.03	-	-	-	-	0.26	0.20
SC3	x̄	58.47	0.54	18.80	3.85	0.15	0.91	3.93	2.89	9.75	0.09	0.30	0.07	0.26	96.81	12.64	3.40
n=20	*s*	1.31	0.04	0.18	0.72	0.03	0.33	0.78	0.25	0.61	0.04	0.12	0.02	0.13	1.33	0.73	0.29
A9	x̄	58.87	0.55	19.13	3.60	0.12	0.59	3.57	3.65	9.81	0.11	0.28	0.14	-	97.10	13.46	2.73
n=16	*s*	1.13	0.24	0.37	0.73	0.10	0.22	0.69	0.38	0.60	0.11	0.14	0.07	-	1.25	0.38	0.41
Sulmona 5-1c	x̄	60.13	0.44	19.05	3.01	0.14	0.55	3.16	3.09	10.33	0.06	0.00	0.11	0.38	95.15	13.42	3.36
n=30	*s*	0.89	0.04	0.43	0.32	0.04	0.14	0.38	0.21	0.21	0.03	0.00	0.02	0.12	1.24	0.26	0.26
FIC-12.9	x̄	55.52	0.63	19.41	4.75	0.19	1.28	5.34	4.38	8.27	0.23	0.43	0.11	0.31	96.51	12.65	1.95
n=22	*s*	1.79	0.08	0.35	0.73	0.05	0.36	0.98	0.53	1.05	0.08	0.11	0.02	0.11	1.77	0.66	0.52
OH-DP-2017	x̄	64.43	0.44	18.27	2.59	0.18	0.29	1.06	5.65	6.32	0.05	0.24	0.36	0.11	94.22	11.97	0.29
n=21	*s*	0.20	0.08	0.12	0.08	0.03	0.02	0.05	0.26	0.14	0.03	0.07	0.02	0.03	0.60	1.12	0.06
A11	x̄	63.68	0.46	18.28	2.73	0.18	0.42	1.44	5.17	7.13	0.15	0.11	0.24	-	96.52	12.30	1.41
n=18	*s*	0.66	0.10	0.33	0.27	0.16	0.17	0.28	0.66	0.40	0.11	0.14	0.09	-	0.84	0.48	0.27
A12	x̄	64.18	0.51	17.85	2.56	0.23	0.30	1.09	6.09	6.57	0.12	0.11	0.39	-	96.37	12.66	1.08
n=17	*s*	0.53	0.12	0.23	0.23	0.16	0.09	0.20	0.33	0.20	0.12	0.13	0.08	-	0.92	0.31	0.08
SC2	x̄	66.20	0.35	16.97	3.01	0.26	0.32	0.98	5.27	5.71	0.02	0.02	0.50	0.40	95.38	10.98	1.09
n=16	*s*	0.58	0.03	0.17	0.21	0.03	0.13	0.26	0.27	0.12	0.02	0.01	0.04	0.10	1.21	0.32	0.05
OH-DP-2060	x̄	44.94	0.78	18.67	8.44	0.29	1.61	10.91	5.39	7.74	0.28	0.91	0.19	0.95	96.34	13.13	1.46
n=19	*s*	1.70	0.17	0.94	1.18	0.05	0.98	1.26	0.76	1.32	0.16	0.23	0.04	0.48	1.81	1.68	0.27
SUL 1-6	x̄	44.73	0.82	19.48	8.17	0.36	1.45	10.90	5.59	8.31	0.18	0.85	0.18	0.75	96.73	13.90	1.53
n=27	*s*	1.16	0.10	0.70	0.77	0.05	0.14	1.16	0.64	0.90	0.03	0.20	0.03	0.27	1.31	0.67	0.40
Oricola tuff	x̄	45.15	0.00	18.83	8.27	0.32	1.52	11.40	4.90	8.33	0.23	0.79	0.13	0.13	100.00	13.23	1.70
n=8	*s*	0.66	0.00	0.31	0.45	0.03	0.11	0.62	0.25	0.67	0.04	0.09	0.02	0.05	-	0.76	0.15
proximal TBA	x̄	45.74	0.76	19.16	7.80	0.30	1.40	10.20	5.49	8.93	0.21	0.86	-	0.85	98.02	14.42	1.63
n=7	*s*	0.79	0.11	0.14	0.19	0.03	0.06	0.46	0.27	0.29	0.03	0.14	-	0.10	0.70	0.27	0.12
Standard 1 - USGS Rhyolite															Total		
n=2	x̄	75.84	0.23	11.16	2.23	0.16	0.05	0.09	4.57	4.51	0.03	0.25	0.18	0.03	99.32		
Recommended		76.00	0.19	11.50	2.02	0.16	0.08	0.10	4.75	4.47	-	-	-	0.03	99.30		

Standard 2 – Kakanui Augite															
n=2	x̄	50.79	0.87	8.36	0.09	6.53	16.27	15.95	1.29	-	-	-	-	-	100.14
Recommended		50.46	0.84	8.28	0.13	6.51	16.28	16.00	1.30	-	-	-	-	-	99.80

Table 2. Depths and ages of tephra layers in the DEEP site succession. $^{40Ar}/^{39}Ar$ ages with 2σ uncertainties (last column) recalculated to ACs at 1.194 Ma for, which corresponds to FCs at 28.02 Ma (Nomade et al., 2005) and the total decay constant of Steiger and Jäger (1977). Tephra layers in bold are not considered for the age-depth modelling (Francke et al., 2016).

Tephra DEEP site	Depth (mcd)	Eruption/ Tephra	Age (ka)	References	recalculated $^{40}Ar/^{39}Ar$ ages
OH-DP-0027	2.773	Mercato	8.43–8.63	Zanchetta et al., 2011	N.A.
OH-DP-0115	11.507	Y-3	28.68-29.42	Albert et al., 2015	N.A.
OH-DP-0169	16.933	Campanian Ignimbrite/Y-5	39.28±0.1	De Vivo et al., 2001	39.6±0.1
OH-DP-0404	40.486	POP2	102±2.4	Regattieri et al., 2015	N.A.
OH-DP-0435	43.513	X-6	109±2	Iori et al., 2014	109±2
OH-DP-0499	49.947	P-11	133.5±2	Satow et al., 2015	N.A.
OH-DP-0617	61.726	Vico "Ignimbrite B"	157±3	Laurenzi and Villa, 1987	162±6
OH-DP-0624	**62.413**	**Pitigliano Tuff**	**158±22**	**Turbeville, 1992a**	**163±22**
OH-DP-1817	181.769	Pozzolane Rosse	457±4	Karner et al., 2001	457±4
			457±2	Giaccio et al., 2013	457±2
OH-DP-1955	195.566	SC5	493.1±10.9	Giaccio et al., 2014	493.1±10.9
OH-DP-2010	**201.049**	**Sabatini Fall A**	**499±3**	**Marra et al., 2014**	**496±3**
OH-DP-2017	201.782	Acerno A11-12	514±6	Petrosino et al., 2014	511±6
OH-DP-2060	206.080	Tufo di Bagni Albule	527±2	Marra et al., 2009	527±2

Figure 1. (a) Location of Lake Ohrid in the Mediterranean region**,** the Italian volcanoes**,** and the locations of archives mentioned in the text **(**1-Ficoncella Site, 2-Carsoli Basin, 3-Paganica-San Demetrio-Castelnuovo basin, 4-Campo Felice, 5-Fucino Basin, 6-Sulmona Basin, 7-PRAD1-2, 8-CM92-42, 9-RF93-77, 10-RF95-11, 11-Veliko Jezero, Island of Mljet, 12-

KET8022, 13-KET8003, 14-KET8011, 15-C-45, 16-KET8004/DED8708, 17-C1202, 18-Cilento coast, 19-C106, 20-SMP1e (CE1/CD1/SMP1), 21-Acerno Basin, 22-San Gregorio Magno basin, 23-Lago Grande di Monticchio, 24-Mercure basin, 25-Montalbano Jonico succession, 26-MD90-917, 27-KET8218, 28-IN68-9, 29-IN68-5, 30-AD91-17, 31-MD90-918, 32-RC9 191, 33-M25/4-12, 34-KET8222, 35-V10 69, 36-ODP 963A, 37-22M-60, 38-KC01B, 39-RC9 183, 40-RC9 181, 41-LC01,-42-V10 58, 43-Lesvos, 44-Tenaghi Philippon, 45-Theopetra Cave, 46-Lake Prespa). **(b)** Geological map of the Lake Ohrid catchment modified after Lindhorst et al. (2015) and the core locations from previous studies (Lz1120, Co1200/1201/1202/1262, and JO2004) and the ICDP main drill site DEEP.

Figure 2. (Litho-) Stratigraphy of the uppermost 247.8 mcd of the DEEP site sequence and the position of recognised tephra layers. Tephra layers coloured in yellow and being labeld are discussed within this paper. The thickness of tephra layers is not to scale and more detailed information about tephra thickness and appearance are provided in the text.

Figure 3. Total alkali-silica diagram after Le Bas et al., 1986 to classify and correlate the DEEP site tephra layers OH-DP-0027–OH-DP-2060 (a–j). The full dataset of the DEEP site record is given in Table 1 and in the supplementary online material. The following references were used: **a) OH-DP-0027/Pomici di Mercato:** Co1262-709 (Wagner et al., 2012), OT0702-3 (Vogel et al., 2010), PT0915-2 (Damaschke et al., 2013TM6a/TM6b (Wulf et al., 2004); MJ1/VJ1 (Jahns and van den Bogaard, 1998); KET8218 V1 (Paterne et al., 1988); IN68-9 125cm, IN68-5 259 cm and RF95-11 320 cm (Calanchi and Dinelli, 2008); 190-191, 195-196 cm AD91-17 (Marchini et al., 2014); 210/223cm MD90-918 (Caron et al., 2012). **b) OH-DP-0115 / Y-3:** OT0520-2; OT0700-1; OT0702-4; JO 187 (Sulpizio et al., 2010), PT0915-5, (Damaschke et al., 2013); TM15 (Wulf et al., 2004); Y-3 M25/4-12, RC9 (Keller et al., 1978; Albert et al., 2015); C7 (Paterne et al., 1988); MD90-917 920/17 (Zanchetta et al., 2008); TP 9.70 (Albert et al., 2015); A2/B2 C106/C45 (Munno and Petrosino, 2004); S19 (Munno and Petrosino, 2007). **c) OH-DP-0169 / CI/Y-5:** OT0520-3, OT0700-2, OT0701-1, OT0702-6, JO-244, PT0704-3 (Sulpizio et al., 2010); Y-5 RC9 191 (Keller et al. 1978); TM-18 (Wulf et al., 2004); S-17 (Munno and Petrosino, 2007)**;** ML 2 (Margari et al., 2007); TP-CI (Lowe et al., 2012); C-13 (Paterne et al., 1988); PRAD1653 (Bourne et al., 2010); I-3, (Insinga et al. 2014); LC21 4.925 (Lowe et al., 2012, Satow et al. 2015); pre-CI deposits (Tomlinson et al., 2012).**d) OH-DP-0404 / TM24a POP2 :** OT-0702-8 (Vogel et al., 2010); TM24a (Wulf et al., 2004; Wulf et al., 2012); POP2 (Regattieri et al., 2015); CM92-42 (710 cm), RF93-77 (797 cm) (Calanchi and

Dinelli, 2008). **e) OH-DP-0435 / X-6:** OT0702-9 (Vogel et al., 2010), JO-575 (Caron et al., 2010); X-6 (Keller et al., 1978); C-31 (Paterne et al., 2008); TM27 (Wulf et al., 2012); POP4 (Regattieri et al., 2015); PRAD-2812 (Bourne et al., 2015); I-9 (Insinga et al., 2014); S10 (Munno and Petrosino, 2007); SM1-2/SA (Marciano et al., 2008); CIL2 (Giaccio et al., 2012); t1 (Iorio et al., 2014). **f) OH-DP-0499 / P-11:** OT0702-10 (Vogel et al., 2010), JO-941 (Caron et al., 2010); P-11 (Paterne et al., 2008); ODP2-4 (Tamburrino et al., 2012); ML5 (Margari et al., 2007); THP-TII5 (Karkanas et al., 2015); LC21 10.345 (Satow et al., 2015). **f) OH-DP-0617 / Vico "Ignimbrite B":** OT0701-6 (Sulpizio et al., 2010); CF-V4 (Giraudi et al., 2011); Vico B (Giraudi et al. 2011). **g) OH-DP-0624 / CF-V5/ PRAD3225:** OT0701-7 (Sulpizio et al., 2010); PRAD3225 (Bourne et al., 2015); CF-V5 tephra (Giraudi and Giaccio, 2015); C-42 (Paterne et al., 2008). **h) OH-DP-1817 / Pozzolane Rosse:** AH-20-PRa (Marra et al., 2009); basal fallout (Freda et al., 2010); Paganica-Raiano-Sulmona (Giaccio et al., 2013a); CF-V11 (Giraudi and Giacco, 2015). **h) OH-DP-1955 / SC5:** SC5 (Giaccio et al., 2014); Fall B (Marra et al., 2014). **i) OH-DP-2010 / Fall A:** Proximal Fall A (Marra et al., 2014); SC3 and SUL 5-1c (Giaccio et al., 20149; A9 (Petrosino et al., 2014b); FIC-12.9 (Aureli et al., 2015). **j) OH-DP-2017/ A11/A12:** A11/12 (Petrosino et al., 2014b); SC2 (Giaccio et al., 2014).

Figure 4. Al_2O_3-FeO_{TOT} diagram for classification of comendites and pantellerites according to MacDonald (1974). Tephra OH-DP-0499 and most of the other P-11 equivalents show the typical bimodal chemical composition of P-11, except for the very distal equivalents LC21 10.345 and THP-TII5, which only have a pantelleritic part (see text for data references).

Figure 5. Harker diagrams of tephra layers OH-DP-0617-OH-DP-1817 and their discussed equivalents. For references of correlated tephra layers, see text, additional Harker diagrams for OH-DP-1817 can be found in the Supplement I Fig. g.

Figure 6. Harker diagrams of tephra layers OH-DP-1955-OH-DP-2060 and their discussed equivalents. For references of correlated tephra layers, see text, additional Harker diagrams for OH-DP-1955 can be found in the Supplement I Fig. h.

Figure 7. Age-depth plot for the selected DEEP site tephra layers. The ages of the tephra layers are based on recalculation of existing $^{40}Ar/^{39}Ar$ ages (Table 2) or according to published data for non $^{40}Ar/^{39}Ar$ ages. Chronological tie points were interpolated on a linear basis (blue line). The dotted lines in the insert indicate a suspicious change in the sedimentation rate for a different age of the Fall A tephra.

Figure 8. Tephrostratigraphic framework of Lake Ohrid and selected archives of the last 637 kyrs corresponding to MIS16. The dashed parts of the archive columns indicate the part of the existing record, where no tephrostratigraphic information are available at present. The following archives and tephra layers are presented: Lago Grande di Montichhio (LgdM, Wulf et al. 2004, 2012), Siciliy Channel: ODP963 (Tamburino et al. 2012), Tyrrhenian Sea: KET8004/DED8708, KET8003,-8011,8022 (C-7,-13,-31,-42, Paterne et al., 1988, 2008); C1202 (t1, Iorio et al. 2014); C45/106 (A2/B2, Munno and Petrosino, 2004), Adriatic Sea: KET8218 (V-1, Paterne et al., 1988), IN68-9, IN68-5, RF95-11, CM92-42, RF93-77 (*125/259/320, 710/797 Calanchi and Dinelli, 2008); AD91-17 ("190-191/195-196, Marchini et al., 2014); MD90-917 (920-17, Zanchetta et al., 2008); MD90-918 (#210/223 Caron et al. 2012); PRAD1-2 (PRAD 1653, 2812, 3225, Bourne et al.,2010, 2015), Ionian Sea: MD25/4-12 (Y-3, Albert et al., 2015); RC9-191, 22M-60, V10 69 (Y-3, Y-5, X-6, Keller et al., 1978); KET-8222 (C-31, P-11, Paterne et al., 2008); KC01B (I-3, I-9, Insinga et al. 2014), Levantine Sea: RC9-183, RC9-181 (Y-5, Keller et al., 1978), Aegean Sea: V10-58 (Y-5, Keller et al., 1978); LC01 (4.925, 10.345, Satow et al., 2015), Tenaghi Philippon: (TP9.70, Albert et al., 2015; CI, Lowe et al., 2012), San Gregorio Magno Basin (Munno and Petrosino, 2007), Campo Felice basin (Giraudi et al., 2011, 2015), Sulmona basin (Giaccio et al. 2013b, Regattieri et al., 2015), Acerno basin (Petrosino et al., 2013b), Mercure basin (Giaccio et al., 2014).

6 References

Aksu, A. E., Jenner, G., Hiscott, R. N., and Isler, E. B.: Occurrence, stratigraphy and geochemistry of Late Quaternary tephra layers in the Aegean Sea and the Marmara Sea, Mar. Geol., 252, 174-192, 2008.

Albert, P. G., Hardiman, M., Keller, J., Tomlinson, E. L., Smith, V. C., Bourne, A. J., Wulf, S., Zanchetta, G., Sulpizio, R., Muller, U. C., Pross, J., Ottolini, L., Matthews, I. P., Blockley, S. P. E., and Menzies, M. A.: Revisiting the Y-3 tephrostratigraphic marker: a new diagnostic glass geochemistry, age estimate, and details on its climatostratigraphical context, Quaternary Sci. Rev., 118, 105-121, 2015.

Le Bas, M. J. L., Maitre, R. W. L., Streckeisen, A., and Zanettin, B.: A Chemical Classification of Volcanic Rocks Based on the Total Alkali-Silica Diagram, J. Petrol., 27, 745-750, 1986.

Baumgarten, H., Wonik, T., Tanner, D. C., Francke, A., Wagner, B., Zanchetta, G., Sulpizio, R., Giaccio, B., and Nomade, S.: Age–depth model of the past 630 kyr for Lake Ohrid (FYROM/Albania) based on cyclostratigraphic analysis of downhole gamma ray data, Biogeosciences, 12, 7453-7465, 2015.

Bear, A. N., Cas, R. A. F., and Giordano, G.: Variations in eruptive style and depositional processes associated with explosive, phonolitic composition, caldera-forming eruptions: The 151 ka Sutri eruption, Vico Caldera, central Italy, J. Volcanol. Geoth. Res., 184, 225-255, 2009.

Bosi, C., Locardi, E., and Villa, I.: Il distretto magmatico abruzzese, Riassunti workshop "Evoluzione dei bacini Neogenici e loro rapporti con il magmatismo Plio-Quaternario nell'area Tosco-Laziale", Pisa 12-13 June 1991, 68-69, 1991.

Bourne, A. J., Lowe, J. J., Trincardi, F., Asioli, A., Blockley, S. P. E., Wulf, S., Matthews, I. P., Piva, A., and Vigliotti, L.: Distal tephra record for the last ca 105,000 years from core PRAD 1-2 in the central Adriatic Sea implications for marine tephrostratigraphy, Quaternary Sci. Rev., 29, 3079-3094, 2010.

Bourne, A. J., Albert, P. G., Matthews, I. P., Trincardi, F., Wulf, S., Asioli, A., Blockley, S. P. E., Keller, J., and Lowe, J. J.: Tephrochronology of core PRAD 1-2 from the Adriatic Sea: insights into Italian explosive volcanism for the period 200-80 ka, Quaternary Sci. Rev., 116, 28-43, 2015.

Calanchi, N. and Dinelli, E.: Tephrostratigraphy of the last 170 ka in sedimentary successions from the Adriatic Sea, J. Volcanol. Geoth. Res., 177, 81-95, 2008.

Calanchi, N., Cattaneo, A., Dinelli, E., Gasparotto, G., and Lucchini, F.: Tephra layers in Late Quaternary sediments of the central Adriatic Sea, Mar. Geol., 149, 191-209, 1998.

Caron, B., Sulpizio, R., Zanchetta, G., Siani, G., and Santacroce, R.: The Late Holocene to Pleistocene tephrostratigraphic record of Lake Ohrid (Albania), Comptes Rendus Geoscience, 342, 453-466, 2010.

Caron, B., Siani, G., Sulpizio, R., Zanchetta, G., Paterne, M., Santacroce, R., Tema, E., and Zanella, E.: Late Pleistocene to Holocene tephrostratigraphic record from the Northern Ionian Sea, Mar. Geol., 311, 41-51, 2012.

Civetta, L., Cornette, Y., Crisci, G., Gillot, P. Y., Orsi, G., and Requejo, C. S.: Geology, Geochronology and Chemical Evolution of the Island of Pantelleria, Geol. Mag., 121, 541-562, 1984.

Civetta, L., Orsi, G., Pappalardo, L., Fisher, R. V., Heiken, G., and Ort, M.: Geochemical zoning, mingling, eruptive dynamics and depositional processes - The Campanian Ignimbrite, Campi Flegrei caldera, Italy, J. Volcanol. Geoth. Res., 75, 183-219, 1997.

Damaschke, M., Sulpizio, R., Zanchetta, G., Wagner, B., Bohm, A., Nowaczyk, N., Rethemeyer, J., and Hilgers, A.: Tephrostratigraphic studies on a sediment core from Lake Prespa in the Balkans, Clim. Past, 9, 267-287, 2013.

De Vivo, B., Rolandi, G., Gans, P. B., Calvert, A., Bohrson, W. A., Spera, F. J., and Belkin, H. E.: New constraints on the pyroclastic eruptive history of the Campanian volcanic Plain (Italy), Miner. Petrol., 73, 47-65, 2001.

Deino, A. L., Southon, J., Terrasi, F., Campajola, L., and Orsi, G.: ^{14}C and $^{40}Ar/^{39}Ar$ Dating of the Campanian Ignimbrite, Phlegran Fields, Italy, 8th International Conference on Geochronology, Cosmochronology and Isotope Geology, Berkeley, CA, USA, Abstracts US Geol. Surv. Circ., 1107, 77, 1994.

Di Vito, M. A., Sulpizio, R., Zanchetta, G., and D'Orazio, M.: The late Pleistocene pyroclastic deposits of the Campanian Plain: New insights into the explosive activity of Neapolitan volcanoes, J. Volcanol. Geoth. Res., 177, 19-48, 2008.

Druitt, T. H., Brenchley, P. J., Gokten, Y. E., and Francaviglia, V.: Late Quaternary Rhyolitic Eruptions from the Acigol Complex, Central Turkey, J. Geol. Soc. London, 152, 655-667, 1995.

Druitt, T. H., Edwards, L., Mellors, R., Pyle, D., Sparks, R., Lanphere, M., Davies, M., and Barreirio, B.: Santorini volcano, Geological Society, London, Memoirs, 19, 1-161, 1999.

Francke, A., Wagner, B., Just, J., Leicher, N., Gromig, R., Baumgarten, H., Vogel, H., Lacey, J. H., Sadori, L., Wonik, T., Leng, M. J., Zanchetta, G., Sulpizio, R., and Giaccio, B.: Sedimentological processes and environmental variability at Lake Ohrid (Macedonia, Albania) between 637 ka and the present, Biogeosciences, 13, 1179-1196, 2016.

Freda, C., Gaeta, M., Giaccio, B., Marra, F., Palladino, D. M., Scarlato, P., and Sottili, G.: CO2-driven large mafic explosive eruptions: the Pozzolane Rosse case study from the Colli Albani Volcanic District (Italy), B. Volcanol., 73, 241-256, 2011.

Galli, P., Giaccio, B., and Messina, P.: The 2009 Central Italy earthquake seen through 0.5 Myr-long tectonic history of the L'Aquila faults system, Quaternary Sci. Rev., 29, 3768-3789, 2010.

Giaccio, B., Nomade, S., Wulf, S., Isaia, R., Sottili, G., Cavuoto, G., Galli, P., Messina, P., Sposato, A., Sulpizio, R., and Zanchetta, G.: The late MIS 5 Mediterranean tephra markers: a reappraisal from peninsular Italy terrestrial records, Quaternary Sci. Rev., 56, 31-45, 2012.

Giaccio, B., Arienzo, I., Sottili, G., Castorina, F., Gaeta, M., Nomade, S., Galli, P., and Messina, P.: Isotopic (Sr-Nd) and major element fingerprinting of distal tephras: an application to the Middle-Late Pleistocene markers from the Colli Albani volcano, central Italy, Quaternary Sci. Rev., 67, 190-206, 2013a.

Giaccio, B., Castorina, F., Nomade, S., Scardia, G., Voltaggio, M., and Sagnotti, L.: Revised Chronology of the Sulmona Lacustrine Succession, Central Italy, J. Quaternary Sci., 28, 545-551, 2013b.

Giaccio, B., Isaia, R., Fedele, F. G., Di Canzio, E., Hoffecker, J., Ronchitelli, A., Sinitsyn, A. A., Anikovich, M., Lisitsyn, S. N., and Popov, V. V.: The Campanian Ignimbrite and Codola tephra layers: Two temporal/stratigraphic markers for the Early Upper Palaeolithic in southern Italy and eastern Europe, J. Volcanol. Geoth. Res., 177, 208-226, 2008.

Giaccio, B., Galli, P., Peronace, E., Arienzo I., Nomade, S., Cavinato, G. P., Mancini, M., Messina, P., and Sottili, G.: A 560-440 ka tephra record from the Mercure Basin, Southern Italy: volcanological and tephrostratigraphic implications, J. Quaternary Sci., 29, 232-248, 2014.

Giaccio, B., Regattieri, E., Zanchetta, G., Nomade, S., Renne, P. R., Sprain, C.J., Drysdale, R.N., Tzedakis, P. C., Messina, P., Scardia, G., Sposato, A., and Bassinot, F.: Duration and dynamics of the best orbital analogue to the present interglacial, Geology 43, 603–606, 2015.

Giordano, G., De Benedetti, A. A., Diana, A., Diano, G., Gaudioso, F., Marasco, F., Miceli, M., Mollo, S., Cas, R. A. F., and Funiciello, R.: The Colli Albani mafic caldera (Roma, Italy): Stratigraphy, structure and petrology, J. Volcanol. Geoth. Res., 155, 49-80, 2006.

Giraudi, C., Bodrato, G., Lucchi, M. R., Cipriani, N., Villa, I. M., Giaccio, B., and Zuppi, G. M.: Middle and late Pleistocene glaciations in the Campo Felice Basin (central Apennines, Italy), Quaternary Res., 75, 219-230, 2011.

Giraudi, C. and Giaccio, B.: Middle Pleistocene glaciations in the Apennines, Italy: new chronological data and preservation of the glacial record, Geological Society, London, Special Publications, 433, 2015.

Grant, K. M., Rohling, E. J., Bar-Matthews, M., Ayalon, A., Medina-Elizalde, M., Ramsey, C. B., Satow, C., and Roberts, A. P.: Rapid coupling between ice volume and polar temperature over the past 150,000 years, Nature, 491, 744-747, 2012.

Hamann, Y., Wulf, S., Ersoy, O., Ehrmann, W., Aydar, E., and Schmiedl, G.: First evidence of a distal early Holocene ash layer in Eastern Mediterranean deep-sea sediments derived from the Anatolian volcanic province, Quaternary Res., 73, 497-506, 2010.

Hoffmann, N., Reicherter, K., Fernandez-Steeger, T., and Grutzner, C.: Evolution of ancient Lake Ohrid: a tectonic perspective, Biogeosciences, 7, 3377-3386, 2010.

Incarbona, A., Bonomo, S., Di Stefano, E., Zgozi, S., Essarbout, N., Talha, M., Tranchida, G., Bonanno, A., Patti, B., Placenti, F., Buscaino, G., Cuttitta, A., Basilone, G., Bahri, T., Massa, F., Censi, P., and Mazzola, S.: Calcareous nannofossil surface sediment assemblages from the Sicily Channel (central Mediterranean Sea): Palaeoceanographic implications, Mar. Micropaleontol., 67, 297-309, 2008.

Insinga, D. D., Tamburrino, S., Lirer, F., Vezzoli, L., Barra, M., De Lange, G. J., Tiepolo, M., Vallefuoco, M., Mazzola, S., and Sprovieri, M.: Tephrochronology of the astronomically-tuned KC01B deep-sea core, Ionian Sea: insights into the explosive activity of the Central Mediterranean area during the last 200 ka, Quaternary Sci. Rev., 85, 63-84, 2014.

Iorio, M., Liddicoat, J., Budillon, F., Incoronato, A., Coe, R. S., Insinga, D. D., Cassata, W. S., Lubritto, C., Angelino, A., and Tamburrino, S.: Combined palaeomagnetic secular variation and petrophysical records to time-constrain geological and hazardous events: An example from the eastern Tyrrhenian Sea over the last 120 ka, Global and Planet. Change, 113, 91-109, 2014.

Jahns, S. and van den Bogaard, C.: New palynological and tephrostratigraphical investigations of two salt lagoons on the island of Mljet, south Dalmatia, Croatia, Veg. His. Archaeobot., 7, 219-234, 1998.

Karkanas, P., White, D., Lane, C. S., Stringer, C., Davies, W., Cullen, V. L., Smith, V. C., Ntinou, M., Tsartsidou, G., and Kyparissi-Apostolika, N.: Tephra correlations and climatic events between the MIS6/5 transition and the beginning of MIS3 in Theopetra Cave, central Greece, Quaternary Sci. Rev., 118, 170-181, 2015.

Karner, D. B., Juvigne, E., Brancaccio, L., Cinque, A., Ermolli, E. R., Santangelo, N., Bernasconi, S., and Lirer, L.: A potential early middle Pleistocene tephrostratotype for the Mediterranean basin: the Vallo Di Diano, Campania, Italy, Global and Planet. Change, 21, 1-15, 1999.

Karner, D. B., Marra, F., and Renne, P. R.: The history of the Monti Sabatini and Alban Hills volcanoes: groundwork for assessing volcanic-tectonic hazards for Rome, J. Volcanol. Geoth. Res., 107, 185-219, 2001.

Keller, J., Ryan,W. B. F., Ninkovich, D., and Altherr, R.: Explosive volcanic activity in the Mediterranean over the past 200,000 yr as recorded in deep-sea sediments, Geol. Soc. Am. Bull., 89, 591–604, 1978.

Keller, J., Gertisser, R., Reusser, E., and Dietrich, V.: Pumice deposits of the Santorini Lower Pumice 2 eruption on Anafi island, Greece: Indications for a Plinian event of exceptional magnitude, J. Volcanol. Geoth. Res., 278, 120-128, 2014.

Kraml, M.: Laser-40Ar/39Ar-Datierungen an distalen marinen Tephren des jung-quartären mediterranen Vulkanismus (Ionisches Meer, METEOR-Fahrt 25/4), Ph.D., Albert-Ludwigs-Universität Freiburg i.Br., 216 pp., 1997.

Kuiper, K. F., Deino, A., Hilgen, F. J., Krijgsman, W., Renne, P. R., and Wijbrans, J. R.: Synchronizing rock clocks of Earth history, Science, 320, 500-504, 2008.

Laskar, J., Robutel, P., Joutel, F., Gastineau, M., Correia, A. C. M., and Levrard, B.: A long-term numerical solution for the insolation quantities of the Earth, Astron. Astrophys., 428, 261-285, 2004.

Laurenzi, M. A. and Villa, I.: 40Ar/39Ar chronostratigraphy of Vico ignimbrites, Period. Mineral., 56, 285-293, 1987.

Lindhorst, K., Krastel, S., Reicherter, K., Stipp, M., Wagner, B., and Schwenk, T.: Sedimentary and tectonic evolution of Lake Ohrid (Macedonia/Albania), Basin Research, 27, 84-101, 2015.

Lisiecki, L. E. and Raymo, M. E.: A Pliocene-Pleistocene stack of 57 globally distributed benthic $\delta^{18}O$ records, Paleoceanography, 20, PA1003, doi:10.1029/2004PA001071, 2005.

Lourens, L. J.: Revised tuning of Ocean Drilling Program Site 964 and KC01B (Mediterranean) and implications for the $\delta^{18}O$, tephra, calcareous nannofossil, and geomagnetic reversal chronologies of the past 1.1 Myr, Paleoceanography, 19, PA3010, doi:10.1029/2003PA000997, 2004.

Lowe, D.J., Tephrochronology and its application: a review. Quaternary Geochronology 6, 107-153, 2011.

Lowe, J., Barton, N., Blockley, S., Ramsey, C. B., Cullen, V. L., Davies, W., Gamble, C., Grant, K., Hardiman, M., Housley, R., Lane, C. S., Lee, S., Lewis, M., MacLeod, A., Menzies, M., Müller, W., Pollard, M., Price, C., Roberts, A. P., Rohling, E. J., Satow, C., Smith, V. C., Stringer, C. B., Tomlinson, E. L., White, D., Albert, P., Arienzo, I., Barker, G., Borić, D., Carandente, A., Civetta, L., Ferrier, C., Guadelli, J.-L., Karkanas, P., Koumouzelis, M., Müller, U. C., Orsi, G., Pross, J., Rosi, M., Shalamanov-Korobar, L., Sirakov, N., and Tzedakis, P. C.: Volcanic ash layers illuminate the resilience of Neanderthals and early modern humans to natural hazards, Proc Natl Acad Sci, 109, 13532-13537, 2012.

Lustrino, M., Duggen, S., and Rosenberg, C. L.: The Central-Western Mediterranean: Anomalous igneous activity in an anomalous collisional tectonic setting, Earth-Sci. Rev., 104, 1-40, 2011.

MacDonald, R.: Nomenclature and petrochemistry of the peralkaline oversaturated extrusive rocks, B. Volcanol., 38, 498-516, 1974.

Mahood, G. A. and Hildreth, W.: Geology of the peralkaline volcano at Pantelleria, Strait of Sicily, B. Volcanol., 48, 143-172, 1986.

Marchini, G., Zanchetta, G., Santacroce, R., Vigliotti, L., Capotondi, L., and Sulpizio, R.: Tephrostratigraphy of marine core AD91-17 (Adriatic Sea) Revised, Alpine and Mediterranean Quaternary, 27, 77-84, 2014.

Marciano, R., Munno, R., Petrosino, P., Santangelo, N., Santo, A., and Villa, I.: Late quaternary tephra layers along the Cilento coastline (southern Italy), J. Volcanol. Geoth. Res., 177, 227-243, 2008.

Margari, V., Pyle, D. M., Bryant, C., and Gibbard, P. L.: Mediterranean tephra stratigraphy revisited: Results from a long terrestrial sequence on Lesvos Island, Greece, J. Volcanol. Geoth. Res., 163, 34-54, 2007.

Marianelli, P. and Sbrana, A.: Risultati di misure di standard di minerali e di vetri naturali in microanalisi a dispersione di energia, Atti della Societa Toscana di Scienze Naturali Memorie Serie A, 105, 57-63, 1998.

Marianelli, P., Sbrana, A., and Proto, M.: Magma chamber of the Campi Flegrei supervolcano at the time of eruption of the Campanian Ignimbrite, Geology, 34, 937-940, 2006.

Marra, F., Karner, D. B., Freda, C., Gaeta, M., and Renne, P.: Large mafic eruptions at Alban Hills Volcanic District (Central Italy): Chronostratigraphy, petrography and eruptive behavior, J. Volcanol. Geoth. Res., 179, 217-232, 2009.

Marra, F., Deocampo, D., Jackson, M. D., and Ventura, G.: The Alban Hills and Monti Sabatini volcanic products used in ancient Roman masonry (Italy): An integrated stratigraphic, archaeological, environmental and geochemical approach, Earth-Sci. Rev., 108, 115-136, 2011.

Marra, F., Sottili, G., Gaeta, M., Giaccio, B., Jicha, B., Masotta, M., Palladino, D. M., and Deocampo, D. M.: Major explosive activity in the Monti Sabatini Volcanic District (central Italy) over the 800-390 ka interval: geochronological-geochemical overview and tephrostratigraphic implications, Quaternary Sci. Rev., 94, 74-101, 2014.

Matter, M., Anselmetti, F. S., Jordanoska, B., Wagner, B., Wessels, M., and Wüest, A.: Carbonate sedimentation and effects of eutrophication observed at the Kališta subaquatic springs in Lake Ohrid (Macedonia), Biogeosciences, 7, 3755-3767, 2010.

Matzinger, A., Jordanoski, M., Veljanoska-Sarafiloska, E., Sturm, M., Muller, B., and Wuest, A.: Is Lake Prespa jeopardizing the ecosystem of ancient Lake Ohrid?, Hydrobiologia, 553, 89-109, 2006a.

Matzinger, A., Spirkovski, Z., Patceva, S., and Wuest, A.: Sensitivity of ancient Lake Ohrid to local anthropogenic impacts and global warming, J.of Great Lakes Res., 32, 158-179, 2006b.

Mele, D., Sulpizio, R., Dellino, P., and La Volpe, L.: Stratigraphy and eruptive dynamics of a pulsating Plinian eruption of Somma-Vesuvius: the Pomici di Mercato (8900 years B.P.), B. Volcanol., 73, 257-278, 2011.

Munno, R. and Petrosino, P.: New constraints on the occurence of Y-3 Upper Pleistocene tephra marker layer in the Tyrrhenian Sea, Il Quaternario, 17, 11-20, 2004.

Munno, R. and Petrosino, P.: The late Quaternary tephrostratigraphical record of the San Gregorio Magno Basin (Southern Italy), J. Quaternary Sci., 22, 247-266, 2007.

Narcisi, B. and Vezzoli, L.: Quaternary stratigraphy of distal tephra layers in the Mediterranean - an overview, Global and Planet. Change, 21, 31-50, 1999.

Nomade, S., Renne, P., Vogel, N., Deino, A., Sharp, W., Becker, T., Jaouni, A., and Mundil, R.: Alder Creek sanidine (ACs-2): a Quaternary 40 Ar/39 Ar dating standard tied to the Cobb Mountain geomagnetic event, Chem. Geol., 218, 315-338, 2005.

Orsi, G., DeVita, S., and diVito, M.: The restless, resurgent Campi Flegrei nested caldera (Italy): Constraints on its evolution and configuration, J. Volcanol. Geoth. Res., 74, 179-214, 1996.

Palladino, D. M., Simei, S., Sottili, G., and Trigila, R.: Integrated approach for the reconstruction of stratigraphy and geology of Quaternary volcanic terrains: An application to the Vulsini Volcanoes (Central Italy), Geol. S. Am. S., 464, 63-84, 2010.

Palladino, D. M., Gaeta, M., Giaccio, B., and Sottili, G.: On the anatomy of magma chamber and caldera collapse: the example of trachy-phonolitic explosive eruptions of the Roman Province (central Italy). J. Volcanol. Geotherm. Res. 281, 12–26, 2014. Pappalardo, L., Civetta, L., de Vita, S., Di Vito, M., Orsi, G., Carandente, A., and Fisher, R. V.: Timing of magma

extraction during the Campanian Ignimbrite eruption (Campi Flegrei Caldera), J. Volcanol. Geoth. Res., 114, 479-497, 2002.

Paterne, M., Guichard, F., Labeyrie, J., Gillot, P. Y., and Duplessy, J. C.: Tyrrhenian Sea Tephrochronology of the Oxygen Isotope Record for the Past 60,000 Years, Mar. Geol., 72, 259-285, 1986.

Paterne, M., Guichard, F., and Labeyrie, J.: Explosive activity of the South Italian volcanoes during the past 80,000 years as determined by marine tephrochronology, J. Volcanol. Geoth. Res., 34, 153-172, 1988.

Paterne, M., Guichard, F., Duplessy, J. C., Siani, G., Sulpizio, R., and Labeyrie, J.: A 90,000–200,000 yrs marine tephra record of Italian volcanic activity in the Central Mediterranean Sea, J. Volcanol. Geoth. Res., 177, 187-196, 2008.

Peccerillo, A.: Plio-Quaternary Volcanism in Italy: Petrology, Geochemistry, Geodynamics, Springer-Verlag Berlin Heidelberg, Berlin, 2005.

Petrosino, P., Ermolli, E. R., Donato, P., Jicha, B., Robustelli, G., and Sardella, R.: Using Tephrochronology and palynology to date the MIS 13 lacustrine sediments of the Mercure Basin (Southern Apennines – Italy), Italian Journal of Geosciences, 133, 169-186, 2014a.

Petrosino, P., Jicha, B. R., Mazzeo, F. C., and Russo Ermolli, E.: A high resolution tephrochronological record of MIS 14–12 in the Southern Apennines (Acerno Basin, Italy), J. Volcanol. Geoth. Res., 274, 34-50, 2014b.

Petrosino, P., Jicha, B. R., Mazzeo, F. C., Ciaranfi, N., Girone, A., Maiorano, P., and Marino, M.: The Montalbano Jonico marine succession: An archive for distal tephra layers at the Early–Middle Pleistocene boundary in southern Italy, Quatern. Int., 383, 89-103, 2015.

Phillips, D. and Matchan, E.: Ultra-high precision 40 Ar/39 Ar ages for Fish Canyon Tuff and Alder Creek Rhyolite sanidine: New dating standards required?, Geochi. et Cosmochim. Ac., 121, 229-239, 2013.

Pross, J., Tzedakis, P. C., Schmiedl, G., Christanis, K., Hooghiemstra, H., Müller, C., Ulrich, K., Ulrich, K., and Stavros, M.: Tenaghi Philippon (Greece) Revisited: Drilling a Continuous Lower-Latitude Terrestirial Climate archive of the Last 250,000 Years, Scientific Drilling, 5, 44-46, 2007.

Pyle, D. M., Ricketts, G. D., Margari, V., van Andela, T. H., Sinitsyn, A. A., Praslov, N. D., and Lisitsyn, S.: Wide dispersal and deposition of distal tephra during the Pleistocene 'Campanian Ignimbrite/Y5' eruption, Italy, Quaternary Sci. Rev., 25, 2713-2728, 2006.

Regattieri, E., Giaccio, B., Zanchetta, G., Drysdale, R. N., Galli, P., Nomade, S., Peronace, E., and Wulf, S.: Hydrological variability over the Apennines during the Early Last Glacial precession minimum, as revealed by a stable isotope record from Sulmona basin, Central Italy, J. Quaternary Sci., 30, 19-31, 2015.

Regattieri, E., Giaccio, B., Galli, P., Nomade, S., Peronace, E., Messina P., Sposato, A., Boschi, C. and Gemelli, M.: A multi-proxy record of MIS 11-12 deglaciation and glacial MIS 12 instability from the Sulmona Basin (central Italy), Quaternary Sci Rev. 132, 129-145, 2016.

Reicherter, K., Hoffmann, N., Lindhorst, K., Krastel, S., Fernández-Steeger, T., Grützner, C., and Wiatr, T.: Active basins and neotectonics: morphotectonics of the Lake Ohrid Basin (FYROM and Albania), Z. Dtsch. Ges. Geowiss., 162, 217-234, 2011.

Renne, P. R., Mundil, R., Balco, G., Min, K., and Ludwig, K. R.: Joint determination of 40 K decay constants and 40 Ar∗/40 K for the Fish Canyon sanidine standard, and improved accuracy for 40 Ar/39 Ar geochronology, Geochim. Cosmochim. Ac., 74, 5349-5367, 2010.

Robertson, A. and Shallo, M.: Mesozoic–Tertiary tectonic evolution of Albania in its regional Eastern Mediterranean context, Tectonophysics, 316, 197-254, 2000.

Rolandi, G., Bellucci, F., Heizler, M. T., Belkin, H. E., and De Vivo, B.: Tectonic controls on the genesis of ignimbrites from the Campanian Volcanic Zone, southern Italy, Miner. Petrol., 79, 3-31, 2003.

Rotolo, S. G., Scaillet, S., La Felice, S., and Vita-Sceillet, G.: A revision of the structure and stratigraphgy of pre-Green Tuff ignimbrites at Pantelleria (Strait of Silicy), J. Volcanol. Geoth. Res., 250, 61-74, 2013.

Rouchon, V., Gillot, P. Y., Quidelleur, X., Chiesa, S., and Floris, B.: Temporal evolution of the Roccamonfina volcanic complex (Pleistocene), Central Italy, J. Volcanol. Geoth. Res., 177, 500-514, 2008.

Roulleau, E., Pinti, D. L., Rouchon, V., Quidelleur, X., and Gillot, P.-Y.: Tephro-chronostratigraphy of the lacustrine interglacial record of Piànico, Italian Southern Alps: Identifying the volcanic sources using radiogenic isotopes and trace elements, Quatern. Int., 204, 31-43, 2009.

Russo Ermolli, E., Aucelli, P. P. C., Di Rollo, A., Mattei, M., Petrosino, P., Porreca, M., and Rosskopf, C. M.: An integrated stratigraphical approach to the Middle Pleistocene succession of the Sessano basin (Molise, Italy), Quatern. Int., 225, 114-127, 2010.

Sagnotti, L., Scardia, G., Giaccio, B., Liddicoat, J. C., Nomade, S., Renne, P. R., and Sprain, C. J.: Extremely rapid directional change during Matuyama-Brunhes geomagnetic polarity reversal, Geophysical Journal International, 199, 1110-1124, 2014.

Santacroce, R., Cioni, R., Marianelli, P., Sbrana, A., Sulpizio, R., Zanchetta, G., Donahue, D. J., and Joron, J. L.: Age and whole rock–glass compositions of proximal pyroclastics from the major explosive eruptions of Somma-Vesuvius: A review as a tool for distal tephrostratigraphy, J. Volcanol. Geoth. Res., 177, 1-18, 2008.

Sarna-Wojcicki, A.: Tephrochronology, in: Quaternary Geochronology, edited by: Noller, J. S., Sowers, J. M., and Lettis, W. R., AGU Reference Shelf, American Geophysical Union, Washington, DC, 2013.

Satow, C., Tomlinson, E. L., Grant, K. M., Albert, P. G., Smith, V. C., Manning, C. J., Ottolini, L., Wulf, S., Rohling, E. J., Lowe, J. J., Blockley, S. P. E., and Menzies, M. A.: A new contribution to the Late Quaternary tephrostratigraphy of the Mediterranean: Aegean Sea core LC21, Quaternary Sci. Rev., 117, 96-112, 2015.

Scaillet, S., Vita-Sceillet, G., and Rotolo, S. G.: Millennial-scale phase relationshhips between ice-core and Mediterranean marine records: insights from high-precision $^{40}Ar/^{39}Ar$ dating of the Green Tuff of Pantelleria, Silicy Strait, Quaternary Sci. Rev., 78, 141-154, 2013.

Siani, G., Sulpizio, R., Paterne, M., and Sbrana, A.: Tephrostratigraphy study for the last 18,000 C-14 years in a deep-sea sediment sequence for the South Adriatic, Quaternary Sci Rev, 23, 2485-2500, 2004.

Sottili, G., Palladino, D. M., and Zanon, V.: Plinian activity during the early eruptive history of the Sabatini volcanic district, central Italy, J. Volcanol. Geoth. Res., 135, 361-379, 2004.

St. Seymour, K., Christanis, K., Bouzinos, A., Papazisimou, S., Papatheodorou, G., Moran, E., and Denes, G.: Tephrostratigraphy and tephrochronology in the Philippi peat basin, Macedonia, Northern Hellas (Greece), Quatern. Int., 121, 53-65, 2004.

Steiger, R. H. and Jäger, E.: Subcommission on geochronology: Convention on the use of decay constants in geo- and cosmochronology, Earth Planet. Sc., 36, 359-362, 1977.

Stoppa, F., Rosatelli, G., Wall, F., and Jeffries, T.: Geochemistry of carbonatite–silicate pairs in nature: A case history from Central Italy, Lithos, 85, 26-47, 2005.

Sulpizio, R., Zanchetta, G., Paterne, M., and Siani, G.: A review of tephrostratigraphy in central and southern Italy during the last 65 ka, Il Quaternario Italian J. Quaternary Sci., 16, 91-108, 2003.

Sulpizio, R., Bonasia, R., Dellino, P., Di Vito, M. A., La Volpe, L., Mele, D., Zanchetta, G., and Sadori, L.: Discriminating the long distance dispersal of fine ash from sustained columns or near ground ash clouds: The example of the Pomici di Avellino eruption (Somma-Vesuvius, Italy), J. Volcanol. Geoth. Res., 177, 263-276, 2008.

Sulpizio, R., Zanchetta, G., D'Orazio, M., Vogel, H., and Wagner, B.: Tephrostratigraphy and tephrochronology of Lakes Ohrid and Prespa, Balkans, Biogeosciences, 7, 3273-3288, 2010.

Sulpizio, R., Alcicek, M. C., Zanchetta, G., and Solari, L.: Recognition of the Minoan tephra in the Acigöl Basin, Western Turkey: implications for inter-archive correlations and fine ash dispersal, J. Quaternary Sci., 28, 329-335, 2013.

Sumita, M. and Schmincke, H.-U.: Impact of volcanism on the evolution of Lake Van II: Temporal evolution of explosive volcanism of Nemrut Volcano (eastern Anatolia) during the past ca. 0.4 Ma, J. Volcanol. Geoth. Res., 253, 15-34, 2013.

Tamburrino, S., Insinga, D. D., Sprovieri, M., Petrosino, P., and Tiepolo, M.: Major and trace element characterization of tephra layers offshore Pantelleria Island: insights into the last 200 ka of volcanic activity and contribution to the Mediterranean tephrochronology, J. Quaternary Sci., 27, 129-140, 2012.

Thunell, R., Federman, A., Sparks, S., and Williams, D.: Age, origin and volcanological significance of the Y-5 ash layer in the Mediterranean, Quaternary Res., 12, 241-253, 1979.

Tomlinson, E. L., Arienzo, I., Civetta, L., Wulf, S., Smith, V. C., Hardiman, M., Lane, C. S., Carandente, A., Orsi, G., Rosi, M., Müller, W., and Menzies, M. A.: Geochemistry of the Phlegraean Fields (Italy) proximal sources for major Mediterranean tephras: Implications for the dispersal of Plinian and co-ignimbritic components of explosive eruptions, Geochim. Cosmochim. Ac., 93, 102-128, 2012.

Tomlinson, E. L., Smith, V. C., Albert, P. G., Aydar, E., Civetta, L., Cioni, R., Çubukçu, E., Gertisser, R., Isaia, R., Menzies, M. A., Orsi, G., Rosi, M., and Zanchetta, G.: The major and trace element glass compositions of the productive Mediterranean volcanic sources: tools for correlating distal tephra layers in and around Europe, Quaternary Sci. Rev., 118, 48-66, 2015.

Ton-That, T., Singer, B., and Paterne, M.: Ar-40/Ar-39 dating of latest Pleistocene (41 ka) marine tephra in the Mediterranean Sea: implications for global climate records, Earth Planet. Sc., 184, 645-658, 2001.

Turbeville, B. N.: Tephra Fountaining, Rheomorphism, and Spatter Flow during Emplacement of the Pitigliano Tuffs, Latera-Caldera, Italy, J. Volcanol. Geoth. Res., 53, 309-327, 1992a.

Turbeville, B. N.: 40Ar/39Ar Ages and stratigraphy of the Latera caldera, Italy, B. Volcanol., 55, 110-118, 1992b.

Tzedakis, P. C.: Long-term tree populations in northwest Greece through multiple Quaternary climatic cycles, Nature, 364, 437-440, 1993.

Vezzoli, L.: Tephra Layers in Bannock Basin (Eastern Mediterranean), Mar. Geol., 100, 21-34, 1991.

Villa, I.M. and Buettner, A.: Chronostratigraphy of Monte Vulture volcano (southern Italy): secondary mineral microtextures and 39Ar-40Ar systematics. B. Volcanol., 71, 1195-1208, 2009.

Vogel, H., Zanchetta, G., Sulpizio, R., Wagner, B., and Nowaczyk, N.: A tephrostratigraphic record for the last glacial-interglacial cycle from Lake Ohrid, Albania and Macedonia, J. Quaternary Sci., 25, 320-338, 2010.

Wagner, B., Reicherter, K., Daut, G., Wessels, M., Matzinger, A., Schwalb, A., Spirkovski, Z., and Sanxhaku, M.: The potential of Lake Ohrid for long-term palaeoenvironmental reconstructions, Palaeogeography Palaeoclimatology Palaeoecology, 259, 341-356, 2008.

Wagner, B., Vogel, H., Zanchetta, G., and Sulpizio, R.: Environmental change within the Balkan region during the past ca. 50 ka recorded in the sediments from lakes Prespa and Ohrid, Biogeosciences, 7, 3187-3198, 2010.

Wagner, B., Francke, A., Sulpizio, R., Zanchetta, G., Lindhorst, K., Krastel, S., Vogel, H., Rethemeyer, J., Daut, G., Grazhdani, A., Lushaj, B., and Trajanovski, S.: Possible earthquake trigger for 6th century mass wasting deposit at Lake Ohrid (Macedonia/Albania), Clim. Past, 8, 2069-2078, 2012.

Wagner, B., Wilke, T., Krastel, S., Zanchetta, G., Sulpizio, R., Reicherter, K., Leng, M. J., Grazhdani, A., Trajanovski, S., Francke, A., Lindhorst, K., Levkov, Z., Cvetkoska, A., Reed, J. M., Zhang, X., Lacey, J. H., Wonik, T., Baumgarten, H., and Vogel, H.: The SCOPSCO drilling project recovers more than 1.2 million years of history from Lake Ohrid, Scientific Drilling, 17, 19-29, 2014.

Washington, H. S.: The Roman comagmatic region, Carnegie Institution of Washington, 1906.

Watzin, M. C., Puka, V., and Naumoski, T. B.: Lake Ohrid and Its Watershed: Our Lake, Our Future. A State of the Environment Report., Tirana, Albania and Ohrid, Macedonia, 134 pp., 2002.

Wulf, S., Kraml, M., Brauer, A., Keller, J., and Negendank, J. F. W.: Tephrochronology of the 100ka lacustrine sediment record of Lago Grande di Monticchio (Southern Italy), Quatern. Int., 122, 7-30, 2004.

Wulf, S., Brauer, A., Mingram, J., Zolitschka, B., and Negendank, J. F. W.: Distal tephras in the sediments of Monticchio maar lakes, Principe, C., Regione Basilicata, Dipartimento Ambiente, Territorio e Politiche della Sostenibilità 2006.

Wulf, S., Keller, J., Paterne, M., Mingram, J., Lauterbach, S., Opitz, S., Sottili, G., Giaccio, B., Albert, P. G., Satow, C., Tomlinson, E. L., Viccaro, M., and Brauer, A.: The 100–133 ka record of Italian explosive volcanism and revised tephrochronology of Lago Grande di Monticchio, Quaternary Sci. Rev., 58, 104-123, 2012.

Zanchetta, G., Sulpizio, R., Giaccio, B., Siani, G., Paterne, M., Wulf, S., and D'Orazio, M.: The Y-3 tephra: A Last Glacial stratigraphic marker for the Central Mediterranean Basin, J. Volcanol. Geoth. Res., 177, 145-154, 2008.

Zanchetta, G., Sulpizio, R., Roberts, N., Cioni, R., Eastwood, W. J., Siani, G., Caron, B., Paterne, M., and Santacroce, R.: Tephrostratigraphy, chronology and climatic events of the Mediterranean basin during the Holocene: An overview, Holocene, 21, 33-52, 2011.

Zanchetta, G., Regattieri, E., Giaccio, B., Wagner, B., Sulpizio, R., Francke, A., Vogel, L. H., Sadori, L., Masi, A., Sinopoli, G., Lacey, J. H., Leng, M. L., and Leicher, N.: Aligning MIS5 proxy records from Lake Ohrid (FYROM) with independently dated Mediterranean archives: implications for core chronology, Biogeosciences Discuss., 12, 16979-17007, 2015.

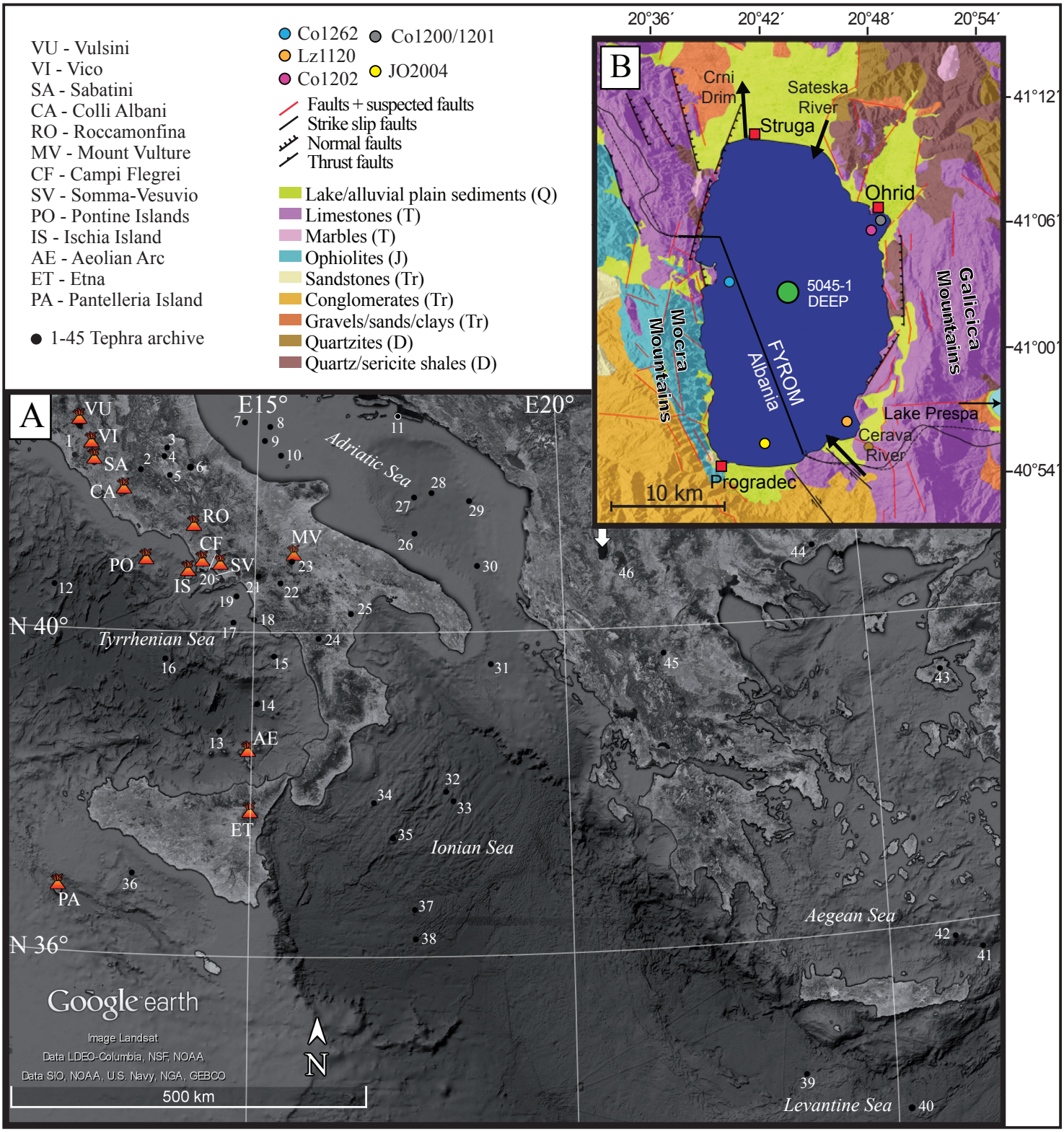
VU - Vulsini
VI - Vico
SA - Sabatini
CA - Colli Albani
RO - Roccamonfina
MV - Mount Vulture
CF - Campi Flegrei
SV - Somma-Vesuvio
PO - Pontine Islands
IS - Ischia Island
AE - Aeolian Arc
ET - Etna
PA - Pantelleria Island
● 1-45 Tephra archive
Co1262
Co1200/1201
Lz1120
Co1202
JO2004
Faults + suspected faults
Strike slip faults
Normal faults
Thrust faults
Lake/alluvial plain sediments (Q)
Limestones (T)
Marbles (T)
Ophiolites (J)
Sandstones (Tr)
Conglomerates (Tr)
Gravels/sands/clays (Tr)
Quartzites (D)
Quartz/sericite shales (D)
A
B
E15°
E20°
N 40°
N 36°
Adriatic Sea
Tyrrhenian Sea
Ionian Sea
Aegean Sea
Levantine Sea
20°36´
20°42´
20°48´
20°54´
41°12´
41°06´
41°00´
40°54´
Crni Drim
Sateska River
Struga
Ohrid
5045-1 DEEP
Galicica Mountains
Mocra Mountains
FYROM
Albania
Lake Prespa
Cerava River
Prigradec
10 km
Google earth
Image Landsat
Data LDEO-Columbia, NSF, NOAA
Data SIO, NOAA, U.S. Navy, NGA, GEBCO
500 km
N

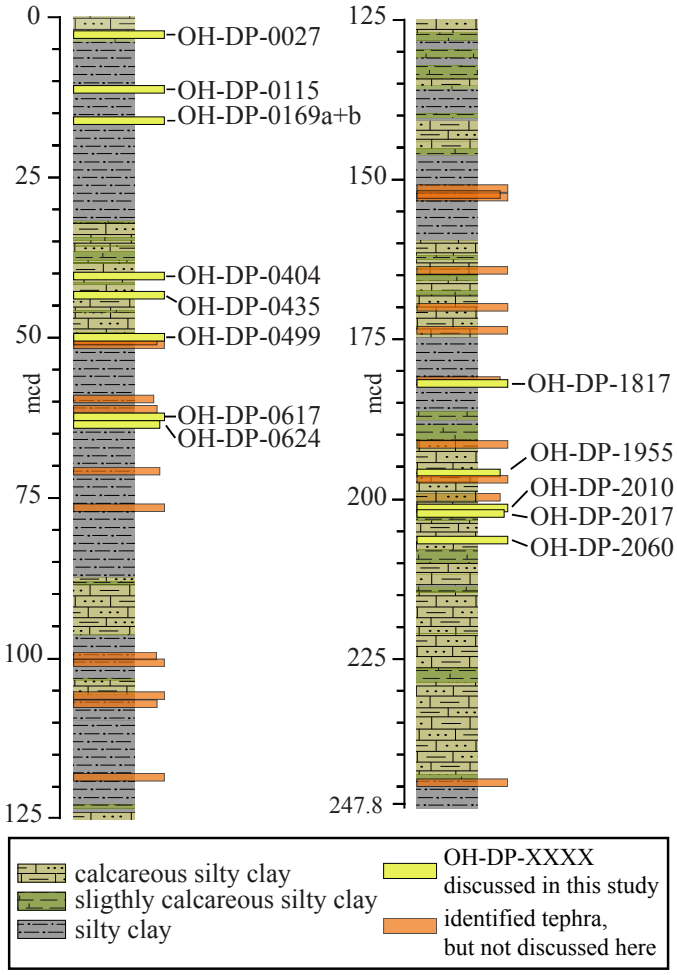
0
25
50
mcd
75
100
125
OH-DP-0027
OH-DP-0115
OH-DP-0169a+b
OH-DP-0404
OH-DP-0435
OH-DP-0499
OH-DP-0617
OH-DP-0624
125
150
175
mcd
200
225
247.8
OH-DP-1817
OH-DP-1955
OH-DP-2010
OH-DP-2017
OH-DP-2060
calcareous silty clay
sligthly calcareous silty clay
silty clay
OH-DP-XXXX
discussed in this study
identified tephra,
but not discussed here

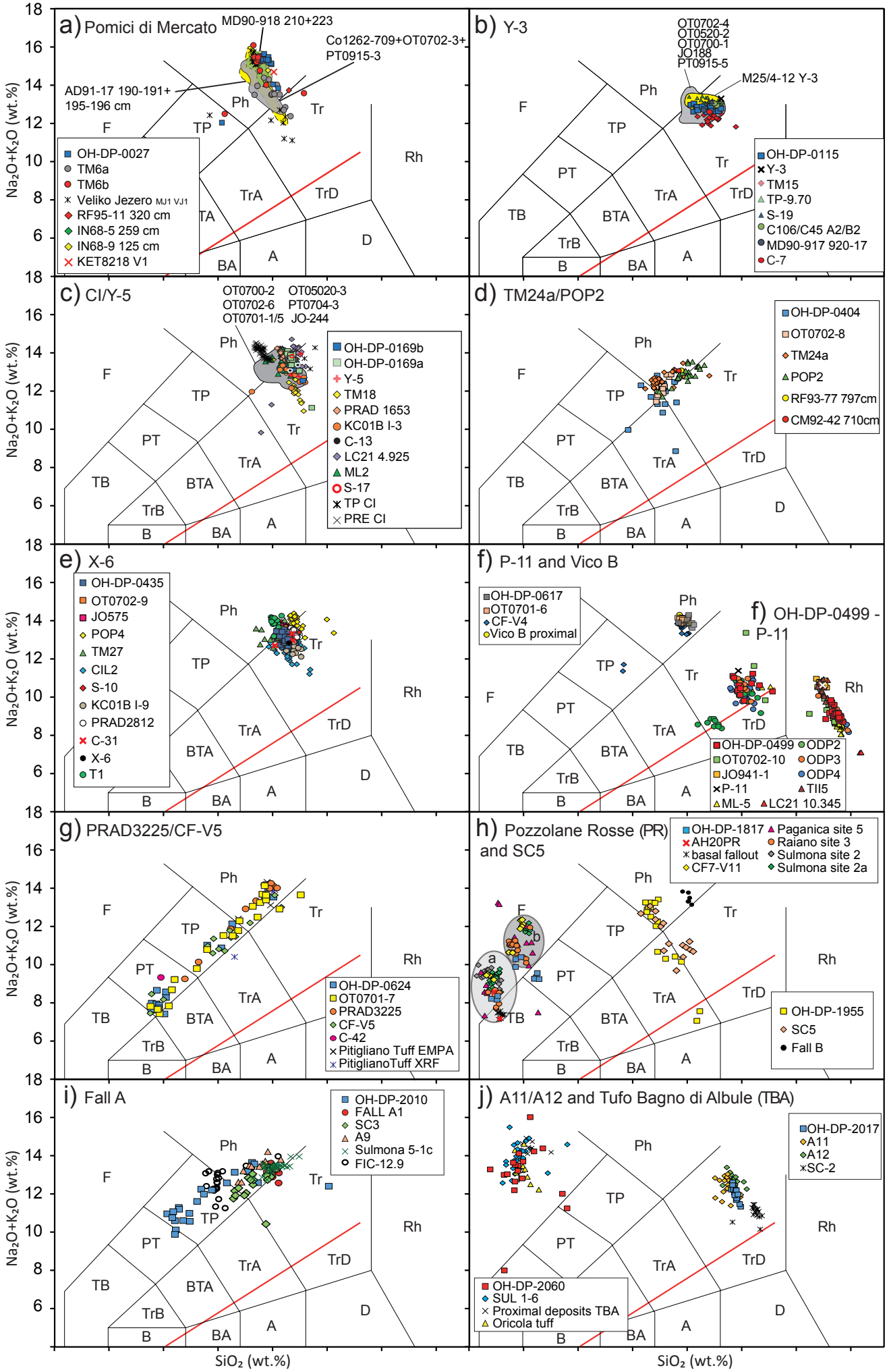
a) Pomici di Mercato
MD90-918 210+223
Co1262-709+OT0702-3+
PT0915-3
AD91-17 190-191+
195-196 cm
OH-DP-0027
TM6a
TM6b
Veliko Jezero MJ1 VJ1
RF95-11 320 cm
IN68-5 259 cm
IN68-9 125 cm
KET8218 V1
b) Y-3
OT0702-4
OT0520-2
OT0700-1
JO188
PT0915-5
M25/4-12 Y-3
OH-DP-0115
Y-3
TM15
TP-9.70
S-19
C106/C45 A2/B2
MD90-917 920-17
C-7
c) CI/Y-5
OT0700-2
OT0702-6
OT0701-1/5
OT05020-3
PT0704-3
JO-244
OH-DP-0169b
OH-DP-0169a
Y-5
TM18
PRAD 1653
KC01B I-3
C-13
LC21 4.925
ML2
S-17
TP CI
PRE CI
d) TM24a/POP2
OH-DP-0404
OT0702-8
TM24a
POP2
RF93-77 797cm
CM92-42 710cm
e) X-6
OH-DP-0435
OT0702-9
JO575
POP4
TM27
CIL2
S-10
KC01B I-9
PRAD2812
C-31
X-6
T1
f) P-11 and Vico B
OH-DP-0617
OT0701-6
CF-V4
Vico B proximal
f) OH-DP-0499 - P-11
OH-DP-0499
OT0702-10
JO941-1
P-11
ML-5
ODP2
ODP3
ODP4
TII5
LC21 10.345
g) PRAD3225/CF-V5
OH-DP-0624
OT0701-7
PRAD3225
CF-V5
C-42
Pitigliano Tuff EMPA
PitiglianoTuff XRF
h) Pozzolane Rosse (PR) and SC5
OH-DP-1817
AH20PR
basal fallout
CF7-V11
Paganica site 5
Raiano site 3
Sulmona site 2
Sulmona site 2a
OH-DP-1955
SC5
Fall B
i) Fall A
OH-DP-2010
FALL A1
SC3
A9
Sulmona 5-1c
FIC-12.9
j) A11/A12 and Tufo Bagno di Albule (TBA)
OH-DP-2017
A11
A12
SC-2
OH-DP-2060
SUL 1-6
Proximal deposits TBA
Oricola tuff
Ph
Tr
Rh
F
TP
PT
TA
TrA
TrD
TB
BTA
TrB
B
BA
A
D
Na2O+K2O (wt.%)
SiO2 (wt.%)

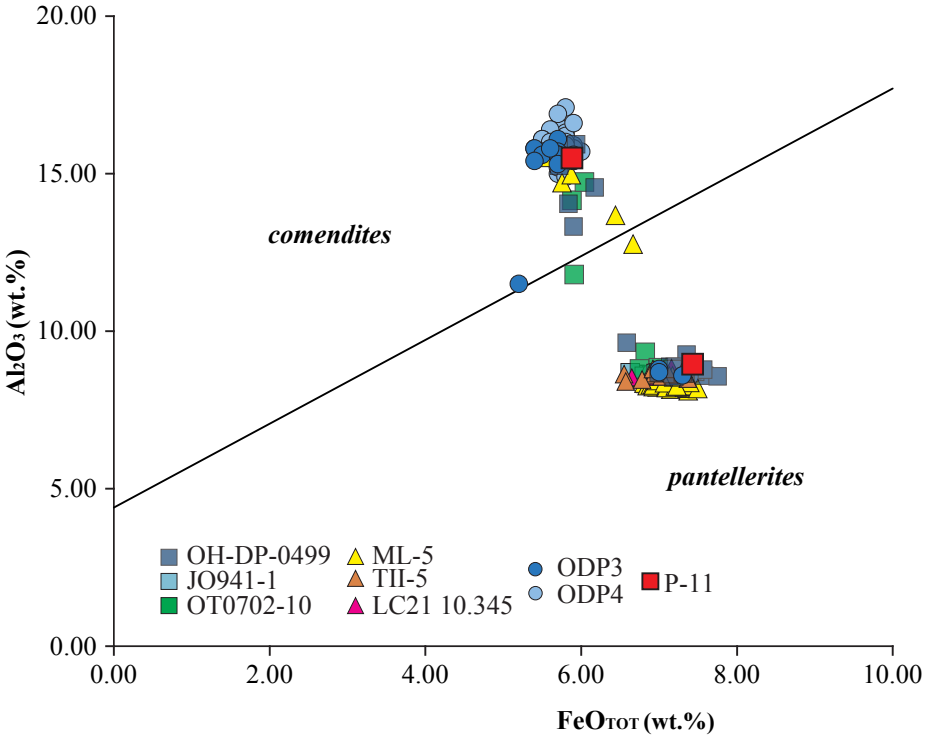
20.00
15.00
10.00
5.00
0.00
0.00
2.00
4.00
6.00
8.00
10.00
Al2O3 (wt.%)
FeOTOT (wt.%)
comendites
pantellerites
OH-DP-0499
JO941-1
OT0702-10
ML-5
TII-5
LC21 10.345
ODP3
ODP4
P-11

a) OH-DP-0617 / Vico B

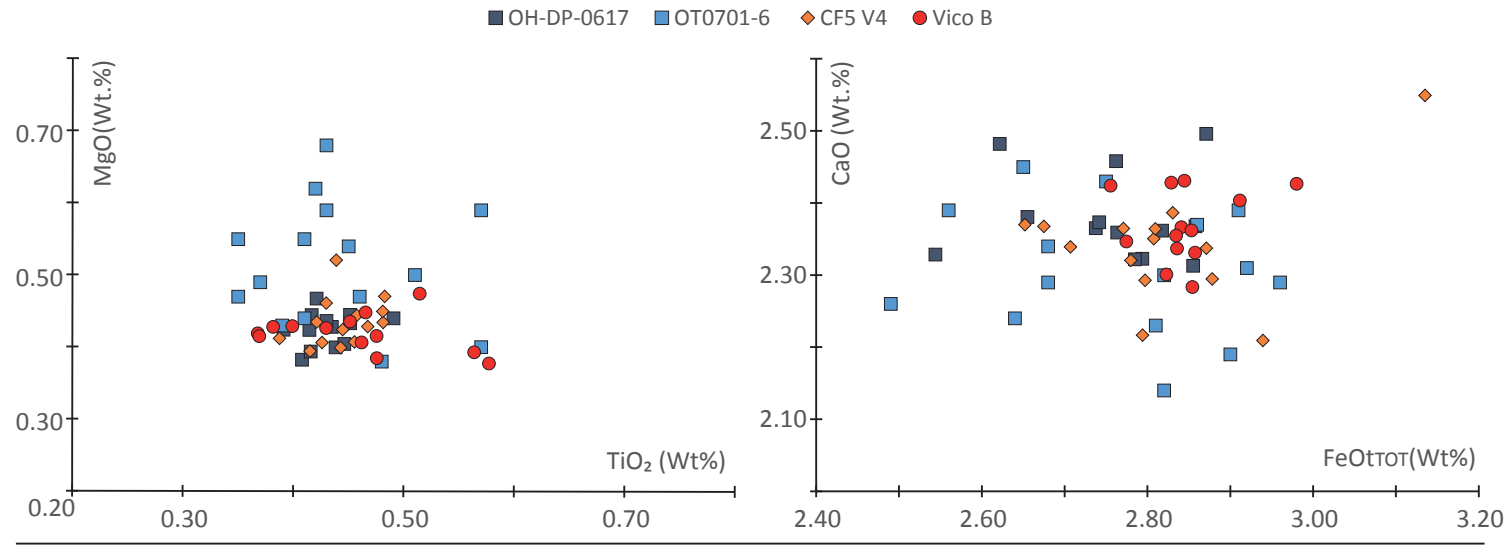

b) OH-DP-06247 / PRAD3225 / CF5-V5

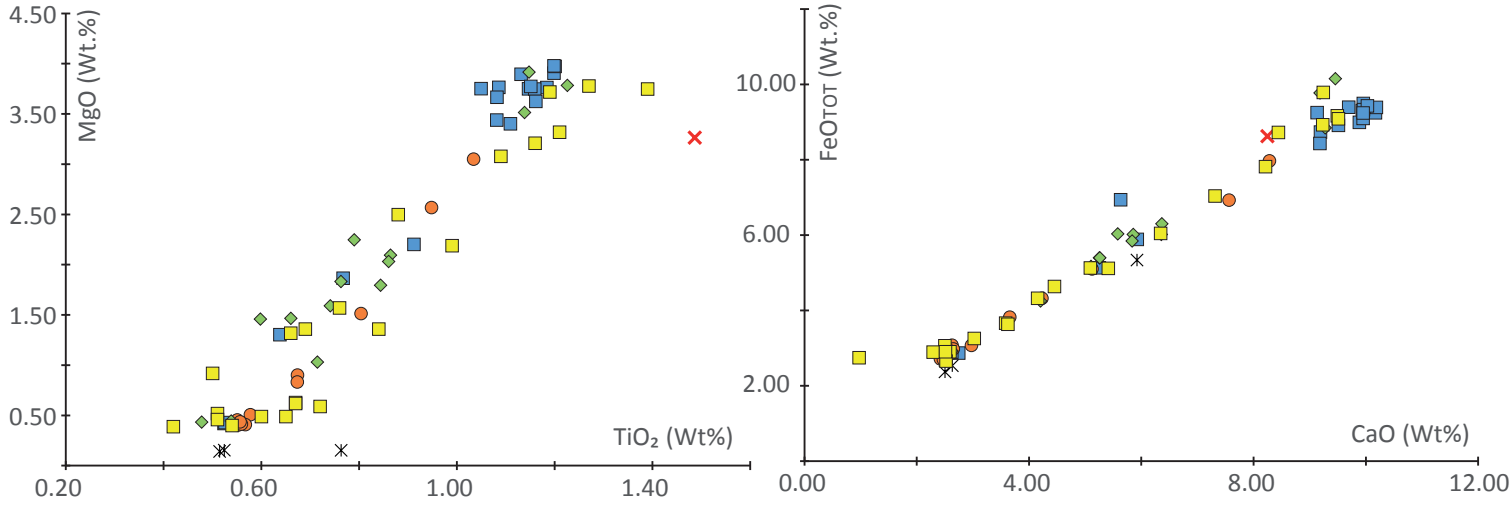

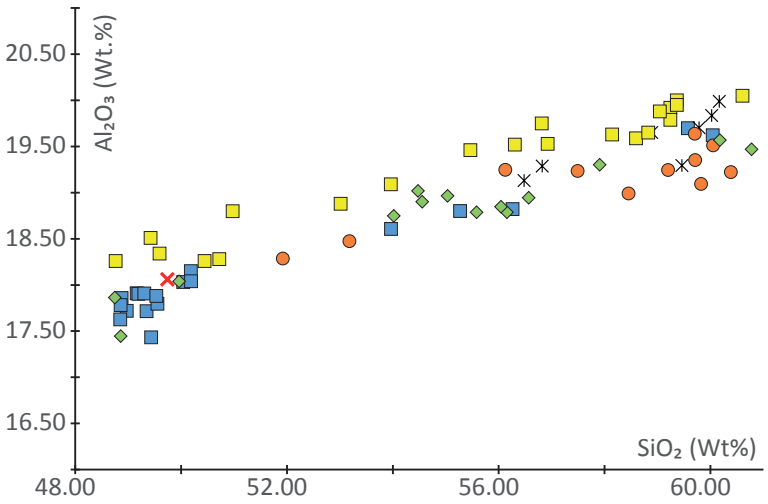

c) OH-DP-1817 / Pozzolane Rosse

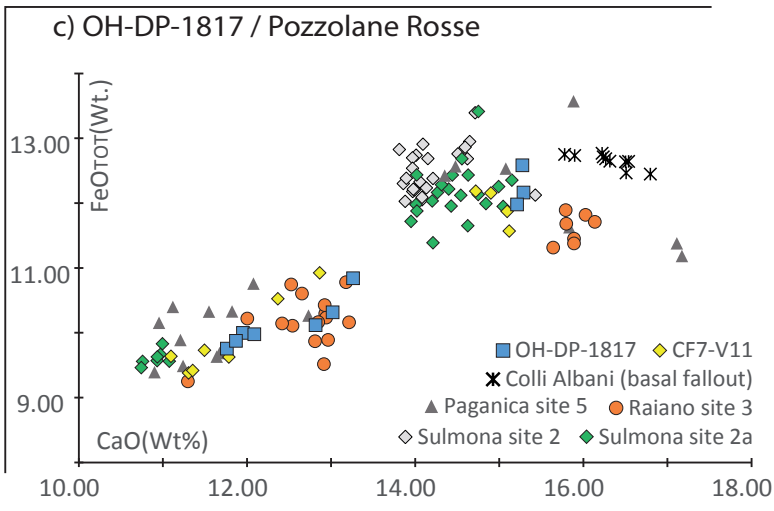

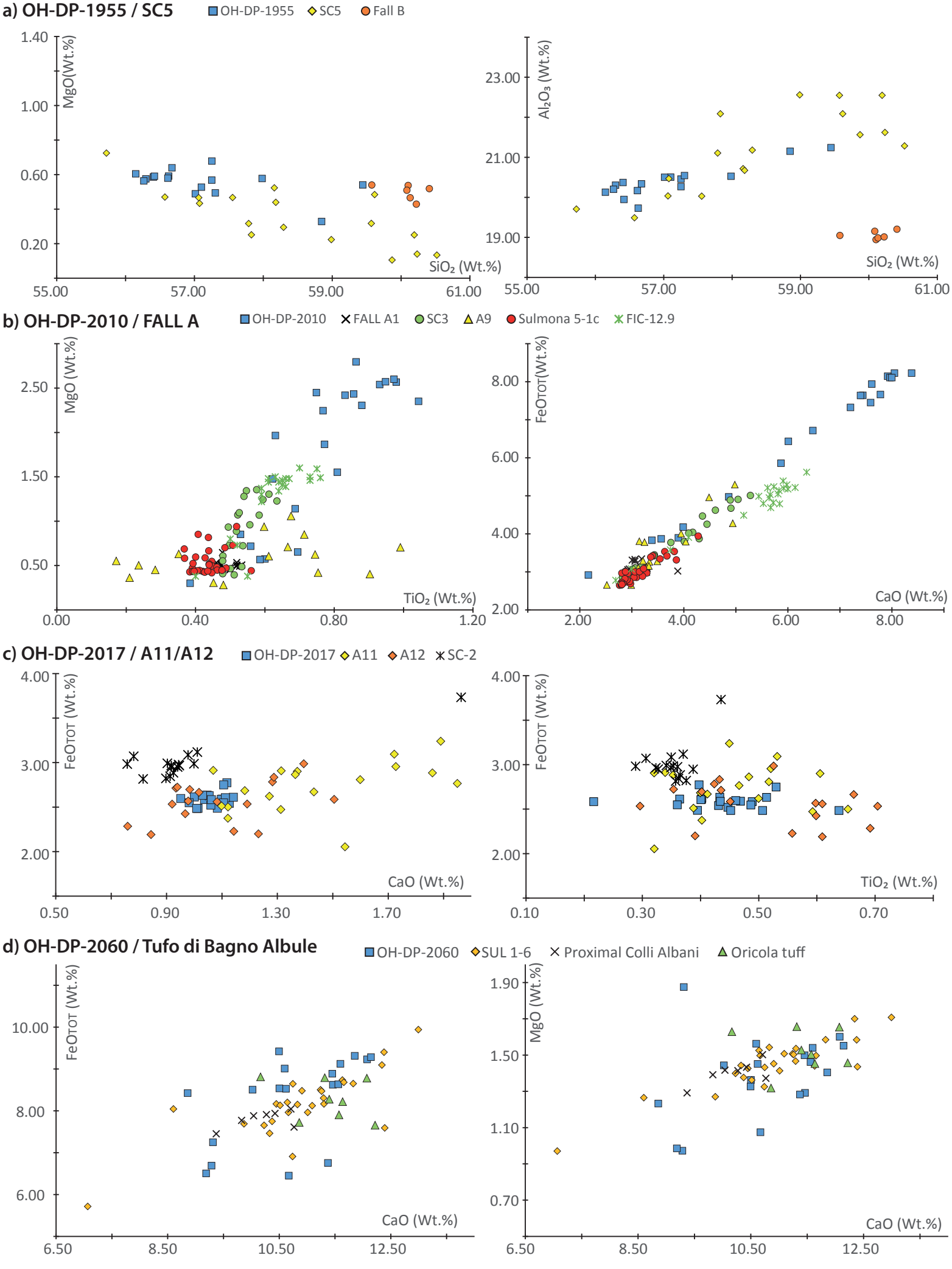
a) OH-DP-1955 / SC5
OH-DP-1955
SC5
Fall B
MgO(Wt.%)
SiO₂ (Wt.%)
Al₂O₃ (Wt.%)
b) OH-DP-2010 / FALL A
OH-DP-2010
FALL A1
SC3
A9
Sulmona 5-1c
FIC-12.9
MgO (Wt.%)
TiO₂ (Wt.%)
FeOTOT(Wt.%)
CaO (Wt.%)
c) OH-DP-2017 / A11/A12
OH-DP-2017
A11
A12
SC-2
FeOTOT (Wt.%)
CaO (Wt.%)
TiO₂ (Wt.%)
d) OH-DP-2060 / Tufo di Bagno Albule
OH-DP-2060
SUL 1-6
Proximal Colli Albani
Oricola tuff
FeOTOT (Wt.%)
MgO (Wt.%)
CaO (Wt.%)

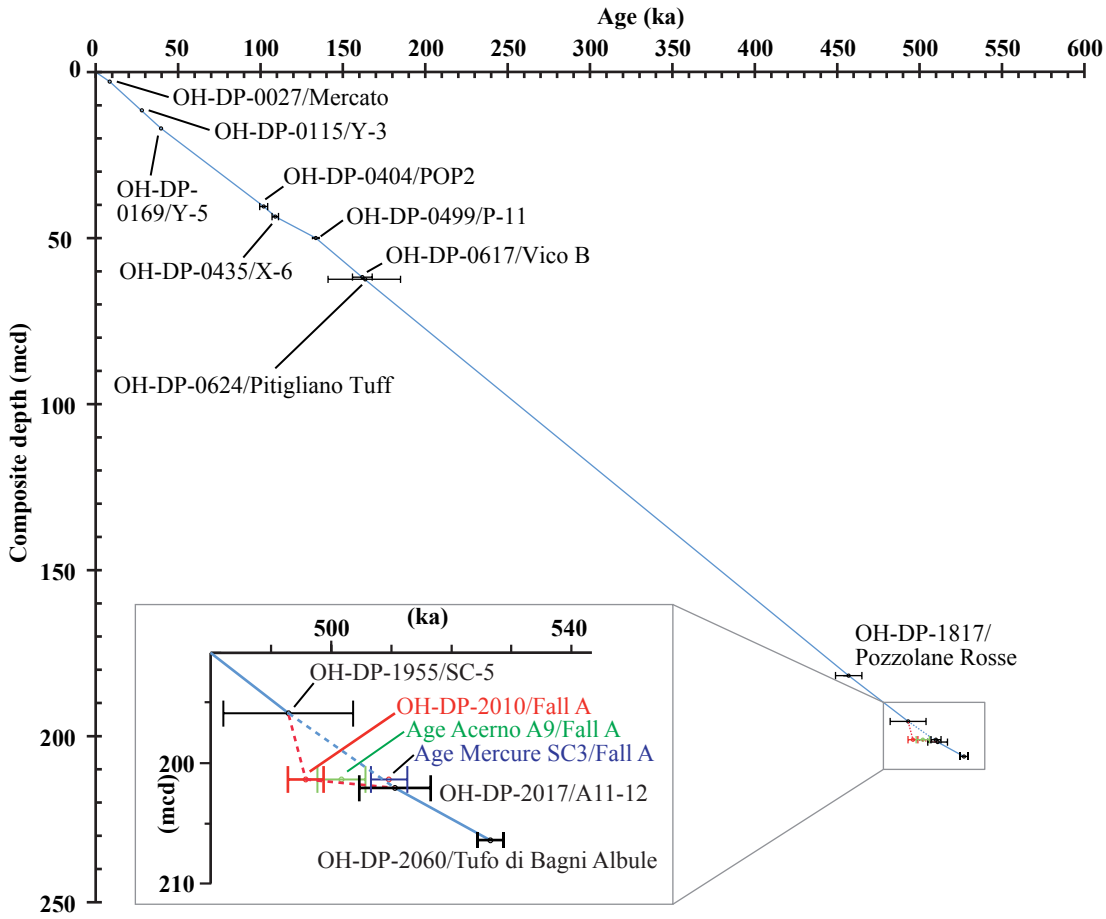
Age (ka)
0
50
100
150
200
250
300
350
400
450
500
550
600
Composite depth (mcd)
OH-DP-0027/Mercato
OH-DP-0115/Y-3
OH-DP-
0169/Y-5
OH-DP-0404/POP2
OH-DP-0499/P-11
OH-DP-0435/X-6
OH-DP-0617/Vico B
OH-DP-0624/Pitigliano Tuff
OH-DP-1817/
Pozzolane Rosse
(ka)
500
540
OH-DP-1955/SC-5
OH-DP-2010/Fall A
Age Acerno A9/Fall A
Age Mercure SC3/Fall A
OH-DP-2017/A11-12
OH-DP-2060/Tufo di Bagni Albule
(mcd)
200
210

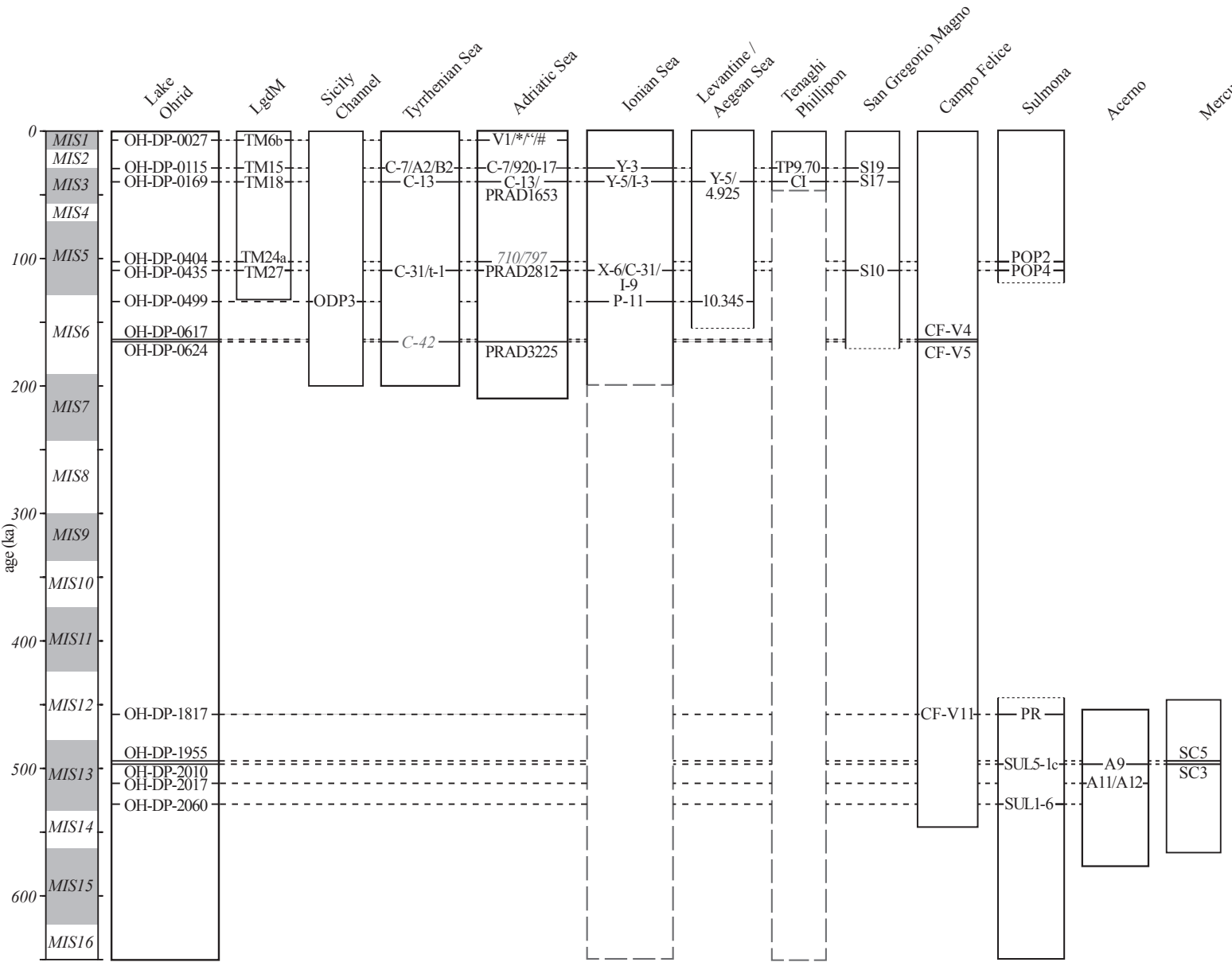
Lake Ohrid
LgdM
Sicily Channel
Tyrrhenian Sea
Adriatic Sea
Ionian Sea
Levantine / Aegean Sea
Tenaghi Phillipon
San Gregorio Magno
Campo Felice
Sulmona
Acerno
Mercure
age (ka)
0
100
200
300
400
500
600
MIS1
MIS2
MIS3
MIS4
MIS5
MIS6
MIS7
MIS8
MIS9
MIS10
MIS11
MIS12
MIS13
MIS14
MIS15
MIS16
OH-DP-0027
OH-DP-0115
OH-DP-0169
OH-DP-0404
OH-DP-0435
OH-DP-0499
OH-DP-0617
OH-DP-0624
OH-DP-1817
OH-DP-1955
OH-DP-2010
OH-DP-2017
OH-DP-2060
TM6b
TM15
TM18
TM24a
TM27
ODP3
V1/*/^/#
C-7/A2/B2
C-13
C-7/920-17
C-13/
PRAD1653
710/797
PRAD2812
C-31/t-1
C-42
PRAD3225
Y-3
Y-5/I-3
X-6/C-31/
I-9
P-11
Y-5/
4.925
10.345
TP9.70
CI
S19
S17
S10
CF-V4
CF-V5
CF-V11
POP2
POP4
PR
SUL5-1c
SUL1-6
A9
A11/A12
SC5
SC3

Supplement I:

a) OH-DP-0027 - Pomici di Mercato

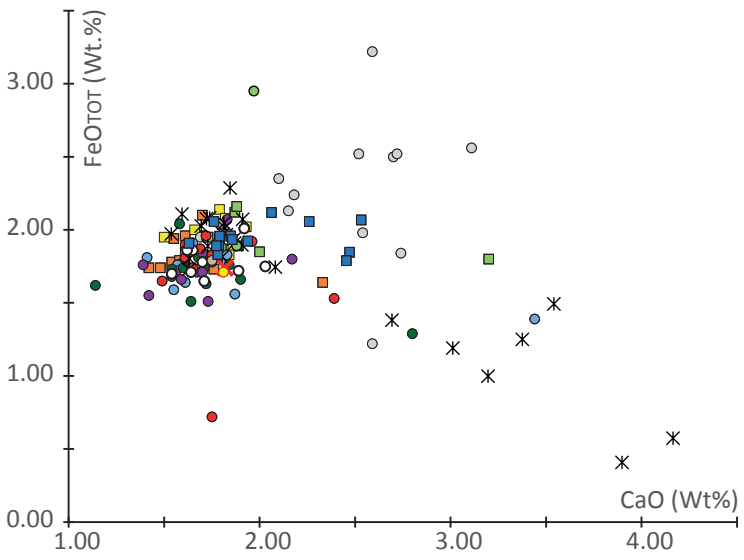

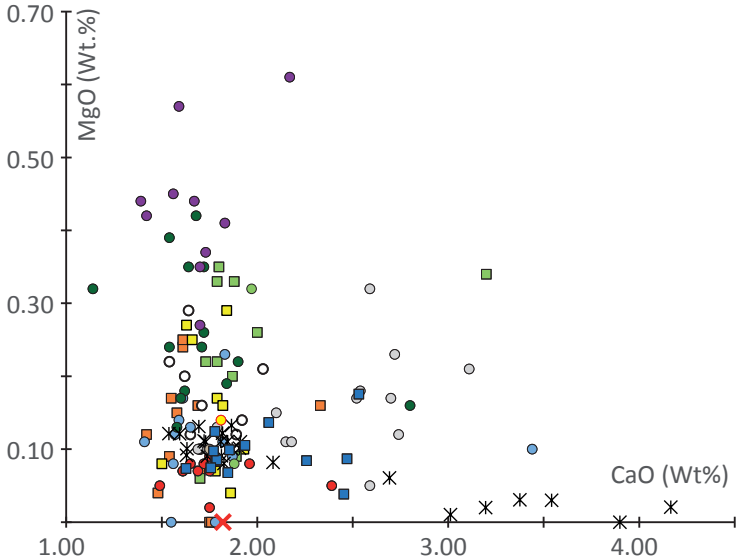

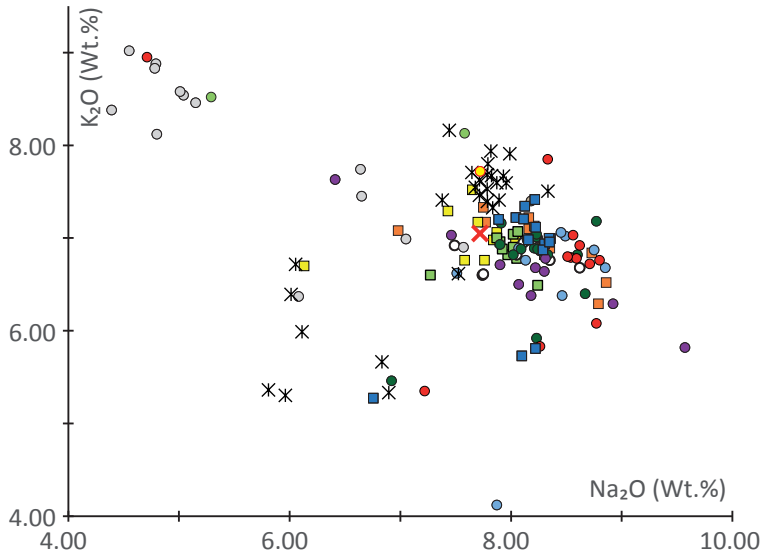

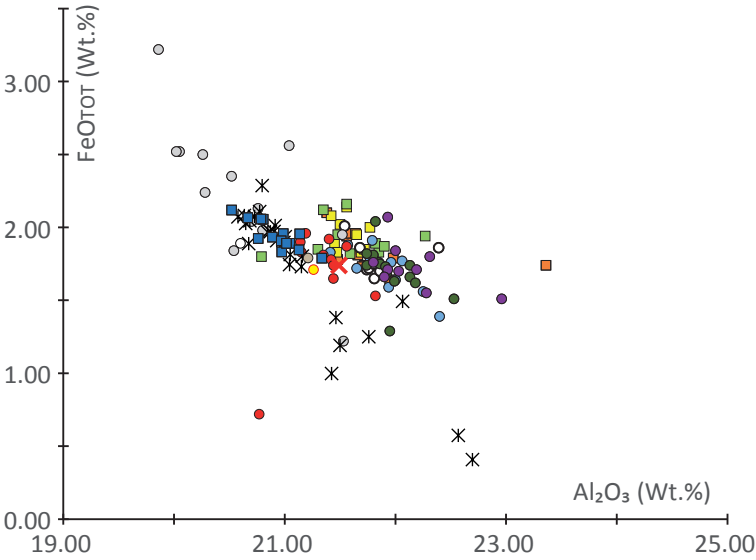

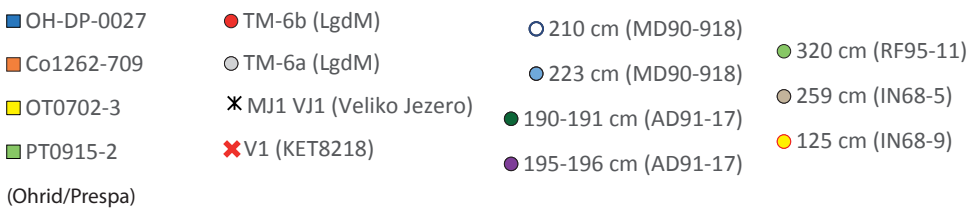

b) OH-DP-0115 - Y-3

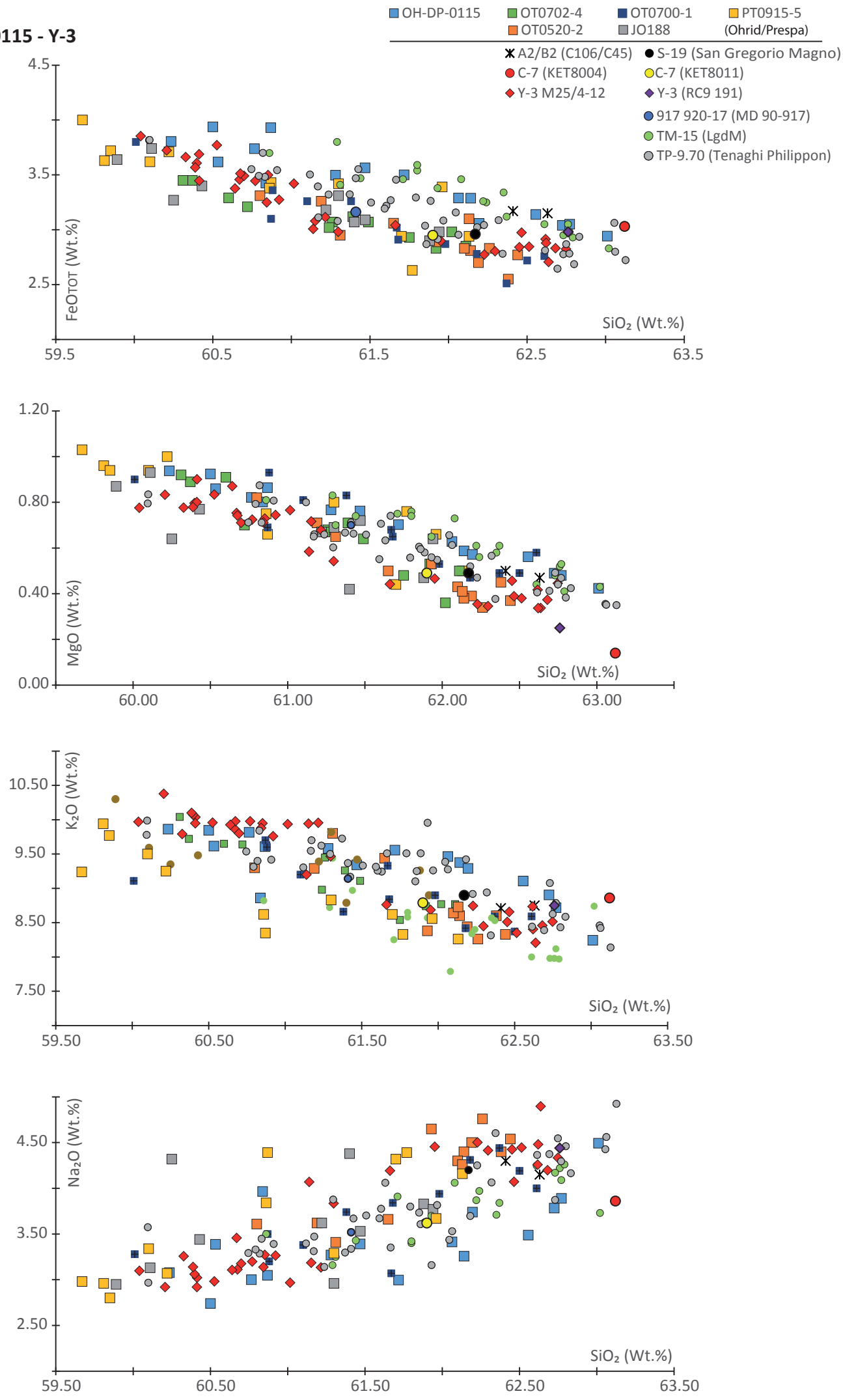

c) OH-DP-0169 - Y-5/CI

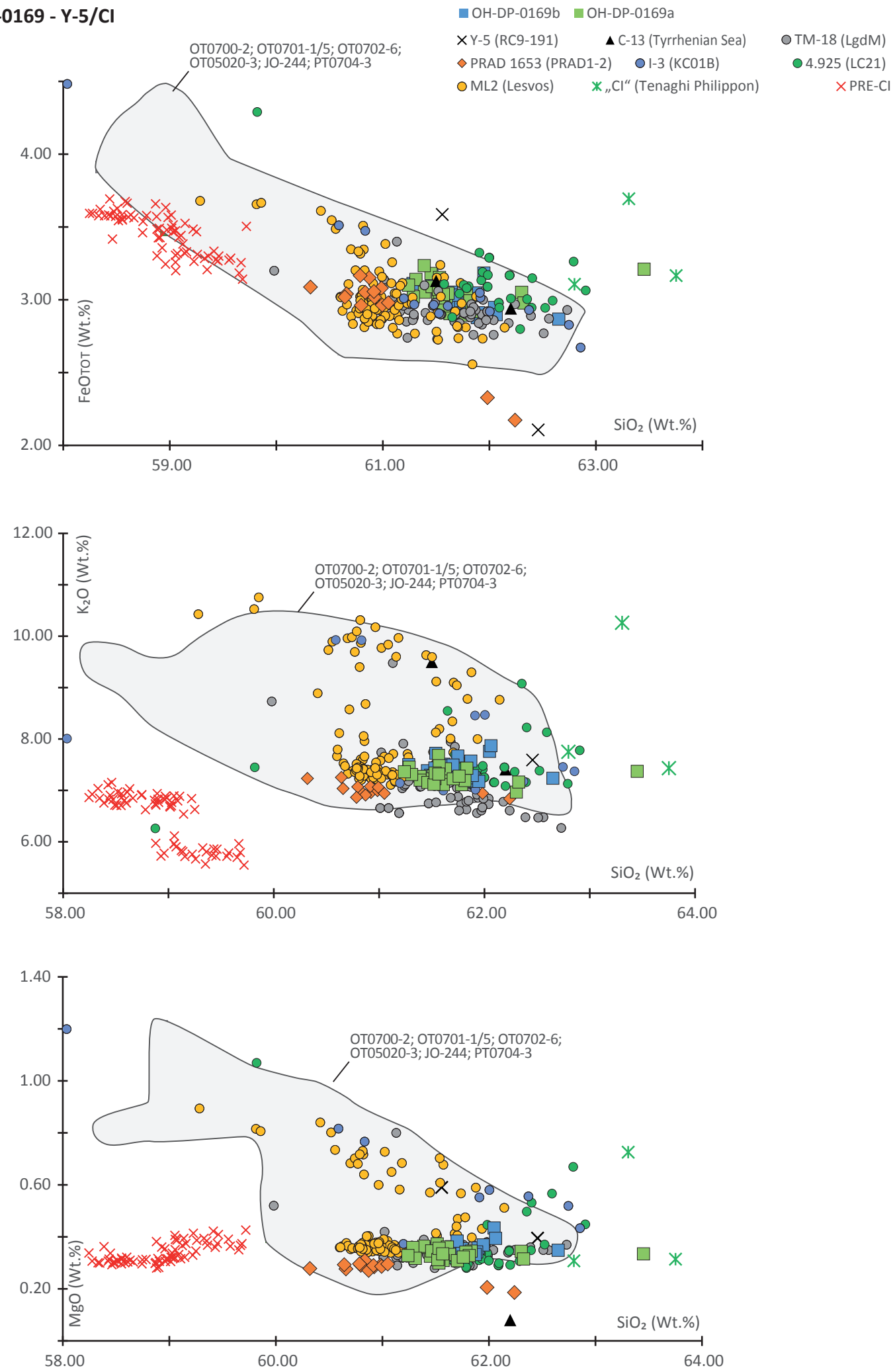

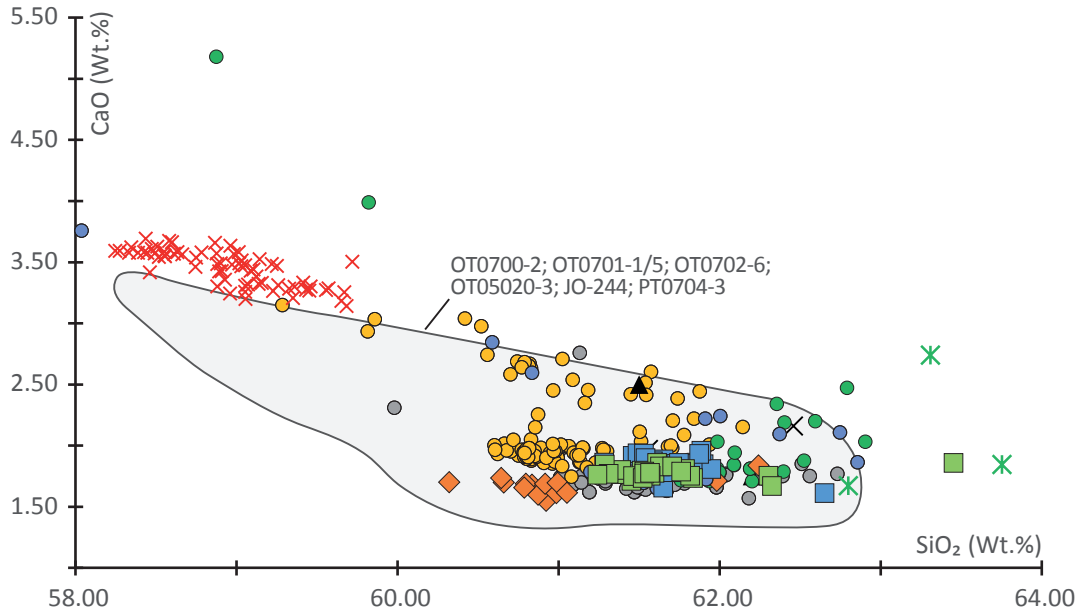

d)OH-DEP-0404 TM24a/POP2

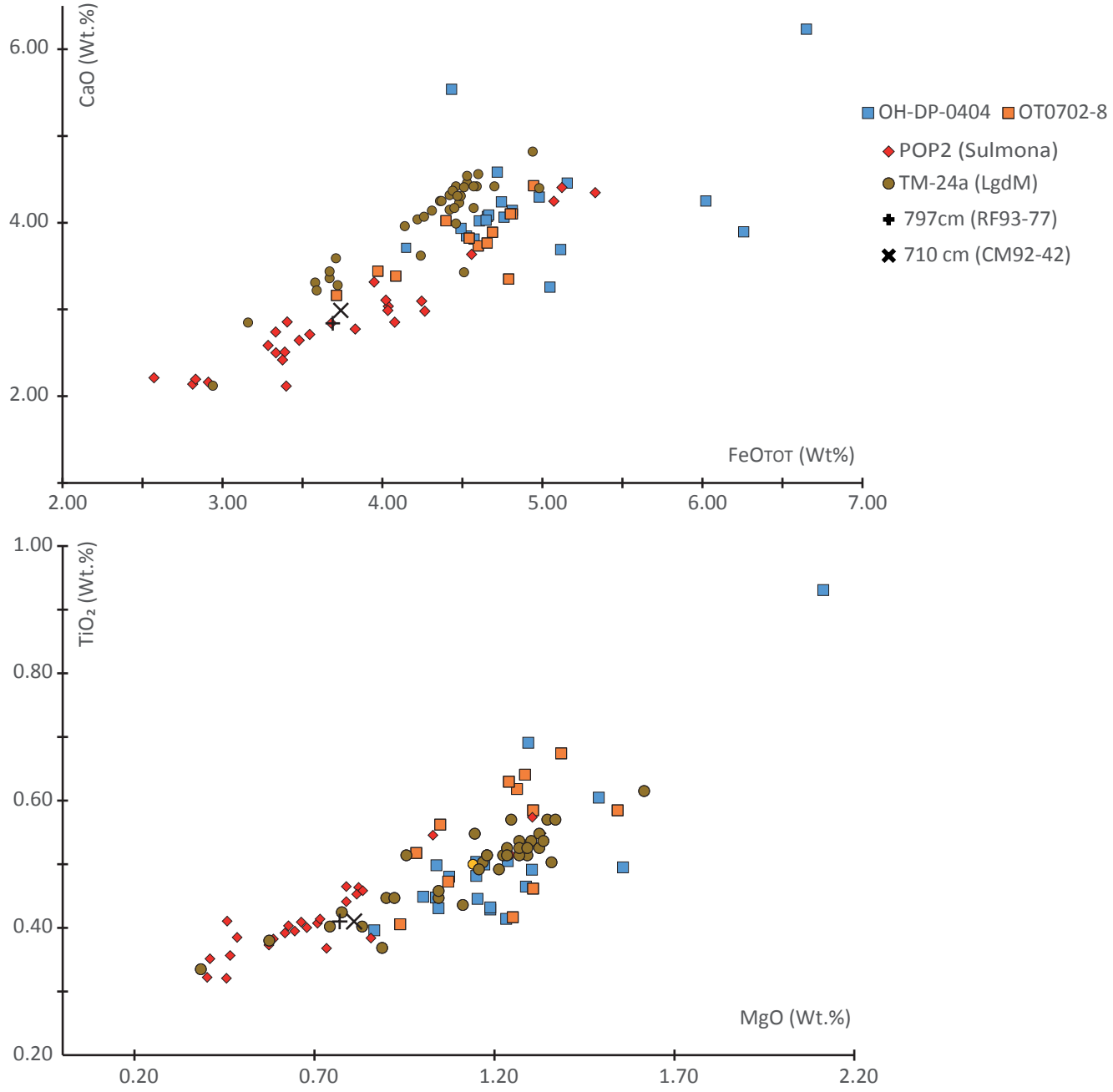

e) OH-DP-0435 - X-6

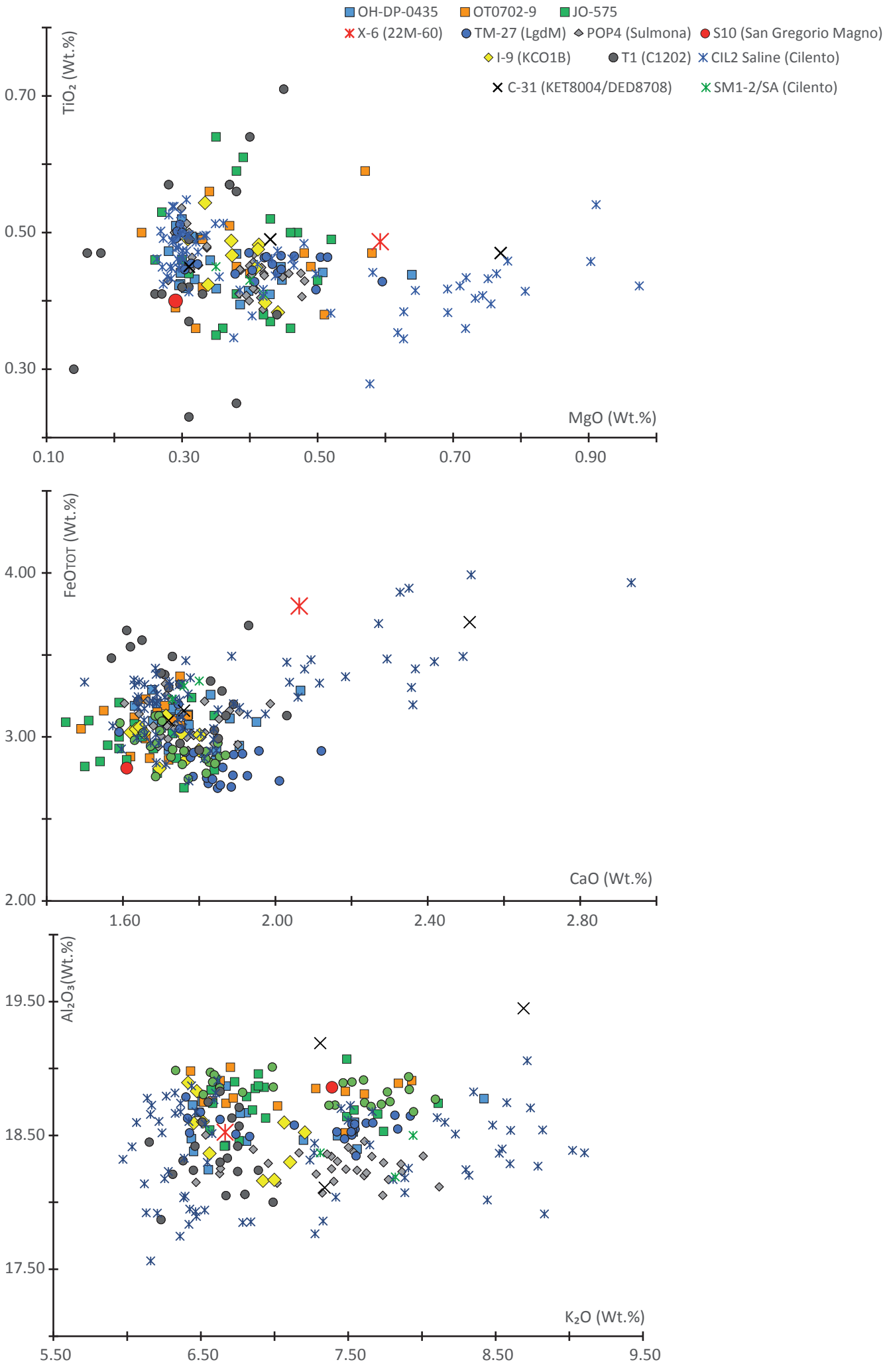

f) OH-DP-0499 - P-11

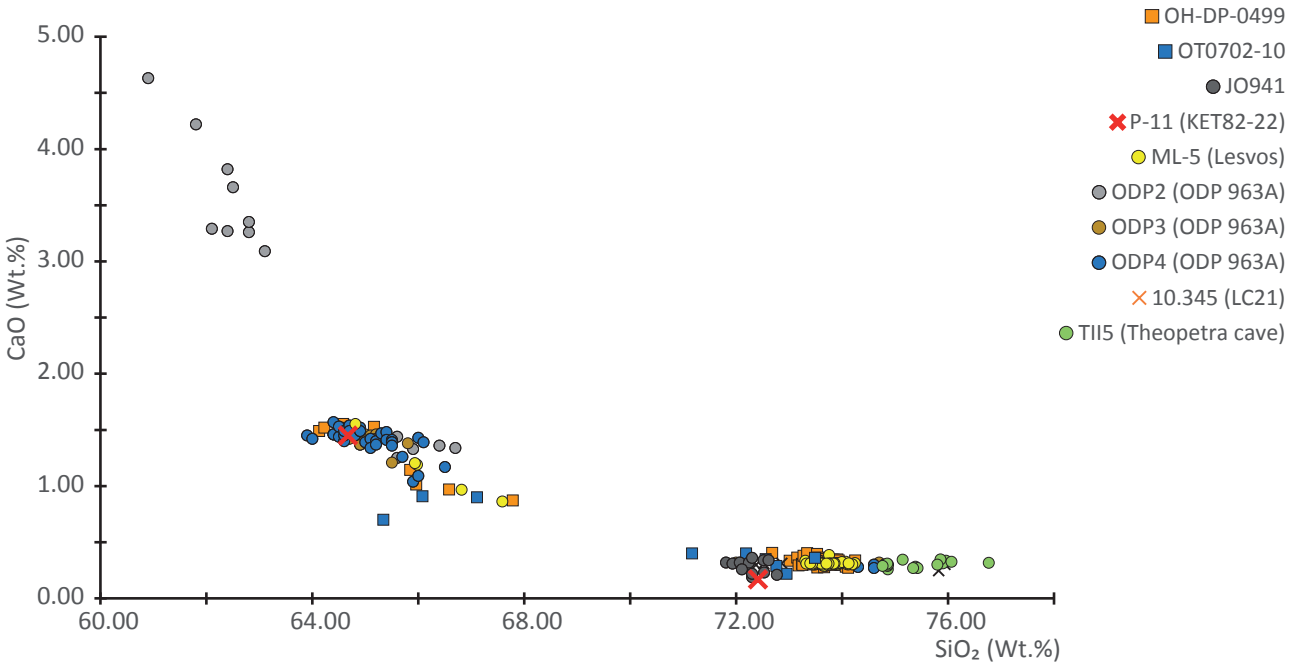

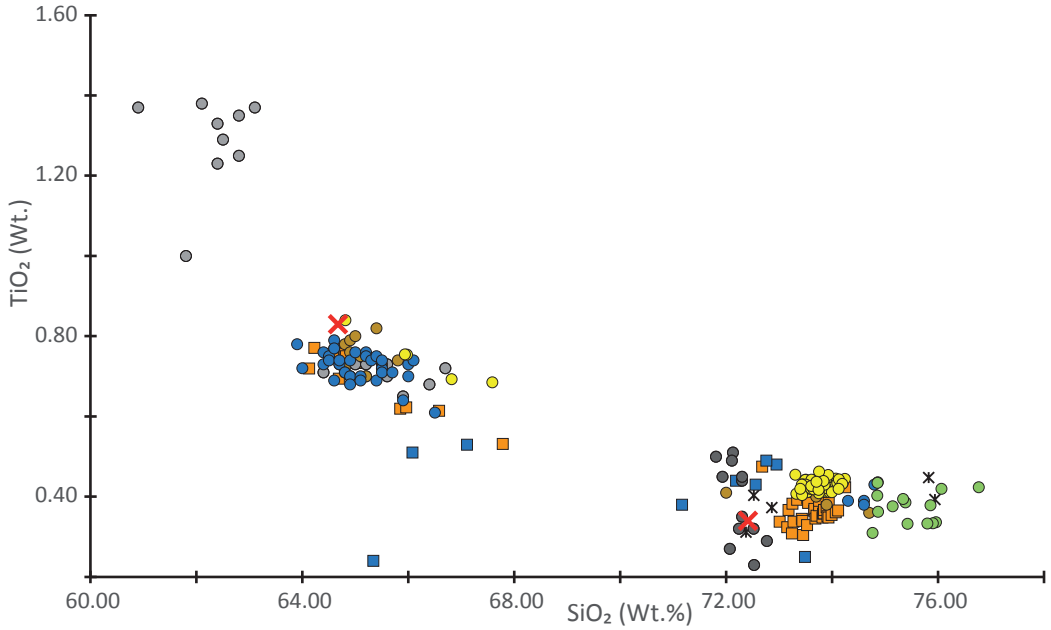

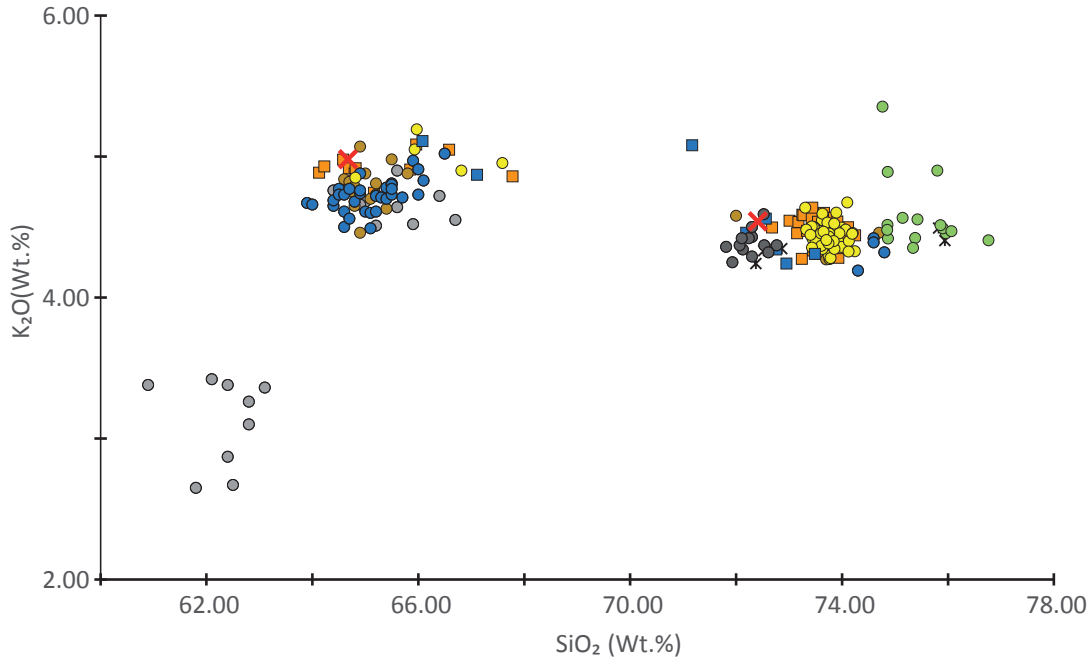

g) OH-DP-1817 - Pozzolane Rosse

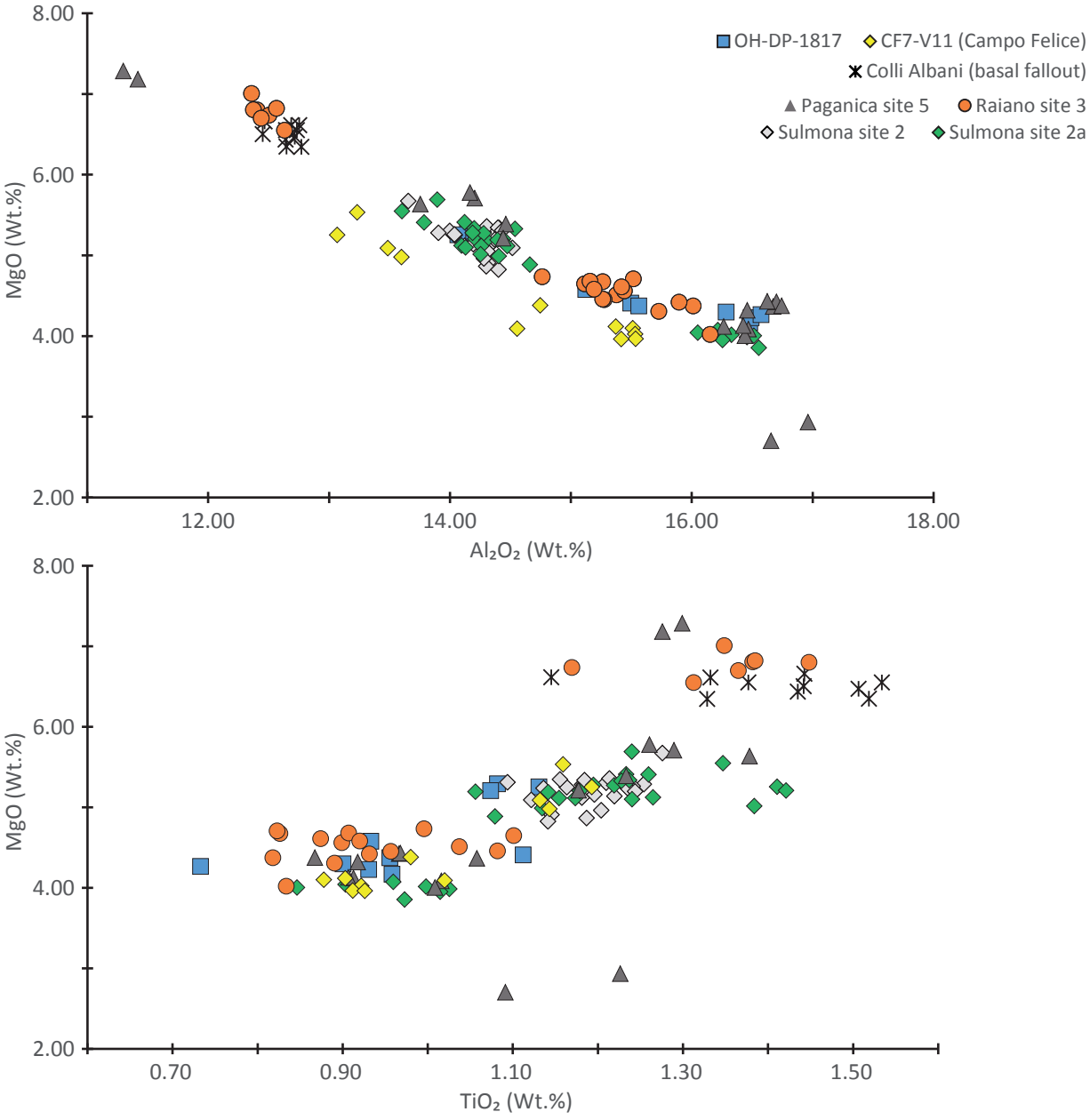

h) OH-DP-1955 - SC5

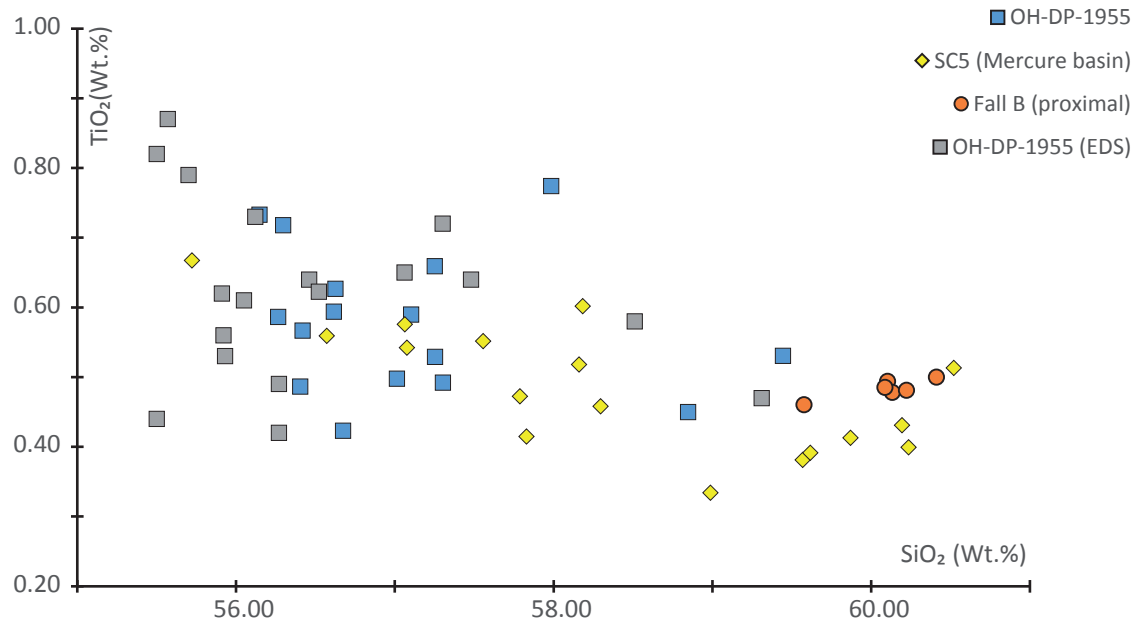

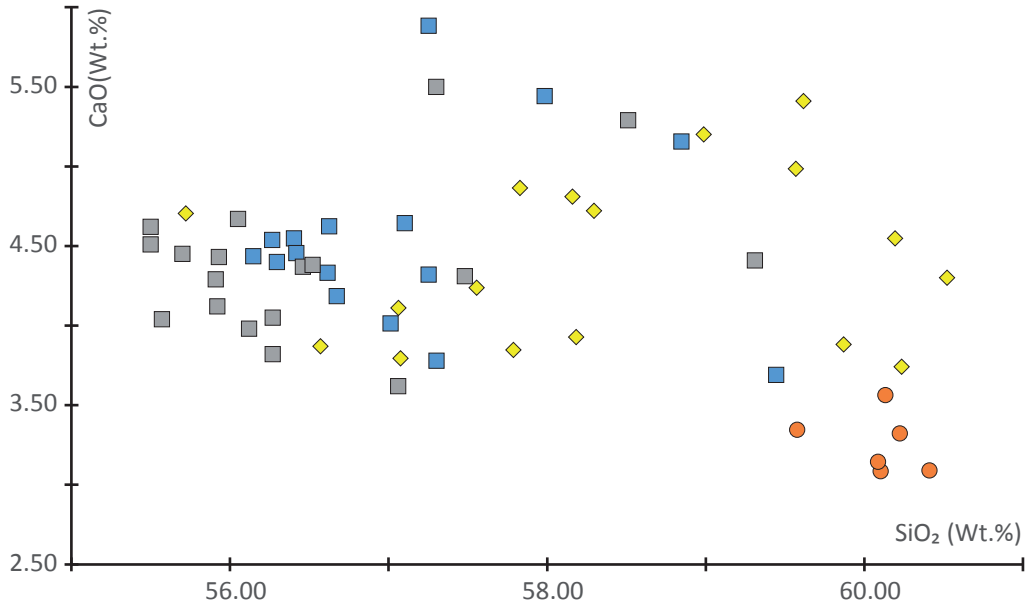

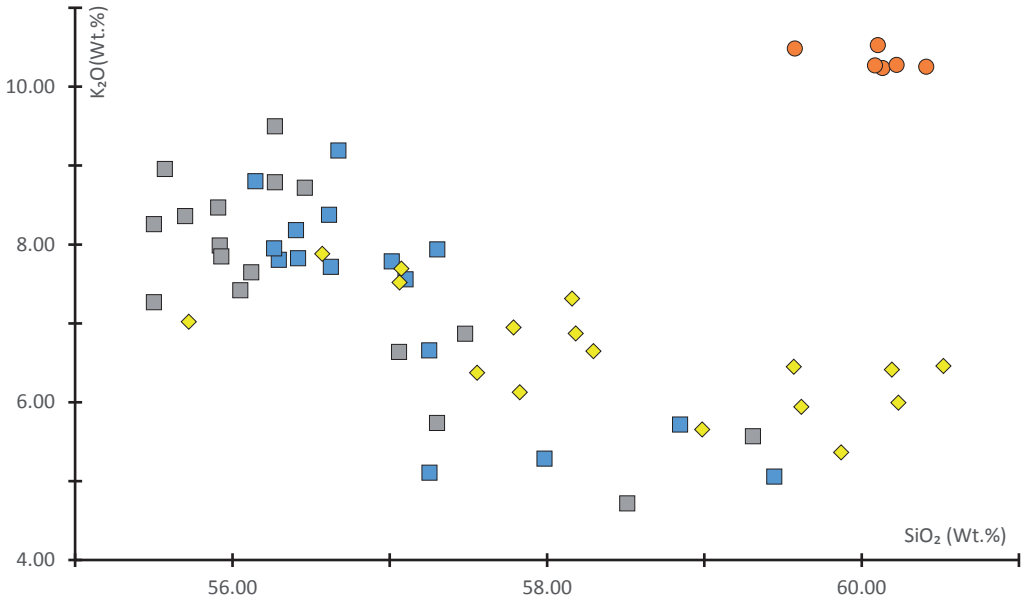

OH-DP-1955
SC5 (Mercure basin)
Fall B (proximal)
OH-DP-1955 (EDS)

Supplement II:

	SiO_2	TiO_2	Al_2O_3	FeO_{tot}	MnO	MgO	CaO	Na_2O	K_2O	P_2O_5	F	Cl	SO_3	Alkali Sum	Alkali Ratio
OH-DP-0027	55.29	0.34	17.48	5.70	0.40	1.56	7.13	6.76	5.28	0.06	0.55	0.47	0.07	12.03	0.78
WDS	59.04	0.11	20.66	2.07	0.12	0.18	2.53	8.05	7.22	0.03	0.59	0.63	0.07	15.27	0.90
	59.08	0.17	20.80	2.06	0.20	0.08	2.26	8.22	7.12	0.02	0.75	0.60	0.09	15.34	0.87
	59.60	0.11	21.04	1.89	0.20	0.08	1.78	8.31	6.94	0.06	0.73	0.61	0.06	15.25	0.84
	60.45	0.05	21.13	1.85	0.12	0.09	2.47	8.10	5.73	0.02	0.61	0.47	0.06	13.83	0.71
	59.59	0.19	20.99	1.96	0.17	0.07	1.84	8.29	6.87	0.02	0.68	0.59	0.09	15.17	0.83
	59.54	0.15	20.89	1.93	0.16	0.10	1.85	8.36	7.00	0.02	0.76	0.63	0.02	15.35	0.84
	59.30	0.21	21.13	1.96	0.18	0.08	1.79	8.35	7.00	0.02	0.78	0.66	0.03	15.35	0.84
	59.83	0.15	20.78	2.06	0.23	0.07	1.76	7.89	7.20	0.02	0.47	0.55	0.05	15.09	0.91
	59.81	0.19	20.97	1.83	0.15	0.12	1.78	8.16	6.98	0.01	0.86	0.64	0.17	15.14	0.86
	59.16	0.16	20.52	2.12	0.12	0.14	2.06	8.22	7.42	0.09	0.87	0.65	0.06	15.63	0.90
	59.56	0.18	20.97	1.91	0.18	0.07	1.62	8.13	7.34	0.03	0.69	0.65	0.06	15.47	0.90
	59.60	0.26	20.76	1.92	0.12	0.10	1.93	8.35	6.96	0.00	0.73	0.58	0.06	15.31	0.83
	59.48	0.17	21.01	1.89	0.22	0.10	1.77	8.12	7.21	0.04	0.60	0.62	0.03	15.32	0.89
	59.97	0.17	21.33	1.79	0.21	0.04	2.45	8.22	5.81	0.01	0.39	0.55	0.07	14.04	0.71
OH-DP-0115	57.35	1.02	18.81	6.30	0.17	2.03	5.61	1.79	6.48	0.45	0.06	0.33	0.01	8.28	3.61
WDS	60.23	0.44	18.26	3.80	0.19	0.94	2.98	3.08	9.86	0.21	0.29	0.43	0.20	12.94	3.20
	60.50	0.41	18.13	3.94	0.14	0.92	3.24	2.74	9.85	0.13	0.01	0.36	0.18	12.59	3.59
low SiO_2 member	60.53	0.43	18.41	3.62	0.08	0.86	2.96	3.39	9.61	0.11	0.25	0.39	0.16	13.00	2.84
high SiO_2 member	60.76	0.40	18.20	3.74	0.15	0.82	2.99	3.00	9.82	0.12	0.08	0.38	0.08	12.82	3.27
	60.84	0.36	18.78	3.43	0.15	0.80	2.76	3.96	8.86	0.06	0.21	0.38	0.00	12.82	2.23
	60.87	0.35	18.17	3.93	0.12	0.86	2.94	3.05	9.61	0.11	0.12	0.42	0.08	12.66	3.15
	61.28	0.42	18.09	3.50	0.11	0.77	2.87	3.27	9.58	0.13	0.10	0.44	0.17	12.85	2.93
	61.47	0.39	18.00	3.57	0.11	0.76	2.83	3.39	9.34	0.13	0.03	0.40	0.14	12.73	2.75
	61.72	0.44	18.11	3.50	0.15	0.70	2.78	3.00	9.56	0.05	0.14	0.43	0.10	12.55	3.19
	62.06	0.35	18.16	3.29	0.07	0.63	2.48	3.41	9.46	0.09	0.04	0.45	0.17	12.88	2.77
	62.14	0.37	18.37	3.29	0.10	0.59	2.42	3.26	9.37	0.09	0.23	0.43	0.04	12.63	2.88
	62.19	0.38	18.25	3.06	0.07	0.57	2.36	3.74	9.29	0.09	0.20	0.40	0.05	13.03	2.48
	62.56	0.38	18.20	3.14	0.04	0.56	2.47	3.49	9.11	0.06	0.00	0.56	0.12	12.60	2.61
	62.72	0.36	18.22	3.04	0.21	0.49	2.22	3.78	8.90	0.05	0.16	0.60	0.06	12.69	2.35
	62.77	0.35	18.26	3.05	0.13	0.48	2.26	3.89	8.72	0.09	0.26	0.67	0.09	12.61	2.24
	63.01	0.34	18.15	2.94	0.19	0.42	2.15	4.49	8.24	0.06	0.16	0.67	0.07	12.74	1.83
OH-DP-0169a	61.58	0.43	18.71	2.98	0.28	0.36	1.87	6.32	7.44	0.03	0.40	0.87	0.02	13.76	1.18
WDS	61.65	0.46	18.69	2.98	0.23	0.36	1.85	6.29	7.43	0.05	0.40	0.84	0.00	13.72	1.18
most evovled group	61.90	0.47	18.89	2.91	0.23	0.36	1.85	6.11	7.25	0.04	0.35	0.83	0.06	13.36	1.19
	61.46	0.39	18.93	3.17	0.23	0.34	1.92	6.15	7.38	0.03	0.32	0.84	0.02	13.54	1.20
intermediate group	61.28	0.43	18.93	3.11	0.26	0.34	1.86	6.22	7.50	0.06	0.28	0.91	0.06	13.73	1.21
	61.62	0.39	18.85	2.97	0.24	0.35	1.85	6.22	7.51	0.00	0.43	0.89	0.08	13.73	1.21
	61.95	0.41	18.96	3.18	0.21	0.37	1.81	5.92	7.18	0.01	0.38	0.84	0.07	13.10	1.21
	61.49	0.40	19.04	3.12	0.30	0.36	1.94	6.01	7.30	0.07	0.25	0.87	0.01	13.30	1.21
	61.65	0.48	18.79	3.05	0.30	0.36	1.66	6.15	7.49	0.07	0.32	0.81	0.06	13.64	1.22
	61.53	0.49	18.88	3.04	0.20	0.34	1.93	6.10	7.44	0.05	0.31	0.88	0.03	13.54	1.22
	61.89	0.45	19.00	2.88	0.29	0.34	1.96	5.86	7.29	0.05	0.40	0.87	0.07	13.15	1.25
	61.75	0.41	18.67	2.91	0.31	0.35	1.86	6.00	7.67	0.06	0.32	0.83	0.06	13.67	1.28

	61.54	0.40	18.72	3.02	0.28	0.36	1.90	5.98	7.73	0.08	0.23	0.81	0.04	13.71	1.29
	61.70	0.46	19.09	3.03	0.24	0.38	1.78	5.80	7.49	0.01	0.35	0.83	0.02	13.30	1.29
	61.87	0.47	18.84	3.05	0.23	0.33	1.93	5.71	7.57	0.00	0.41	0.91	0.06	13.28	1.33
	62.65	0.44	19.23	2.87	0.28	0.35	1.61	5.27	7.24	0.07	0.31	0.66	0.06	12.50	1.37
	62.05	0.40	18.70	2.95	0.18	0.43	1.94	5.55	7.76	0.05	0.22	0.67	0.08	13.31	1.40
	62.06	0.39	18.64	2.90	0.26	0.39	1.90	5.54	7.87	0.04	0.20	0.70	0.07	13.41	1.42
OH-DP-0169b	61.52	0.42	18.85	3.07	0.27	0.31	1.73	6.65	7.12	0.05	0.38	0.85	0.03	13.77	1.07
WDS	61.53	0.41	18.78	3.01	0.24	0.30	1.79	6.63	7.23	0.07	0.35	0.88	0.05	13.85	1.09
	61.76	0.38	18.69	2.89	0.23	0.32	1.79	6.63	7.28	0.03	0.36	0.90	0.09	13.91	1.10
most evovled group	61.46	0.38	19.05	3.09	0.27	0.35	1.75	6.45	7.16	0.04	0.24	0.83	0.03	13.61	1.11
	61.39	0.38	18.89	3.05	0.28	0.36	1.77	6.55	7.28	0.05	0.26	0.85	0.05	13.83	1.11
intermediate group	61.39	0.38	18.88	3.24	0.24	0.36	1.80	6.47	7.20	0.05	0.29	0.87	0.02	13.67	1.11
	61.78	0.38	18.81	3.06	0.33	0.34	1.81	6.36	7.11	0.01	0.38	0.85	0.08	13.48	1.12
	61.31	0.45	18.85	3.14	0.27	0.32	1.77	6.53	7.31	0.04	0.38	0.87	0.06	13.85	1.12
	61.24	0.40	18.96	3.10	0.25	0.33	1.76	6.57	7.36	0.02	0.29	0.87	0.02	13.93	1.12
	61.53	0.39	18.68	3.15	0.19	0.36	1.77	6.52	7.34	0.06	0.40	0.85	0.04	13.86	1.13
	61.29	0.45	18.64	3.02	0.28	0.36	1.85	6.62	7.46	0.03	0.42	0.84	0.00	14.08	1.13
	61.45	0.41	18.94	3.18	0.27	0.33	1.71	6.42	7.23	0.06	0.37	0.94	0.04	13.65	1.13
	61.71	0.39	18.93	2.88	0.30	0.31	1.83	6.38	7.22	0.05	0.42	0.91	0.06	13.60	1.13
	61.61	0.41	19.08	3.05	0.25	0.36	1.86	6.22	7.12	0.05	0.37	0.83	0.07	13.33	1.15
	61.57	0.42	18.89	3.04	0.23	0.34	1.78	6.39	7.32	0.03	0.31	0.81	0.04	13.71	1.15
	61.63	0.42	18.72	2.91	0.23	0.33	1.83	6.47	7.42	0.03	0.32	0.78	0.07	13.89	1.15
	61.60	0.42	18.91	3.02	0.37	0.33	1.78	6.30	7.25	0.03	0.30	0.83	0.02	13.55	1.15
	62.30	0.42	18.90	3.05	0.20	0.35	1.75	6.02	6.97	0.03	0.34	0.92	0.04	13.00	1.16
	61.82	0.43	18.94	2.99	0.30	0.33	1.76	6.20	7.19	0.04	0.42	0.80	0.01	13.39	1.16
	61.57	0.36	18.80	2.96	0.27	0.31	1.75	6.44	7.48	0.05	0.31	0.90	0.03	13.92	1.16
	61.52	0.39	19.05	3.03	0.28	0.37	1.79	6.21	7.28	0.09	0.43	0.78	0.02	13.49	1.17
	61.83	0.40	18.91	2.92	0.27	0.35	1.74	6.13	7.43	0.04	0.33	0.80	0.05	13.56	1.21
	62.33	0.40	18.98	2.98	0.27	0.32	1.67	5.86	7.17	0.03	0.53	0.81	0.10	13.03	1.22
	61.56	0.45	18.82	2.94	0.22	0.35	1.76	6.22	7.68	0.00	0.34	0.91	0.05	13.90	1.24
	63.45	0.46	19.33	3.21	0.22	0.34	1.86	3.70	7.37	0.06	0.53	0.86	0.07	11.08	1.99
OH-DP-0404	57.52	0.53	19.36	4.65	0.13	1.24	3.95	4.33	8.09	0.20	0.24	0.48	0.12	12.41	1.87
WDS	57.94	0.49	19.21	4.69	0.18	1.13	4.11	4.10	7.90	0.24	0.14	0.59	0.01	12.00	1.93
	55.67	0.46	20.73	4.86	0.12	1.32	4.25	4.55	7.77	0.27	0.27	0.58	0.16	12.32	1.71
	57.79	0.47	18.89	4.79	0.16	1.25	4.20	4.12	8.11	0.23	0.10	0.51	0.14	12.23	1.97
	57.72	0.48	18.97	4.71	0.22	1.08	4.11	4.17	8.26	0.27	0.16	0.57	0.07	12.43	1.98
	58.88	0.72	19.02	6.59	0.28	1.38	4.10	3.23	5.64	0.17	0.09	0.42	0.13	8.86	1.75
	58.95	0.51	19.10	4.70	0.12	1.15	3.92	3.22	8.20	0.12	0.20	0.35	0.05	11.42	2.55
	57.37	0.49	19.07	5.05	0.14	1.33	4.36	4.19	7.73	0.27	0.27	0.48	0.12	11.91	1.84
	57.06	0.54	19.01	4.98	0.15	1.31	4.29	4.70	7.75	0.22	0.10	0.51	0.15	12.45	1.65
	57.16	0.52	18.76	5.17	0.22	1.34	3.74	4.70	8.13	0.25	0.30	0.54	0.04	12.83	1.73
	57.21	0.65	18.53	5.47	0.16	1.58	4.73	3.63	7.71	0.34	0.23	0.44	0.14	11.33	2.13
	56.60	0.53	18.42	6.24	0.21	1.61	4.40	3.82	7.90	0.28	0.16	0.49	0.06	11.71	2.07
	57.79	0.51	18.86	4.81	0.17	1.20	4.11	4.12	8.26	0.18	0.13	0.47	0.03	12.38	2.01
	57.77	0.48	19.04	4.78	0.18	1.22	4.14	4.10	8.07	0.22	0.18	0.57	0.08	12.17	1.97
	57.63	0.53	18.92	4.83	0.15	1.21	4.32	4.43	7.73	0.25	0.09	0.59	0.09	12.16	1.75

	58.77	0.43	19.03	4.22	0.17	0.95	3.77	4.21	8.29	0.15	0.22	0.59	0.09	12.50	1.97
	57.90	0.48	19.06	4.93	0.14	1.14	4.79	3.68	7.66	0.22	0.22	0.60	0.23	11.34	2.08
	54.49	0.93	18.65	6.84	0.13	2.10	6.40	3.17	6.80	0.48	0.15	0.29	0.05	9.98	2.14
	57.68	0.46	19.28	4.49	0.14	1.24	5.61	3.46	7.43	0.22	0.03	0.35	0.09	10.88	2.15
	57.86	0.54	19.14	5.27	0.17	1.13	3.40	5.34	6.90	0.25	0.34	0.67	0.04	12.24	1.29
OH-DP-0435	61.16	0.44	18.77	3.09	0.21	0.51	1.95	5.19	7.83	0.06	0.16	0.61	0.03	13.01	1.51
WDS	60.67	0.49	18.67	3.26	0.39	0.32	1.83	6.45	6.31	0.03	0.55	0.99	0.05	12.76	0.98
	60.33	0.44	18.67	3.28	0.20	0.64	2.07	5.05	8.42	0.14	0.21	0.46	0.09	13.47	1.67
	61.27	0.43	18.73	2.90	0.35	0.32	1.81	5.94	6.81	0.05	0.37	1.00	0.02	12.75	1.15
	60.95	0.42	18.87	3.29	0.30	0.30	1.68	6.41	6.49	0.02	0.40	0.87	0.01	12.89	1.01
	61.36	0.42	18.67	3.06	0.38	0.30	1.70	6.25	6.44	0.05	0.40	0.94	0.02	12.70	1.03
	60.95	0.42	18.42	3.13	0.33	0.35	1.73	6.32	6.67	0.09	0.55	0.96	0.06	13.00	1.05
	61.11	0.46	18.37	3.14	0.00	0.34	1.77	6.63	6.77	0.05	0.33	0.98	0.06	13.40	1.02
	61.48	0.42	18.38	3.14	0.34	0.31	1.69	6.35	6.67	0.03	0.26	0.95	0.00	13.01	1.05
	60.60	0.52	18.53	3.20	0.39	0.30	1.69	6.76	6.45	0.00	0.57	0.95	0.04	13.21	0.95
	61.24	0.39	18.24	3.07	0.28	0.39	1.77	5.91	7.53	0.06	0.35	0.69	0.06	13.45	1.27
	61.10	0.44	18.40	3.06	0.37	0.30	1.75	6.48	6.72	0.04	0.37	0.89	0.09	13.21	1.04
	61.15	0.51	18.75	3.03	0.30	0.29	1.65	6.34	6.55	0.00	0.38	1.00	0.03	12.89	1.03
	61.52	0.41	18.48	2.86	0.29	0.40	1.84	5.52	7.56	0.05	0.22	0.77	0.08	13.08	1.37
	61.06	0.50	18.50	3.19	0.44	0.29	1.63	6.36	6.51	0.07	0.52	0.92	0.02	12.87	1.02
	60.28	0.47	18.46	3.17	0.46	0.28	1.73	7.03	6.44	0.04	0.61	1.00	0.03	13.47	0.91
	61.07	0.49	18.50	3.14	0.33	0.32	1.75	6.16	6.81	0.05	0.36	0.97	0.06	12.97	1.11
	61.47	0.45	18.46	2.91	0.23	0.45	1.85	5.59	7.57	0.09	0.19	0.73	0.01	13.16	1.35
	61.45	0.41	18.60	3.11	0.20	0.43	1.88	5.43	7.43	0.05	0.18	0.75	0.08	12.86	1.37
	61.00	0.47	18.30	2.92	0.28	0.38	1.72	6.37	7.20	0.04	0.37	0.85	0.09	13.57	1.13
	61.34	0.43	18.51	2.95	0.24	0.45	1.91	5.52	7.54	0.04	0.28	0.73	0.07	13.06	1.37
	60.81	0.49	18.29	3.10	0.37	0.31	1.68	6.68	6.76	0.06	0.48	0.92	0.04	13.44	1.01
OH-DP-0499	64.13	0.72	15.78	5.89	0.32	0.42	1.49	6.25	4.89	0.11	0.11	0.13	0.06	11.14	0.78
WDS	64.23	0.77	15.89	5.74	0.27	0.37	1.52	6.11	4.93	0.18	0.09	0.09	0.06	11.04	0.81
	64.58	0.76	15.95	5.93	0.30	0.38	1.55	5.40	4.98	0.17	0.00	0.14	0.01	10.38	0.92
	64.69	0.69	15.99	5.72	0.24	0.41	1.52	5.74	4.92	0.09	0.00	0.11	0.08	10.65	0.86
	64.80	0.76	15.87	6.17	0.26	0.36	1.51	5.27	4.88	0.14	0.12	0.14	0.02	10.15	0.93
	64.82	0.75	15.90	5.84	0.23	0.37	1.45	5.58	4.92	0.15	0.01	0.11	0.08	10.49	0.88
	65.16	0.73	15.94	5.90	0.36	0.40	1.53	5.10	4.74	0.13	0.10	0.13	0.07	9.84	0.93
	65.85	0.62	15.25	5.73	0.29	0.28	1.14	5.84	4.91	0.09	0.04	0.13	0.06	10.75	0.84
	65.96	0.62	14.56	6.06	0.24	0.25	1.01	6.17	5.09	0.05	0.08	0.17	0.05	11.25	0.82
	66.58	0.61	14.04	6.62	0.29	0.19	0.97	5.60	5.05	0.05	0.16	0.21	0.11	10.65	0.90
	67.78	0.53	13.32	6.58	0.31	0.17	0.87	5.47	4.86	0.10	0.14	0.26	0.08	10.33	0.89
	72.68	0.48	9.63	7.58	0.27	0.07	0.41	4.39	4.50	0.00	0.10	0.54	0.04	8.89	1.02
	73.01	0.34	9.12	7.43	0.41	0.13	0.34	4.66	4.55	0.02	0.37	0.85	0.11	9.21	0.98
	73.15	0.32	8.71	7.18	0.30	0.10	0.36	5.42	4.45	0.00	0.37	0.86	0.08	9.87	0.82
	73.18	0.37	8.67	7.35	0.34	0.07	0.29	5.15	4.54	0.05	0.29	0.90	0.07	9.68	0.88
	73.24	0.31	8.59	7.35	0.33	0.07	0.31	5.49	4.27	0.04	0.28	0.85	0.08	9.76	0.78
	73.25	0.38	8.74	7.19	0.33	0.07	0.30	5.14	4.59	0.00	0.18	0.86	0.03	9.73	0.89
	73.27	0.34	8.53	7.75	0.33	0.10	0.38	4.71	4.58	0.01	0.38	0.90	0.08	9.30	0.97

	73.34	0.39	9.25	6.99	0.38	0.07	0.40	4.65	4.47	0.04	0.36	0.75	0.05	9.12	0.96
	73.43	0.34	8.82	7.46	0.46	0.09	0.31	4.48	4.56	0.02	0.34	0.89	0.12	9.05	1.02
	73.44	0.34	8.56	7.35	0.32	0.09	0.32	4.94	4.64	0.01	0.32	0.90	0.06	9.57	0.94
	73.45	0.30	8.57	7.26	0.40	0.09	0.30	5.29	4.33	0.00	0.30	0.83	0.04	9.63	0.82
	73.53	0.33	8.69	7.38	0.37	0.10	0.40	4.71	4.49	0.03	0.27	0.84	0.02	9.19	0.95
	73.53	0.40	8.71	7.43	0.43	0.09	0.28	4.63	4.50	0.00	0.28	0.89	0.10	9.13	0.97
	73.54	0.39	8.74	7.57	0.35	0.06	0.32	4.71	4.31	0.01	0.15	0.89	0.06	9.02	0.91
	73.55	0.38	8.81	7.20	0.38	0.05	0.36	4.70	4.54	0.02	0.42	0.87	0.05	9.24	0.96
	73.66	0.37	8.70	7.39	0.33	0.07	0.28	4.58	4.60	0.02	0.12	0.87	0.08	9.18	1.00
	73.67	0.37	8.76	7.25	0.31	0.09	0.34	4.78	4.38	0.04	0.31	0.89	0.04	9.16	0.92
	73.68	0.35	8.78	7.25	0.38	0.07	0.35	4.63	4.49	0.03	0.28	0.88	0.06	9.12	0.97
	73.70	0.35	8.81	7.14	0.43	0.06	0.33	4.70	4.44	0.03	0.39	0.85	0.02	9.14	0.94
	73.75	0.38	8.67	7.34	0.31	0.09	0.32	4.70	4.44	0.00	0.32	0.84	0.08	9.15	0.94
	73.76	0.39	8.74	7.33	0.26	0.09	0.31	4.63	4.45	0.04	0.33	0.81	0.05	9.08	0.96
	73.82	0.35	8.64	7.26	0.28	0.08	0.34	4.84	4.38	0.01	0.21	0.78	0.09	9.22	0.90
	73.83	0.36	8.87	7.32	0.29	0.07	0.33	4.46	4.43	0.04	0.39	0.81	0.06	8.89	0.99
	73.84	0.36	8.71	7.20	0.38	0.07	0.35	4.59	4.50	0.00	0.35	0.81	0.02	9.10	0.98
	73.85	0.37	8.65	7.24	0.32	0.08	0.30	4.63	4.56	0.00	0.31	0.88	0.11	9.19	0.99
	73.90	0.37	8.75	7.30	0.32	0.05	0.32	4.66	4.31	0.02	0.26	0.89	0.07	8.96	0.93
	73.91	0.35	8.81	7.17	0.30	0.08	0.35	4.48	4.54	0.02	0.24	0.90	0.02	9.02	1.01
	73.93	0.35	8.88	7.30	0.36	0.09	0.32	4.49	4.28	0.00	0.26	0.82	0.01	8.78	0.95
	73.94	0.38	8.80	7.17	0.40	0.09	0.34	4.51	4.35	0.02	0.15	0.95	0.03	8.86	0.96
	73.99	0.35	8.75	7.15	0.29	0.07	0.31	4.62	4.43	0.03	0.45	0.85	0.08	9.05	0.96
	74.07	0.36	8.64	7.16	0.36	0.08	0.28	4.60	4.44	0.02	0.26	0.87	0.08	9.05	0.97
	74.12	0.37	8.69	7.25	0.27	0.09	0.27	4.46	4.50	0.00	0.29	0.88	0.06	8.95	1.01
	74.25	0.42	8.80	7.14	0.24	0.09	0.34	4.29	4.44	0.00	0.18	0.91	0.05	8.73	1.04
OH-DP-0617	59.20	0.43	20.71	2.76	0.16	0.43	2.36	5.19	8.70	0.05	0.58	0.24	0.10	13.89	1.67
WDS	59.96	0.42	19.76	2.87	0.11	0.47	2.50	5.04	8.81	0.05	0.48	0.26	0.14	13.86	1.75
	60.18	0.42	19.77	2.76	0.12	0.44	2.46	4.96	8.87	0.02	0.41	0.22	0.06	13.83	1.79
	60.17	0.45	19.69	2.86	0.13	0.43	2.37	4.69	9.16	0.06	0.36	0.23	0.06	13.84	1.95
	60.37	0.44	19.83	2.66	0.15	0.40	2.38	5.09	8.63	0.05	0.51	0.25	0.14	13.72	1.69
	60.19	0.43	19.66	2.86	0.20	0.44	2.31	5.08	8.78	0.05	0.72	0.23	0.08	13.86	1.73
	60.11	0.45	19.69	2.62	0.20	0.44	2.48	4.88	9.09	0.02	0.51	0.23	0.15	13.97	1.86
	60.47	0.49	19.67	2.82	0.12	0.44	2.36	5.13	8.49	0.02	0.52	0.21	0.12	13.62	1.66
	60.10	0.41	19.71	2.79	0.11	0.42	2.32	4.87	9.19	0.05	0.54	0.28	0.14	14.06	1.89
	60.14	0.41	19.62	2.54	0.20	0.38	2.33	4.94	9.35	0.09	0.40	0.23	0.12	14.28	1.89
	60.00	0.45	19.82	2.74	0.12	0.40	2.37	5.24	8.80	0.07	0.51	0.26	0.11	14.04	1.68
	60.44	0.39	19.54	2.78	0.16	0.42	2.32	5.21	8.66	0.06	0.43	0.23	0.19	13.87	1.66
	60.61	0.42	19.54	2.74	0.11	0.39	2.37	5.22	8.56	0.04	0.36	0.23	0.10	13.77	1.64
OH-DP-0624	50.18	1.08	18.15	8.74	0.20	3.44	9.19	2.97	5.32	0.72	0.28	0.29	0.57	8.29	1.79
WDS	50.04	1.18	18.03	9.25	0.21	3.76	9.13	2.27	5.14	0.97	0.29	0.34	0.48	7.42	2.26
	60.04	0.52	19.62	2.87	0.17	0.42	2.74	4.21	9.36	0.04	0.17	0.49	0.19	13.57	2.22
	50.18	1.11	18.04	8.43	0.16	3.40	9.18	3.04	5.54	0.91	0.21	0.28	0.60	8.58	1.82
	49.16	1.15	17.91	9.50	0.20	3.75	9.95	2.81	4.81	0.76	0.18	0.28	0.75	7.62	1.72
	48.97	1.20	17.72	9.25	0.23	3.91	10.17	2.74	5.04	0.78	0.13	0.31	0.31	7.78	1.84
	48.87	1.13	17.86	9.30	0.21	3.90	9.93	2.94	5.05	0.80	0.08	0.28	0.30	7.98	1.72

	55.27	0.77	18.80	5.89	0.17	1.87	5.92	3.89	7.01	0.41	0.19	0.35	0.34	10.90	1.80
	49.34	1.05	17.72	8.92	0.22	3.75	9.51	2.95	5.71	0.83	0.32	0.30	0.29	8.66	1.93
	48.85	1.20	17.78	9.40	0.13	3.97	10.18	2.79	4.87	0.81	0.18	0.27	0.48	7.66	1.75
	49.19	1.09	17.90	9.33	0.24	3.77	9.96	2.83	4.83	0.87	0.22	0.32	0.50	7.66	1.71
	53.96	0.91	18.61	6.94	0.16	2.20	5.63	4.09	6.95	0.54	0.17	0.54	0.02	11.05	1.70
	56.26	0.64	18.82	5.14	0.15	1.30	5.25	4.73	7.43	0.28	0.07	0.40	0.31	12.16	1.57
	49.30	1.16	17.91	9.00	0.21	3.75	9.88	2.89	5.06	0.84	0.11	0.33	0.46	7.95	1.75
	49.55	1.16	17.80	9.10	0.19	3.63	9.95	2.80	5.08	0.75	0.24	0.29	0.33	7.88	1.81
	48.85	1.20	17.63	9.43	0.25	3.98	10.02	2.79	4.86	0.98	0.18	0.27	0.21	7.66	1.74
	49.43	1.15	17.43	9.40	0.21	3.77	9.69	2.83	5.16	0.91	0.14	0.29	0.25	7.99	1.82
	49.53	1.08	17.88	9.24	0.14	3.67	9.95	2.78	4.96	0.76	0.23	0.28	0.41	7.74	1.78
	59.57	0.53	19.70	2.90	0.17	0.43	2.62	4.46	9.59	0.04	0.17	0.47	0.18	14.05	2.15
OH-DP-1817	46.12	0.90	16.28	10.00	0.20	4.30	11.95	3.40	5.96	0.90	0.30	0.11	0.57	9.35	1.75
WDS	46.22	0.96	16.48	9.76	0.15	4.17	11.76	3.46	6.11	0.93	0.25	0.12	0.60	9.58	1.77
	45.95	0.93	16.49	9.98	0.23	4.23	12.08	3.50	5.78	0.83	0.41	0.13	0.66	9.28	1.65
	46.39	0.73	16.57	9.88	0.26	4.27	11.87	3.38	5.88	0.77	0.30	0.14	0.56	9.26	1.74
	44.23	1.11	15.50	10.32	0.17	4.41	13.01	4.72	5.59	0.95	0.34	0.15	0.34	10.31	1.18
	44.21	0.93	15.12	10.84	0.22	4.58	13.26	4.44	5.46	0.94	0.29	0.16	0.46	9.90	1.23
	44.71	0.96	15.56	10.12	0.21	4.37	12.81	4.91	5.51	0.84	0.28	0.11	0.30	10.42	1.12
	42.49	1.08	14.14	12.17	0.27	5.29	15.29	3.27	4.90	1.10	0.59	0.14	0.16	8.17	1.50
	42.55	1.07	14.18	11.98	0.26	5.21	15.21	3.46	4.91	1.16	0.55	0.16	0.19	8.37	1.42
	41.96	1.13	14.06	12.59	0.38	5.26	15.27	3.53	4.69	1.13	0.27	0.16	0.22	8.22	1.33
OH-DP-1955	57.25	0.53	20.27	4.22	0.20	0.68	5.88	5.60	5.11	0.09	0.38	0.27	0.18	10.71	0.91
WDS	58.85	0.45	21.15	3.11	0.15	0.33	5.16	4.75	5.72	0.08	0.26	0.15	0.27	10.46	1.20
	60.86	0.54	21.47	4.08	0.21	0.57	4.82	2.95	4.14	0.10	0.21	0.15	0.26	7.09	1.40
	57.10	0.59	20.51	4.07	0.17	0.53	4.64	4.50	7.56	0.14	0.38	0.19	0.19	12.07	1.68
	56.63	0.63	19.73	4.63	0.20	0.59	4.62	4.84	7.72	0.11	0.33	0.32	0.31	12.56	1.60
	59.44	0.53	21.24	3.90	0.17	0.54	3.69	5.13	5.06	0.06	0.36	0.26	0.23	10.19	0.99
	56.40	0.49	20.37	4.27	0.09	0.59	4.55	4.78	8.18	0.10	0.31	0.23	0.17	12.97	1.71
	56.30	0.72	20.31	4.26	0.22	0.58	4.40	5.12	7.81	0.09	0.55	0.27	0.21	12.93	1.52
	56.42	0.57	19.95	4.39	0.19	0.59	4.46	5.24	7.83	0.09	0.29	0.24	0.29	13.06	1.50
	57.25	0.66	20.46	3.98	0.16	0.57	4.32	5.65	6.66	0.12	0.38	0.23	0.17	12.31	1.18
	56.61	0.59	20.17	4.21	0.20	0.58	4.33	4.68	8.38	0.10	0.39	0.24	0.14	13.06	1.79
	61.12	0.52	21.37	3.70	0.16	0.53	4.69	3.27	4.32	0.10	0.00	0.10	0.20	7.59	1.32
	57.98	0.77	20.53	3.88	0.13	0.58	5.44	5.06	5.29	0.09	0.28	0.26	0.25	10.35	1.04
	56.15	0.73	20.13	4.18	0.18	0.60	4.44	4.50	8.80	0.09	0.39	0.26	0.20	13.30	1.96
	56.67	0.42	20.34	3.93	0.17	0.64	4.19	4.11	9.19	0.11	0.34	0.22	0.21	13.30	2.24
	56.27	0.59	20.20	4.40	0.28	0.56	4.54	4.85	7.95	0.07	0.24	0.26	0.30	12.80	1.64
	57.30	0.49	20.54	3.58	0.21	0.49	3.78	5.52	7.94	0.02	0.39	0.25	0.11	13.46	1.44
	57.01	0.50	20.50	3.79	0.16	0.49	4.01	5.49	7.79	0.09	0.19	0.21	0.17	13.28	1.42
OH-DP-2010	52.37	0.88	17.70	7.45	0.19	2.30	7.59	3.23	7.38	0.47	0.31	0.09	0.44	10.61	2.28
WDS	51.76	1.04	17.83	7.66	0.12	2.35	7.78	3.01	7.63	0.46	0.31	0.07	0.35	10.65	2.53
	50.31	0.93	17.50	8.23	0.21	2.54	8.05	2.77	8.23	0.56	0.21	0.07	0.68	11.00	2.97
	51.36	0.75	17.80	7.64	0.16	2.45	7.44	2.78	8.55	0.47	0.05	0.04	0.59	11.33	3.07

	51.01	0.98	17.57	8.14	0.14	2.57	7.92	2.66	7.98	0.55	0.40	0.07	0.48	10.64	3.00
	51.39	0.83	17.75	7.64	0.17	2.42	7.40	2.65	8.59	0.60	0.49	0.07	0.56	11.24	3.24
	65.09	0.38	16.37	2.92	0.15	0.30	2.16	3.22	9.23	0.01	0.30	0.14	0.17	12.45	2.87
	53.04	0.63	18.30	6.72	0.13	1.97	6.48	2.45	9.20	0.41	0.24	0.07	0.68	11.65	3.75
	50.85	0.95	17.59	7.94	0.18	2.57	7.61	2.47	8.64	0.57	0.17	0.03	0.63	11.12	3.49
	54.40	0.81	18.38	5.86	0.15	1.55	5.87	3.23	9.02	0.30	0.35	0.08	0.44	12.25	2.80
	50.77	0.86	17.36	8.11	0.12	2.80	7.96	2.45	8.35	0.49	0.27	0.05	0.74	10.80	3.42
	51.09	0.97	17.86	8.11	0.19	2.60	8.00	2.83	7.32	0.51	0.37	0.09	0.53	10.15	2.59
	55.76	0.69	19.14	4.97	0.16	1.14	4.86	4.65	7.97	0.22	0.44	0.09	0.43	12.62	1.72
	52.34	0.77	17.80	7.32	0.14	2.25	7.20	2.95	8.08	0.45	0.39	0.06	0.71	11.03	2.74
	57.68	0.56	19.06	4.18	0.12	0.72	3.99	3.45	9.76	0.13	0.26	0.08	0.35	13.21	2.83
	58.07	0.60	18.98	3.87	0.14	0.57	3.56	3.54	10.16	0.16	0.31	0.10	0.35	13.70	2.87
	58.28	0.59	19.13	3.83	0.15	0.57	3.38	3.36	10.25	0.09	0.41	0.09	0.37	13.62	3.05
	58.60	0.69	19.17	3.90	0.16	0.65	3.89	3.42	9.22	0.06	0.43	0.09	0.23	12.63	2.70
	53.42	0.77	18.13	6.43	0.14	1.87	6.01	2.98	9.31	0.37	0.22	0.08	0.57	12.29	3.13
	51.01	0.86	17.86	8.23	0.14	2.43	8.38	2.98	6.95	0.53	0.35	0.09	0.64	9.92	2.33
	56.48	0.53	18.70	4.36	0.21	0.85	5.25	3.62	9.56	0.14	0.52	0.14	0.30	13.18	2.64
	53.67	0.62	18.99	5.84	0.14	1.48	6.37	2.95	9.09	0.23	0.23	0.06	0.64	12.03	3.08
OH-DP-2017	64.47	0.51	18.32	2.49	0.16	0.26	1.01	5.70	6.30	0.07	0.26	0.38	0.07	12.01	1.11
WDS	64.44	0.43	18.27	2.63	0.16	0.26	1.05	5.74	6.38	0.01	0.18	0.36	0.09	12.11	1.11
	64.46	0.43	18.30	2.54	0.18	0.30	1.13	5.64	6.32	0.06	0.16	0.38	0.12	11.96	1.12
	64.30	0.47	18.14	2.59	0.15	0.29	1.10	5.75	6.29	0.04	0.36	0.36	0.16	12.04	1.09
	64.57	0.36	18.39	2.61	0.14	0.29	1.00	5.53	6.35	0.03	0.25	0.38	0.11	11.88	1.15
	64.33	0.36	18.22	2.55	0.19	0.28	0.98	5.87	6.36	0.02	0.33	0.40	0.12	12.22	1.08
	64.89	0.39	18.44	2.49	0.21	0.33	1.08	5.05	6.24	0.03	0.31	0.37	0.16	11.29	1.24
	64.15	0.43	17.87	2.59	0.17	0.30	1.10	6.26	6.30	0.06	0.29	0.35	0.14	12.56	1.01
	64.79	0.49	18.36	2.59	0.18	0.28	1.04	5.38	6.05	0.07	0.32	0.36	0.10	11.43	1.13
	64.56	0.40	18.39	2.77	0.21	0.27	1.12	5.32	6.35	0.01	0.16	0.36	0.08	11.68	1.19
	64.44	0.64	18.16	2.49	0.22	0.28	1.01	5.82	6.19	0.05	0.28	0.36	0.06	12.01	1.06
	64.03	0.40	18.29	2.61	0.22	0.29	1.14	5.74	6.45	0.05	0.28	0.38	0.12	12.19	1.12
	64.14	0.40	18.17	2.63	0.17	0.29	1.05	5.98	6.43	0.07	0.22	0.36	0.10	12.41	1.07
	64.22	0.40	18.39	2.61	0.13	0.32	1.11	5.41	6.77	0.10	0.10	0.30	0.12	12.18	1.25
	64.43	0.46	18.18	2.60	0.17	0.32	0.95	5.84	6.32	0.09	0.22	0.37	0.06	12.16	1.08
	64.47	0.53	18.24	2.75	0.20	0.29	1.11	5.30	6.34	0.07	0.24	0.36	0.11	11.64	1.20
	64.38	0.45	18.30	2.52	0.23	0.30	1.06	5.75	6.20	0.06	0.26	0.37	0.12	11.95	1.08
	64.52	0.51	18.45	2.63	0.16	0.31	1.03	5.52	6.20	0.02	0.20	0.37	0.07	11.73	1.12
	64.33	0.49	18.26	2.55	0.21	0.30	1.11	5.67	6.22	0.06	0.31	0.36	0.14	11.89	1.10
	64.49	0.22	18.24	2.58	0.21	0.31	1.06	5.71	6.43	0.09	0.11	0.38	0.15	12.15	1.13
	64.64	0.45	18.27	2.49	0.23	0.30	1.01	5.64	6.29	0.05	0.20	0.33	0.11	11.93	1.12
OH-DP-2060	43.22	0.81	18.57	9.31	0.32	1.40	11.85	5.78	7.15	0.29	0.85	0.21	1.28	12.94	1.24
WDS	44.18	0.77	18.44	9.23	0.29	1.60	12.07	4.68	7.46	0.25	0.79	0.19	1.03	12.14	1.60
	43.53	0.89	18.05	9.28	0.35	1.55	12.14	5.58	7.39	0.21	0.86	0.16	1.03	12.97	1.32
	41.96	0.85	19.49	8.62	0.34	1.29	11.46	6.65	6.58	0.33	1.21	0.32	2.43	13.22	0.99
	44.22	0.56	18.80	9.12	0.35	1.54	11.60	5.46	7.13	0.28	0.75	0.17	0.94	12.59	1.30
	48.57	0.91	18.55	8.43	0.33	1.23	8.86	5.23	6.73	0.31	1.15	0.17	0.86	11.95	1.29
	44.59	0.68	18.72	8.53	0.27	1.45	10.62	5.56	8.48	0.25	1.09	0.19	0.84	14.04	1.53

	44.50	0.85	19.37	8.54	0.28	1.36	10.50	4.99	8.43	0.32	0.62	0.17	0.86	13.42	1.69
	45.62	0.63	19.83	6.69	0.30	0.97	9.29	5.86	10.08	0.15	1.05	0.17	0.58	15.94	1.72
	45.72	0.61	19.85	6.50	0.30	0.99	9.19	5.88	10.19	0.20	0.96	0.18	0.56	16.08	1.73
	44.89	0.73	19.03	9.42	0.29	1.33	10.50	5.34	7.41	0.29	0.94	0.17	0.77	12.75	1.39
	44.25	0.74	18.44	8.89	0.27	1.50	11.45	5.63	7.83	0.14	0.85	0.17	0.85	13.46	1.39
	44.07	0.76	18.46	8.64	0.32	1.46	11.56	5.78	7.80	0.27	1.03	0.17	0.89	13.58	1.35
	43.25	1.06	15.27	11.17	0.24	5.66	14.19	3.06	4.90	0.93	0.45	0.17	0.26	7.96	1.60
	49.00	0.82	18.26	7.25	0.22	1.88	9.31	5.91	5.29	0.26	0.99	0.32	1.81	11.20	0.90
	44.97	0.98	18.78	8.51	0.23	1.44	10.02	4.56	9.07	0.27	0.55	0.17	1.17	13.63	1.99
	44.49	1.11	18.77	9.01	0.18	1.56	10.60	4.51	8.64	0.28	0.62	0.19	0.84	13.15	1.91
	45.97	0.57	18.83	6.76	0.36	1.28	11.37	5.99	8.17	0.14	1.21	0.18	0.56	14.16	1.36
	46.78	0.46	19.30	6.45	0.29	1.07	10.67	5.96	8.36	0.16	1.29	0.18	0.50	14.32	1.40
EDS standard															
KE12 (glass)															
Measured mean	70.83	0.29	7.82	8.67	0.29	0.35	7.23	4.19	0.33	-	-	-	-	100.00	
Recommended	70.99	0.20	7.82	8.38	0.21	0.35	7.43	4.33	0.30	-	-	-	-		
CFA47 (glass)															
Measured mean	62.16	0.42	18.62	2.66	0.18	0.42	1.85	5.40	8.02	0.07	-	-	-	100.00	
Recommended	61.60	0.35	18.92	2.73	0.22	0.52	1.73	5.43	7.93	0.00	-	-	-	100.00	
Olivine															
Measured mean	41.49	-	7.72	50.86	-	-	-	-	-	-	-	-	-	100.00	
Recommended	41.37	-	7.53	50.97	-	-	-	-	-	-	-	-	-	100.00	
Albite															
Measured mean	68.15	19.77	-	-	-	0.38	-	11.46	0.23	-	-	-	-	100.00	
Recommended	67.75	20.55	-	-	-	0.00	-	11.55	0.15	-	-	-	-	100.00	
WDS standard															
Standard 1 - USGS Rhyolite															
Test1	76.04	0.15	11.09	2.16	0.14	0.06	0.08	4.47	4.49	0.01	0.26	0.18	0.03	99.17	
Test2	75.64	0.31	11.23	2.29	0.17	0.05	0.11	4.68	4.52	0.04	0.24	0.18	0.02	99.47	
Measured mean	75.84	0.23	11.16	2.23	0.16	0.05	0.09	4.57	4.51	0.03	0.25	0.18	0.03	99.32	
Recommended	76.00	0.19	11.50	2.02	0.16	0.08	0.10	4.75	4.47	-	-	-	0.03	99.30	
Standard 2 - Kakanui Augite															
test1	50.91	0.88	8.39	0.08	6.48	16.17	15.86	1.37	-	-	-	-	-	100.15	
test2	50.67	0.86	8.32	0.09	6.58	16.36	16.04	1.22						100.14	
Measured mean	50.79	0.87	8.36	0.09	6.53	16.27	15.95	1.29						100.14	
Recommended	50.46	0.84	8.28	0.13	6.51	16.28	16.00	1.30	-	-	-	-	-	99.80	